

A Faint Progenitor System for the Faint Supernova 2024vjm

Erez A. Zimmerman^{1*}, Avishay Gal-Yam¹, Paul J. Groot^{2,3,4},
Eran O. Ofek¹, Jan van Roestel^{5,6}, Andrea Pastorello⁷,
Stefano Valenti⁸, Aravind P. Ravi⁸, Ping Chen^{9,10},
Steve Schulze^{1,11}, Nadejda Blagorodnova^{12,13,14},
Maxime Wavasseur^{12,15}, Marco A. Gómez-Muñoz^{12,15},
Hugo Tranin^{12,14,15}, Simon de Wet¹⁶, Giorgos Leloudas¹⁶,
Paul M. Vreeswijk¹⁷, Lindsey A. Kwok¹¹, Michaela Schwab^{18,19},
Saurabh W. Jha¹⁸, Kate Maguire²⁰, David J. Sand²¹,
Eric Stringer²², Thomas Kupfer²², Tamar Faran¹,
Joseph P. Anderson²³, Jennifer Andrews²⁴, Moira Andrews^{25,26},
Avshalom Badash¹, Steven Bloemen², K. Azalee Bostroem^{21,27},
Ting-Wan Chen²⁸, Massimo Della Valle²⁹, Georgios Dimitriadis³⁰,
Yize Dong³¹, Joseph R. Farah^{25,32}, James H. Gillanders³³,
Benjamin Godson³⁴, Mariusz Gromadzki³⁵, Daichi Hiramatsu¹³,
Emily Hoang⁸, D. Andrew Howell^{25,26}, Daryl Janzen³⁶,
Hanindyo Kuncarayakti^{37,38}, Jiaxuan Li³⁹, Joseph D. Lyman³⁴,
Keiichi Maeda⁴⁰, Mark R. Magee³⁴, Darshana Mehta⁸,
Andrew Milligan³⁰, Shane Moran⁴¹, Yuan Qi Ni^{25,42},
David O'Neill⁴³, Jeniveve Pearson²¹, Daniëlle L. A. Pieterse²,
Giuliano Pignata⁴⁴, Andrea Reguitti^{7,45}, Daniel E. Reichart⁴⁶,
Nicolás Meza Retamal⁸, Rita P. Santos^{23,47}, Simone Scaringi^{48,29},
Manisha Shrestha^{49,50}, Shubham Srivastav³³, Fiorenzo Stoppa³³,
Bhagya Subrayan²¹, Giorgio Valerin⁷, Xiaofeng Wang⁵¹,
Kathryn Wynn^{25,32}, Ofer Yaron¹, Weicheng Zang⁵²

¹Department of Particle Physics and Astrophysics, Weizmann Institute of Science, 234 Herzl St, 7610001, Rehovot, Israel.

²Department of Mathematics/IMAPP, Radboud University, PO Box 9010, 6500 GL, Nijmegen, The Netherlands.

³Department of Astronomy and Inter-University Center for Data Intensive Astronomy, University of Cape Town, Private Bag, X3 7701, Rondebosch, South Africa.

⁴South African Astronomical Observatory, P.O. Box 9, 7935, Observatory, South Africa.

⁵Institute of Science and Technology Austria, Am Campus 1, 3400 Klosterneuburg, Austria.

⁶Anton Pannekoek Institute for Astronomy, University of Amsterdam, P.O. Box 94249, 1090 GE, Amsterdam, The Netherlands.

⁷INAF – Osservatorio Astronomico di Padova, Vicolo dell’Osservatorio 5, I-35122, Padova, Italy.

⁸Department of Physics and Astronomy, University of California, Davis, 1 Shields Avenue, CA 95616-5270, Davis, USA.

⁹Institute for Advanced Study in Physics, Zhejiang University, Hangzhou 310027, China.

¹⁰Institute for Astronomy, School of Physics, Zhejiang University, Hangzhou 310027, China.

¹¹Center for Interdisciplinary Exploration and Research in Astrophysics (CIERA), 1800 Sherman Ave., IL 60201, Evanston, USA.

¹²Institut de Ciències del Cosmos (ICCUB), Universitat de Barcelona (UB), c. Martí i Franquès, 1, 08028, Barcelona, Spain.

¹³Department of Astronomy, University of Florida, Bryant Space Science Center, FL 32611-2055, Gainesville, USA.

¹⁴Institut d’Estudis Espacials de Catalunya (IEEC), c/ Esteve Terradas, 1, Edifici RDIT, Despatx 212, Campus del Baix Llobregat UPC - Parc Mediterrani de la Tecnologia, 08860, Castelldefels, Spain.

¹⁵Departament de Física Quàntica i Astrofísica (FQA), Universitat de Barcelona (UB), c. Martí i Franquès, 1, 08028, Barcelona, Spain.

¹⁶DTU Space, Technical University of Denmark, Building 327, Elektrovej, 2800, Kgs. Lyngby, Denmark.

¹⁷Department of Astrophysics/IMAPP, Radboud University, P.O. Box 9010, 6500 GL, Nijmegen, The Netherlands.

¹⁸Department of Physics and Astronomy, Rutgers, The State University of New Jersey, 136 Frelinghuysen Road, NJ 08854-8019, Piscataway, USA.

¹⁹Department of Astronomy, University of Virginia, Charlottesville VA 22904-4325, USA.

²⁰School of Physics, Trinity College Dublin, The University of Dublin, Dublin 2, Ireland..

²¹Steward Observatory, University of Arizona, 933 North Cherry Avenue, AZ 85721-0065, Tucson, USA.

²²Hamburger Sternwarte, University of Hamburg, Gojenbergsweg 112, 21029, Hamburg, Germany.

²³European Southern Observatory, Alonso de Córdova 3107, Vitacura, Casilla 19001, Santiago, Chile.

²⁴Gemini Observatory, 670 North A'ohoku Place, HI 96720-2700, Hilo, USA.

²⁵Las Cumbres Observatory, 6740 Cortona Drive, Suite 102, CA 93117-5575, Goleta, USA.

²⁶Department of Physics, University of California, CA 93106-9530, Santa Barbara, USA.

²⁷LSSTC Catalyst Fellow.

²⁸Graduate Institute of Astronomy, National Central University, 300 Jhongda Road, 32001, Jhongli, Taiwan.

²⁹INAF – Osservatorio Astronomico di Capodimonte, Napoli, Italy.

³⁰Department of Physics, Lancaster University, Lancaster, LA1, 4YB, UK.

³¹Center for Astrophysics |Harvard & Smithsonian, 60 Garden Street, MA 02138-1516, Cambridge, USA.

³²Department of Physics, University of California, CA 93106-9530, Santa Barbara, USA.

³³Astrophysics sub-Department, Department of Physics, University of Oxford, Keble Road, Oxford, OX1, 3RH, UK.

³⁴Department of Physics, University of Warwick, Gibbet Hill Road, Coventry CV4 7AL, UK.

³⁵Astronomical Observatory, University of Warsaw, Al. Ujazdowskie 4, 00-478, Warszawa, Poland.

³⁶Department of Physics and Engineering Physics, University of Saskatchewan, 116 Science Place, Saskatoon, SK S7N 5E2, Canada.

³⁷Tuorla Observatory, Department of Physics and Astronomy, FI-20014, University of Turku, Finland.

³⁸Finnish Centre for Astronomy with ESO (FINCA), FI-20014 University of Turku, Finland.

³⁹Department of Astrophysical Sciences, 4 Ivy Lane, Princeton University, NJ 08540, Princeton, USA.

⁴⁰Department of Astronomy, Kyoto University,

Kitashirakawa-Oiwake-cho, Sakyo-ku, Kyoto 606-8502, Japan.

⁴¹School of Physics and Astronomy, University of Leicester, University Road, Leicester LE1 7RH, UK.

⁴²Kavli Institute for Theoretical Physics, University of California, Santa Barbara, 552 University Road, CA 93106-4030, Goleta, USA.

⁴³School of Physics and Astronomy, University of Birmingham, Edgbaston, B15 2TT, Birmingham, UK.

⁴⁴Instituto de Alta Investigación, Universidad de Tarapacá, Casilla 7D, Arica, Chile.

⁴⁵INAF – Osservatorio Astronomico di Brera, Via E. Bianchi 46, I-23807, Merate (LC), Italy.

⁴⁶Department of Physics and Astronomy, University of North Carolina, 120 East Cameron Avenue, NC 27599, Chapel Hill, USA.

⁴⁷CENTRA, Departamento de Física, Instituto Superior Técnico – IST, Universidade de Lisboa – UL, Avenida Rovisco Pais 1, 1049-001, Lisboa, Portugal.

⁴⁸Centre for Extragalactic Astronomy, Department of Physics, Durham University, DH1, 3LE, United Kingdom.

⁴⁹School of Physics and Astronomy, Monash University, Clayton, Australia.

⁵⁰OzGrav: The ARC Center of Excellence for Gravitational Wave Discovery, Australia.

⁵¹Physics Department, Tsinghua University, Beijing 100084, China.

⁵²Department of Astronomy, Westlake University, Hangzhou 310030, Zhejiang Province, China.

Contributing authors: erez.zimmerman@weizmann.ac.il;

Abstract

Type Ia Supernovae (SNe Ia) are well known for their role as standardizable cosmological candles. Their uniformity is credited to their single origin as thermonuclear explosions of White dwarf (WD) stars (e.g., [1, 2]). Nevertheless, some SNe Ia break this regularity. Prominently, the Iax subclass [3] are less energetic and remarkably diverse, raising questions about their progenitor systems. While no progenitor system of a normal SN Ia has ever been detected, a luminous blue star was identified in pre-explosion images of the site of the bright SN Iax SN 2012Z [4], suggested to be a helium giant companion star acting as a mass donor to a WD SN progenitor. This is in line with models of weak mass accretion of a WD from a binary companion (e.g., [5]), producing an explosion that does not fully disrupt the star. However, these models fail to explain the properties of the faintest Type Iax explosions [6], suggesting either they originate from other WD binary systems, or even from massive progenitor stars [7, 8]. Here, we present the faint SN Iax SN 2024vjm - possibly the faintest supernova observed to date. Using a deep pre-explosion image taken by the recently launched *Euclid* space mission, we show that its progenitor system must be fainter than the helium giant

SN Iax progenitor candidate of SN 2012Z, as well as that of the luminous red companion or remnant of the faint SN 2008ha [9], and may require a subdwarf helium star as a mass donor. The deep image also provides strong arguments against a massive star origin for this faint supernova. Our observations argue that SN 2024vjm is a WD explosion, but we find that remarkably faint SNe Iax fade more slowly than bright ones, i.e., they evolve in an opposite manner from the famous Phillips relation that makes regular SNe Ia cosmological candles [10].

Keywords: Supernovae, Type Iax supernovae, White dwarf stars

SN 2024vjm was discovered on 2024 September 13 at 23:59:05 UTC (MJD = 60567.00) by the BlackGEM (BG) Local Transient Survey (LTS;[11]). The supernova (SN) exploded within a spiral arm in the outskirts of the nearby NGC 6744 galaxy (distance 9.39 ± 0.43 Mpc, Fig 1b; Methods 2.1), north-west of its centre, at right ascension $\alpha = 19^{\text{hr}}09^{\text{m}}25^{\text{s}}.79$ and declination $\delta = -63^{\circ}50'01''.77$ (J2000). A classification spectrum was taken on 2024 September 15 at 00:40:56 UTC [12], revealing a plethora of narrow ($v \sim 3000 \text{ km s}^{-1}$) absorption lines, including low mass elements (LME) such as C II, O I, intermediate mass elements (IME) such as S II, Si II, Mg II and Ca II and iron group elements (IGE), namely Fe II. The SN was subsequently classified as a Type Iax SN [13] based on its spectral similarity to other faint (reaching peak *B*-band absolute magnitude of $M_B > -15$) SNe Iax 2008ha [7, 14], 2010ae [15], and 2019gsc [16, 17]. Following discovery, we initiated a multiwavelength follow-up campaign to study the SN (Methods 2.3 – 2.4), as well as an archival search for pre-explosion imaging of the explosion site. SN 2024vjm reached peak in *B*-band brightness on MJD = 60572.18, which we use as a reference time (Methods 2.3).

The host galaxy NGC 6744 was serendipitously observed by the *Euclid* space mission [18] as part of an Early Release Observations (ERO) program [19, 20] on 2023 October 4 [21], a mere 11 months before the discovery of SN 2024vjm. This presented the opportunity to study the SN explosion site, shown in Figure 1c, in search of its progenitor system. To detect or constrain such progenitor systems, we determine the location of the explosion site in the *Euclid* pre-explosion image to within 10 milliarcseconds (mas), less than a single *Euclid* VIS-band (500–900 nm) pixel ($0.1''$), using astrometry derived by averaging multiple ground-based seeing-limited images taken by BlackGEM (Methods 2.2). Inspecting the *Euclid* VIS-band image, we find no point source in the SN explosion site pixel. The nearest source detected by the *Euclid* source identification pipeline in the vicinity of the explosion site is at a separation of $0.12''$, exceeding our astrometric accuracy and corresponding to an offset of at least 5.5 pc in the host itself (Methods 2.2). We refer to this source as S1 for clarity. S1 is classified as an extended source, implying that it is inconsistent with the light from a single point source, and originates from diffuse stellar or nebular emission (Methods 2.2). S1 is therefore not the SN progenitor, however its light distribution extends into the location of SN 2024vjm. To place a limit on a possible progenitor at the SN location we measure the brightness of a point source at the SN location, assuming all the light included in the *Euclid* Point Spread Function (PSF) centred on this location

originates from such a putative progenitor rather than S1 (Methods 2.2). We find such a point source would have a brightness of $m_{\text{VIS}} = 26.6 \pm 0.16$ mag, corresponding to an extinction corrected absolute magnitude of $M_{\text{VIS}} = -3.84 \pm 0.19$ mag. However, since diffuse light from S1 must contribute to the light within the PSF, any progenitor system is likely fainter and this brightness limit is a conservative upper limit.

From the limit set by the *Euclid* image (Fig. 2), we find that the progenitor system of SN 2024vjm must have been fainter than previously proposed progenitor systems of SNe Iax (Methods 2.2). Specifically, the SN 2024vjm system was fainter than the luminous blue star coincident with bright Iax SN SN 2012Z [4], suggested to be the He giant companion to the supernova and which may still be visible in deep observations today [22]. The progenitor system of SN 2024vjm is also fainter than the luminous red companion or remnant of the faint SN 2008ha [9], and the Helium (He) star companion of the Galactic He-Nova V445 Pup [23] as well as the limits placed by the SN 2014dt progenitor search [24]. Our work therefore shows, for the first time, that not all SNe Iax progenitor systems contain a luminous source.

We further compare the *Euclid* VIS-band brightness limit to theoretical stellar evolution models calculated using the BPASS binary stellar evolution code [25, 26]. Based on deep observations of the SN 2024vjm immediate environment using the Multi Unit Spectroscopic Explorer [27] (MUSE), we chose sets of models with a solar abundance of metals (Methods 2.1). We use both single star models that simulate the evolution of typical hydrogen-rich stars, as well as binary models leading to stripped stars devoid of hydrogen (H), through Roche-lobe overflow. Comparison to stripped stars is motivated both as massive star progenitors [8], as well as mass-donor companion He-stars to a WD progenitor, similar to the SN 2012Z progenitor candidate and suggested by theoretical works [5, 28]. Finally, we also compare known Wolf-Rayet (WR) stars [29] and hot sub-dwarf (SdB)-WD systems (Methods 2.2) observed in our own galaxy to the brightness limit. The Hertzsprung–Russell (H-R) diagram presented in Figure 2 compares our limits to these systems and the calculated stellar tracks.

Most calculated stellar evolution tracks exceed the luminosity limit and are ruled out. These systems include massive H-rich stars, massive He-star channels (analogous to the SN 2012Z progenitor candidate), the majority (34 of 48) of WR stars, and the terminal luminosities calculated for most (81%) massive stripped star progenitor system models. We note that while these massive systems are intrinsically luminous, their spectral energy distributions (SED) peak in the blue, resulting in fainter emission in the redder *Euclid*-VIS band. Therefore, the effect of dust, while obscuring such sources, would also reprocess emission to the redder bands, mitigating its effect on detectability. Although a subset of massive star systems could evade detection, we find that the absence of other luminous point sources in the vicinity of the explosion site implies a population age inconsistent with the short lifetimes of such progenitors. We therefore consider a massive-star progenitor for SN 2024vjm unlikely.

Possible progenitor channels for SN 2024vjm that are left unexcluded are WD systems with faint companions such as low-mass main-sequence or He-star companions, as well as double degenerate systems consisting of just WD stars. Specifically, known binary Galactic hot sdB-WD systems are much fainter than our limit. These systems have been proposed to lead to faint thermonuclear explosions [30–33] and are therefore

interesting candidates for a progenitor system. Regardless, as the permitted companions are not expected to explode as SNe themselves, SN 2024vjm is likely the result of a thermonuclear explosion of a WD star.

The thermonuclear nature of SN 2024vjm is further confirmed by the shape of its light curve and spectral features, as shown in Figure 3. Thermonuclear SNe (i.e. Ia SNe) are powered by the decay of radioactive nickel, the ^{56}Ni isotope [34, 35], through the deposition of energy by γ -rays and positrons into the ejecta. Using the multi-band lightcurve of SN 2024vjm, we calculate its bolometric lightcurve (Methods 2.3) from B-band to the near-infrared (NIR), until SN 2024vjm fades in B-band beyond detection ~ 50.7 days after its B-band peak. We then compare its luminosity, normalised by its time-integration to that of ^{56}Ni deposition normalised in the same manner, a method known as the Katz integral [36] (Methods 2.5). This method requires fitting only one parameter - the γ -ray escape time, t_0 , after which γ -ray energy deposition becomes inefficient as the ejecta become optically thin. We find the lightcurve strictly adheres to the energy conservation expected from ^{56}Ni decay, indicating that ^{56}Ni is sufficient to explain the lightcurve. Our data do not require any additional power source.

SN 2024vjm reached a B-band peak magnitude of $M_B = -12.7 \pm 0.1$, when accounting for extinction (Methods 2.4), making it the faintest SN observed to date, with the possible exception of SN 2021fcg [37] for which no colour information is available and dust extinction correction is unreliable. The faintness of SN 2024vjm indicates that only a small amount of ^{56}Ni was synthesised by the explosion. To measure this nickel mass, we further fit a ^{56}Ni deposition curve directly to the late-time bolometric curve (the nickel tail; Methods 2.5). We find good agreement between the best-fit t_0 value determined using this method and the values previously inferred from the Katz integral, and measure a ^{56}Ni mass of $3.6 \times 10^{-3} M_\odot$. This value is similar to that derived for other faint SNe Iax [14, 15, 37], and is two orders of magnitude lower than regular SN Ia ^{56}Ni yields [38].

While the low nickel yield is expected in a low-energy explosion, the bolometric analysis reveals an unexpectedly long timescale for γ -ray trapping in the SN ejecta. Both the tail fit and the Katz integral method yield a γ -ray escape time of 70–80 days (Methods 2.5), meaning the ejecta remained optically thick to γ -rays post-explosion. This value is significantly longer than for regular type Ia SNe where the γ -ray escape time is typically $t_0 \approx 30 - 45$ days [39, 40] and larger ^{56}Ni yields are correlated with longer γ -ray escape times.

As shown in Figure 4, SN 2024vjm breaks this trend as its low ^{56}Ni ejecta remained optically thick to γ -rays for a long duration after explosion. Observationally, this causes the lightcurve of SN 2024vjm to fade more slowly than its peak brightness would suggest (Methods 2.3). The initial decline rate of Type Ia SNe is parameterised by ΔM_{15} – the drop in magnitudes 15 days after peak. Regular Type Ia SNe follow the Phillips relation [10] whereby fainter events fade more quickly (larger ΔM_{15}). While SNe Iax do not follow this exact relation due to their heterogeneous nature, bright SNe Iax still typically follow a trend where fainter SNe fade more quickly [41]. However, SN 2024vjm reverses this behavior entirely. Compared to other well-observed faint SNe Iax, it fades significantly more slowly (smaller ΔM_{15} in all optical bands; Methods 2.3). As SN 2024vjm is fainter than other SNe Iax, its slow decline robustly confirms

the hypothesis by ref. [41] that faint Iax SNe follow a trend opposite to the Phillips relation.

We identify the cause for the “faint-yet-slow” evolution of SN 2024vjm as the inability of the low-energy explosion to rapidly expand its ejecta (Methods 2.5), keeping the ejecta optically thick to γ -rays. The γ -ray escape time of Type Ia SNe ejecta is governed by the average ejecta column density (Σ) [42], which scales as $\Sigma \propto M_{ej} v^{-2}$, where M_{ej} is the ejecta mass and v is the ejecta expansion velocity. The NIR and optical spectra of SN 2024vjm reveal that most features expand in an exceptionally low velocity (Methods 2.4), ranging from $v \approx 3000 \text{ km s}^{-1}$ measured in the earliest spectroscopic epoch to $v < 1000 \text{ km s}^{-1}$ 20 days post B-band peak brightness. Of particular interest are the distinct Co II features in the NIR spectra of SN 2024vjm, since ^{56}Co is the product of ^{56}Ni . The slow expansion velocity of these Co II features therefore demonstrates that the radioactive products themselves are moving slowly. This slow evolution is also consistent with that of Ni II in the mid-infrared spectrum of SN 2024vjm taken with the *James Webb Space Telescope (JWST)* [43].

While other faint SNe Iax have also shown low-velocity expansion, the low ejecta mass characterizing faint SNe Iax [44] can compensate for the effect of their slow ejecta expansion on γ -ray trapping. With a slow expansion velocity and a large t_0 we find that the ejecta mass of SN 2024vjm must be of order $M_{ej} \approx 0.1 M_{\odot}$. To confirm this by an independent measurement, we apply a scaling relation between the luminosity rise time, sensitive to the photon diffusion time through the ejecta, and the ejecta mass [14]. The measured rise-time of ~ 11 days indicates an ejecta mass of $M_{ej} \approx 0.1 M_{\odot}$, confirming the low ejecta mass does not compensate for the low expansion velocity in determining the slow evolution of SN 2024vjm.

Our constraints on the ejecta mass provide a strong confirmation to previous suggestions regarding the existence of surviving bound remnants left behind Iax SN explosions due to their ejecta-mass budget [44], as well as very late-time luminosity excess [45, 46]. Our evidence for a WD progenitor system confirms that SN 2024vjm must have left behind a gravitationally bound remnant, as even the lowest mass WD systems [47] have more mass than the estimated ejecta mass produced by SN 2024vjm. Despite this, we find that the late-time lightcurve of SN 2024vjm shows no additional excess luminosity beyond that expected from a single thermonuclear explosion, and follows its expected decay rate (Methods 2.5). This suggests that, in contrast to brighter members of the class, where a surviving remnant may contribute additional luminosity via secondary ejecta or disruption of the remnant [45], the remnant of SN 2024vjm did not contribute significant energy to its light curve. We further find the optical late-time lightcurve to be very red at ~ 200 days post peak (Methods 2.5), possibly due to dust formation, which Iax SNe have been suggested to efficiently produce [48]. The SED shifts even more to the red in later epochs (~ 350 days), reminiscent of dust accumulation. Deep infrared studies of SN 2024vjm with space telescopes such as *JWST* would better probe dust formation and possible later signatures from the bound remnant.

Faint SNe Iax occupy the very faint end of the SN population as a whole. Our work provides a strong indication that the progenitor systems of these faintest known SNe are themselves also faint and likely composed of low-mass binary systems. The

advent of deep wide-field surveys such as BlackGEM and, in particular, the Rubin Observatory’s Legacy Survey of Space and Time (LSST) [49], could put this suggestion to a strong test, providing deep multicolour observations of the sites of similar future events. When combined with deep, wide-field space surveys such as *Euclid* and the future Nancy Grace Roman Space Telescope [50], the progenitor systems of such events, and those of brighter SNe, will be directly constrained. SN 2024vjm provides unprecedented high-quality observations of an event within a previously unexplored regime of very faint Type Iax explosions, placing strict new constraints on the allowed progenitor systems and demonstrating that such objects follow different physical correlations compared to both brighter SNe Iax and normal SNe Ia.

1 Figures

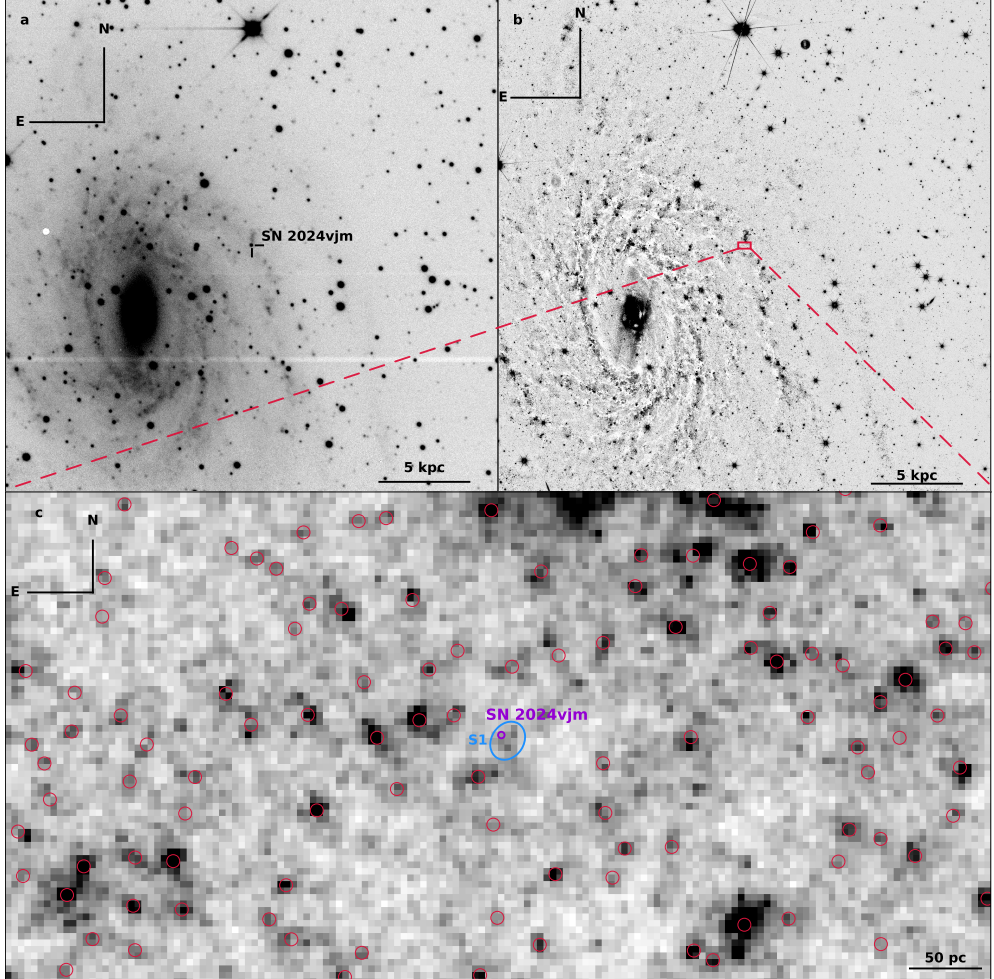


Fig. 1: No bright stars at the location of SN 2024vjm. **a**, post explosion q-band BG image of SN 2024vjm. SN 2024vjm is clearly seen at a spiral arm in the north-west of NGC 6744 (marked by a crosshair) **b**, the pre-explosion *Euclid* VIS-band image of NGC 6744 with the nearest 10'' to the explosion site marked with a red rectangle. **c**, A zoom in on the 7.5'' by 15'' around the explosion site. The tip of the large star-forming region to the north of the explosion site is visible in the cutout. The astrometric location of SN 2024vjm is marked in a 0.1'' diameter circle (purple) corresponding to a single *Euclid* pixel. Sources identified by the *Euclid* pipeline are marked with 0.2'' diameter circles (red). S1, the nearest extended source to the location of SN 2024vjm, is marked in a cyan ellipse marking its extent. SN 2024vjm lies just north of S1's centre and is unlikely to be physically associated with the source.

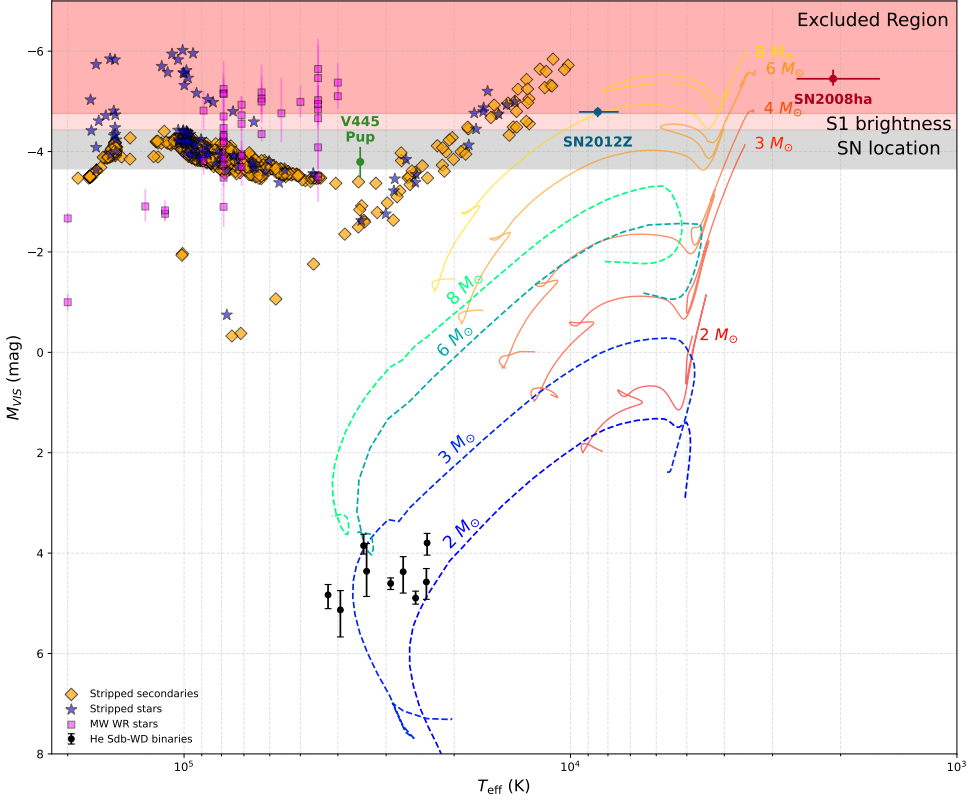


Fig. 2: The progenitor system of SN 2024vjm is fainter than previous Iax progenitor candidates. A Hertzsprung–Russell diagram showing the *Euclid*–VIS band brightness vs temperature. Two sets of BPASS stellar tracks are plotted; single-star H-rich (yellow-red shades) and stripped He tracks (green-blue). The terminal position of massive stripped BPASS tracks is also plotted with blue stars (for primary stars) and orange diamonds (secondary stars). The region occupied by the brightness of S1 is marked in translucent red, and the region occupied by the brightness at the SN location itself is marked in translucent grey. We note that the latter is likely contaminated by S1, and is therefore a strict upper limit of a possible progenitor brightness. We mark the region brighter than both with a darker shade of red. The progenitor system of SN 2024vjm is fainter than the inferred companion of SN 2012Z (blue circle), as well as the possible remnant of SN 2008ha (red circle), and also from that of galactic He Nova V445 Pup (green circle). Known Galactic WR stars [29] (pink squares) are mostly excluded, though some are slightly fainter than the limit. Low-mass hot subdwarf-WD binary systems (black; Methods 2.2) lie well within the permitted brightness range. Such faint systems are possible progenitor systems for faint SNe Iax. Error bars represent 1σ uncertainties.

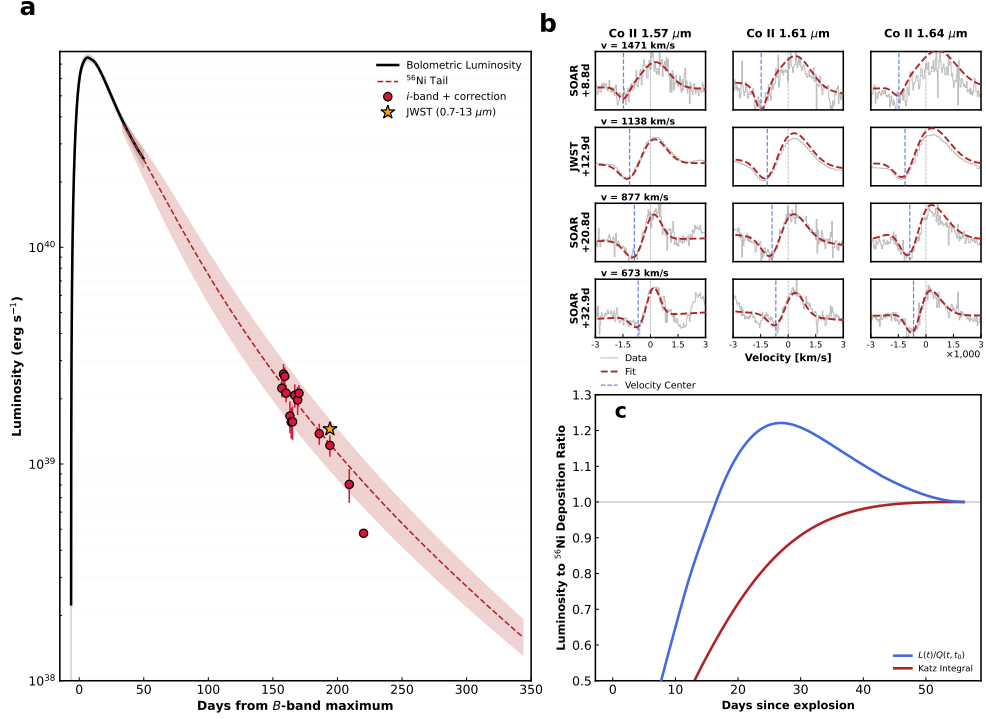


Fig. 3: Thermonuclear Diagnostics and Ejecta Evolution of SN 2024vjm. **a.** Bolometric light curve and radioactive model. The bolometric luminosity evolution of SN 2024vjm (black solid line, grey region shows the 1σ uncertainties) calculated from multi-band photometry covering the B -band through NIR bands. The late light curve is consistent with ^{56}Ni power (red dashed line). The total flux derived from a +194 days *JWST* spectrum (yellow star; Methods 2.5) agrees with the flux expected from a single ^{56}Ni decay curve. Late-time i -band detections (red circles with 1σ errors), follow the trend of ^{56}Ni decay, confirming that the supernova is consistent with a single radioactive deposition curve up to at least $t \approx 200$ days. We apply a single bolometric correction to the i -band measurements to highlight they follow the ^{56}Ni trend. As the SED shifts to the red, this correction no longer applies. **b.** NIR Co II evolution. Sequence of multi-epoch near-infrared spectra (gray steps) centred on the Co II triplet ($\lambda\lambda 1.57, 1.61, 1.64 \mu\text{m}$). The Co II features trace ^{56}Ni decay as ^{56}Co is its product. A model (red dashed lines) is fit to the Co lines, tracking their development. Blue vertical dashed lines mark the photospheric velocity (v) for each epoch, decreasing from $\sim 1,500 \text{ km s}^{-1}$ to $\sim 670 \text{ km s}^{-1}$. These exceptionally low velocities show the low-energy explosion failed to rapidly expand the ejecta, producing a slow declining lightcurve. **c.** Katz Integral Energy Deposition Curve. The ratio between the bolometric luminosity (L), and the radioactive ^{56}Ni deposition (Q ; blue line), as well as the time-integrated ratio of the two (the Katz integral; red line). Both values converge to unity, suggesting no energy source other than ^{56}Ni decay is needed, with a long γ -ray escape time ($t_0 \approx 70\text{--}80$ days).

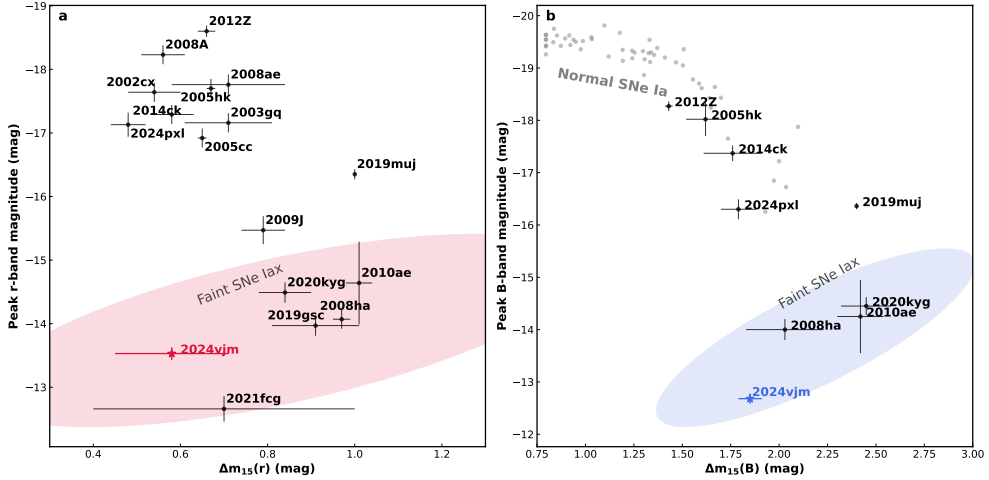


Fig. 4: Peak absolute magnitude versus 15-day magnitude decline for SN 2024vjm. **a.** Absolute peak r -band magnitude (M_r) versus the 15-day decline rate ($\Delta M_{15}(r)$). **b.** Absolute peak B -band magnitude (M_B) versus $\Delta M_{15}(B)$. In both panels, SN 2024vjm is denoted by a coloured star, while comparison Type SNe Iax are shown as black circles. The shaded regions highlight other particularly faint SNe Iax. Panel **b** also shows regular Type Ia supernovae from the Carnegie Supernova Project [51] (gray points), that follow the famous Phillips relation, whereby fainter events fade faster than bright ones. SN 2024vjm however fades slower than brighter Iax events, due to its low velocity ejecta. The physics responsible for the decline trend of the Phillips relation holds, perhaps, for bright SNe Iax, but not for the faintest events like SN 2024vjm. Error bars represent 1σ uncertainties.

2 Methods

2.1 The environment of SN 2024vjm

2.1.1 The host galaxy

We adopt a distance of 9.39 ± 0.43 Mpc to NGC 6744, derived by tip of the red giant branch analysis of the PHANGS-HST survey [52]. This corresponds to a distance modulus of 29.86 ± 0.1 . For the redshift, we adopt the value of $z = 0.0028$ reported by NED. This value matches the SN spectral features and the host's interstellar Na I D doublet observed in the SN spectra.

2.1.2 Extinction

We adopt the Galactic foreground extinction from NASA Extragalactic Database (NED) [53] of $E(B - V) = 0.043$ mag based on ref. [54] and recalibrated by ref. [55]. To measure the host galaxy extinction, we use the relations from [56] between the sum equivalent width (EW) of the Na I D doublet and $E(B - V)$ reddening. To measure the EW of the lines we use the -2.1 days X-shooter spectrum being the highest resolution spectrum in our dataset. We first remove the continuum by fitting a 3rd degree polynomial to the area around the Na I D doublet. We then directly measure the EW of each line in the spectrum by integrating the area up to 2 \AA around the line. We measure $EW(D1) = 0.47 \text{ \AA}$ and $EW(D2) = 0.52 \text{ \AA}$ corresponding to an extinction value of $E(B - V) = 0.21$ mag.

2.1.3 Immediate environment and metallicity

To study the immediate environment of SN 2024vjm, we obtained a single epoch of observations with the Multi Unit Spectroscopic Explorer (MUSE) [27] instrument mounted on the Very Large Telescope (VLT) in the ESO Paranal observatory through a director's discretionary time (DDT) program 114.28GZ (PI Zimmerman). The observations were conducted using the instrument's Narrow Field Mode (NFM) utilizing Adaptive Optics (AO) [57, 58]. This mode allows observation with a spaxel resolution as small as 25 mas, meaning that at the distance of NGC 6744 each spaxel represents just 1 pc upon the host. Since no bright star exists within the narrow $7.5''$ field of view, we used SN 2024vjm itself as a tip-tilt star for the AO guiding. Further details on the reduction process are described in the supplementary material section 4.4.

SN 2024vjm exploded within a spiral arm in the outskirts of NGC 6744 northwest of its centre. The $\text{H}\alpha$ MUSE slice, presented in Extended Data Figure 1, shows that SN 2024vjm lies approximately 90 pc south of the edge of a large star formation region, suggesting recent star formation in the vicinity of the SN site. A second, more diffuse star-forming region lies approximately 165 pc southwest of SN 2024vjm, as well as diffuse star-formation directly west of SN 2024vjm. This suggests that while the explosion site does not lie in a region with ongoing star formation, it is surrounded by star-forming regions and therefore a young stellar population. This is in line with the explosion sites of other SNe Iax, which are often found near star formation in their host galaxies [59].

We further analyze the strong emission lines in the star-forming region to the north. To gather enough signal for this analysis, we sum the contribution of a 70 spaxel circle capturing the star-forming region to the north of SN 2024vjm. We find that many emission lines are well detected in the summed spectrum including $H\alpha$, $H\beta$, [O III] $\lambda\lambda 5008$, [N II] $\lambda\lambda 6548, 6583$ and [Si II] $\lambda\lambda 6716, 6730$. We then measure the flux of each line by fitting a Gaussian to each emission line and integrating the total emission as set by the best-fit Gaussian. We present the result of this measurement in *Supplementary Material Table 2*. We attempted to make the same measurement around the more distant south-west star-forming region; however, the signal for this region was low, and many lines were not well detected.

We use the measured fluxes to assess the metallicity of the star-forming region using the O3N2 metallicity indicator, and adopting the calibration of [60]. We find the oxygen abundance to be $12 + \log(\text{O/H}) = 8.73 \pm 0.09$ dex. Compared to the solar composition [61], this indicates a metallicity of $\frac{[\text{Fe}/\text{H}]}{[\text{Fe}/\text{H}]_{\odot}} = 1.09^{+0.25}_{-0.20}$. We therefore conclude the immediate environment of SN 2024vjm is consistent with a solar abundance of metals.

SNe Iax have been found in solar abundance environments in the past [62, 63]. In particular, they have been shown to follow a similar metallicity distribution as core-collapse SNe [59]. However, the metallicity measurement around SN 2024vjm is in contradiction with the hypothesis raised by ref. [16], that faint SNe Iax explode in more metal-poor environments. This was based on their measurement of sub-solar metallicity at the host of SN 2019gsc and the slightly sub-solar environment measurements of SN 2008ha [14] and SN 2010ae [15]. Regardless, all faint Type Iax explosion sites are found near star-forming regions and hence younger stellar populations.

2.1.4 Radio

We obtained a single epoch of radio continuum follow-up observations with the MeerKAT radio telescope [64] in the L-band (900–1670 MHz) and S4-band (2625–3500 MHz) through DDT proposal DDT-20240920-SD-01 (PI de Wet). The total integration time on source was one hour each for the L and S4-band observations, with J1939-6342 used as the flux, bandpass and gain calibrator. The mid-times of the S4-band and L-band observations were 18:26 and 20:17 UT on 2024 September 21. Inspecting the SARA0 Science Data Processor (SDP) images, we do not detect a radio source at the position of SN 2024vjm. The median RMS noise was 17 and 11 μJy in the L and S-band images from which we derive 3σ upper limits of 51 and 33 μJy , respectively, on any radio emission. This corresponds to luminosity limits of 4.9 and $7.6 \times 10^{33} \text{ erg s}^{-1}$ in the L and S-band respectively.

2.2 Search for progenitor system

We conducted an archival data search for deep pre-explosion images of SN 2024vjm's location. While the host NGC 6744 was observed in the past by *HST*, we found the SN location within the galaxy has not been previously observed. However, NGC 6744 was observed by the *Euclid* space mission [18] as part of their Early Release Observations

(ERO) program [19, 20]. Owing to the mission’s large field of view, the entire galaxy was visible, including the SN location.

2.2.1 Precision Astrometry

It is common to achieve precise astrometry using another space-based or adaptive optics imaging. However, here we present a careful astrometric analysis of the seeing-limited BlackGEM (BG) images. To improve upon the astrometric solution derived by the standard BG pipeline for single images, we derived a joint astrometric solution based on 234 q -band images and 54 i -band images. The solution was calculated using the *AstroPack/MAATv2* tools[65–67] developed for the Large Array Survey Telescope (LAST) [68, 69] and the ULTRASAT space mission [70]. The astrometry was conducted with respect to the GAIA-DR3 catalog [71, 72], considering the sources’ proper motion and parallax.

For each BG image, a section of 1001×1001 pixels was cropped around the approximate SN position. Next, we searched for sources, measured their positions via PSF-fitting, and solved the astrometry for each image. The astrometry based on Gaia DR3 was solved for each field, including distortions represented by third-order polynomials. This is enough to represent differential atmospheric refraction to better than 1 milliarcsecond (mas). The typical asymptotic rms (i.e., the terms of the astrometric solution at the bright end of $\lesssim 18$ mag) was about 15 mas. Next, we matched the sources over all images by coordinates. For each source, we calculated its median position and its standard deviation (std) across all images obtained with a specific filter. The median astrometric position of identified Gaia sources in i -band is presented in Extended Data Figure 2, showing the improvement in astrometric noise by binning multiple images. At the bright end, the typical rms per image is about 10 mas, and can reach at least 3 mas by binning a large number of observations. However, this method does not consider chromatic aberrations (in the atmosphere or telescope). Therefore, we adopted the median i -band position (which is less affected by chromatic effects) as the final SN position. The difference between the median i -band and q -band position of the SN was less than 9 mas (in each axis), while the robust std of the i -band measurements was about 20 mas (in each axis). However, since this is larger than the possible systematic effect (e.g., chromatic), we adopted a 10 mas error in each axis. The adopted positions are: $\alpha = 19^{\text{hr}}09^{\text{m}}25^{\text{s}}.7876$ and $\delta = -63^{\circ}50'01''.7718$

2.2.2 Brightness limits from *Euclid*

To search for a progenitor candidate in the *Euclid* data we analyze the VIS-band image, since it has a smaller pixel size of just $0.01''$ instead of $0.02''$ in the Y, J and H bands and typically goes 1.5 mag deeper [21]. The astrometric accuracy of *Euclid* ERO has been shown to be better than 10 mas [21] in the VIS band, thus the SN location can be associated with a single pixel within the *Euclid* VIS image.

Euclid employs multiple source detection algorithms to identify astrophysical objects in its imaging data [21]. S1, along with other sources marked in Figure 1, were identified by the **SExtractor** [73] catalog distributed in the *Euclid* ERO. We note that other elongated sources are not detected in the catalog and that S1 itself is flagged as an elongated source with a **CLASS_STAR** value of 0.09. This suggests that S1

is the result of the congregation of multiple stellar systems or diffuse star formation too faint to be detected in our MUSE data. The total brightness of S1 as determined by a Kron-like automated aperture magnitude (`MAG_AUTO`) is $m_{VIS} = 25.83 \pm 0.13$ mag. Since SN 2024vjm lies within the extent of S1, its location is likely contaminated by its light. Therefore, to obtain an upper limit to the brightness of a possible progenitor system we perform a forced PSF-photometry measurement at the SN location. We use the PSF shape distributed as part of the ERO, the *Euclid* pipeline weights file for the background error-estimation, and the gain and zeropoint values from the image header, consistent with the values for NGC 6744 in the *Euclid* ERO pipeline paper [21]. We perform the PSF photometry using the `PSFPhotometry` function in the `Photutils` Python package [74]. To verify our custom pipeline we compare our measurement to that of all point sources (`CLASS_STAR > 0.8`) within $20''$ of the SN location in the *Euclid* catalogue. We find a mean offset of 0.06 mag between our measurement and that of the catalogue `MAG_PSF` values, confirming its accuracy. We then measure a brightness of $m_{VIS} = 26.58 \pm 0.16$ mag at the SN location, which can be used as a strict upper limit to any progenitor system, if it were not contaminated by S1.

We compared the VIS magnitude limits to theoretical BPASS models of binary stellar evolution. Specifically, we use the v2.2.1 set of stellar tracks [25, 26] with a solar abundance of metals ($Z = 0.014$). To probe hot sdB progenitor companion star channels, we chose to plot the full tracks of a subset of low ($< 8 M_{\odot}$) mass stripped stars according to the following criteria: (a) The stars are secondary stars, (b) The primary has turned into a $\sim 1 M_{\odot}$ WD, (c) They have no surface hydrogen. For the rest of the stripped stars, we only plot their end-state to probe them as direct progenitors, rather than binary companions. We calculate the *Euclid*-VIS band magnitude for each track by estimating the SED from the calculated standard filter brightness provided in the BPASS code. We then calculate the *Euclid*-VIS absolute magnitude by running synthetic photometry on the SED using the *Euclid*-VIS band transmission function. We also plot the full evolutionary tracks for a subset of single-star models ($> 8 M_{\odot}$) in Figure 2.

For the SN 2012Z [15] and SN 2008ha [9] systems, we calculate the perceived *Euclid*-VIS magnitudes by fitting a blackbody to the corresponding *HST* detections and deriving their synthetic photometry in the *Euclid* VIS-band. For the V445 Pup companion [23, 75], we assume a blackbody at a temperature of 35 kK. Assuming a colder temperature pushes the companion further into the excluded region, as the SED becomes redder. Figure 2 also shows WR stars from ref. [29], for which we apply a V-band to VIS-band correction, which corrects the underlying blackbody SED instead. This is to avoid excluding additional flux from V-band emission lines that can contribute substantial flux in WR stars. Since this method does not take into account corrections from red emission lines, it may be underestimating the stars' brightness. We also plot several known Milky Way subdwarf(SD)-WD binary systems: CD -30 11223[76], PTF J0823 [77], OW J0741 [78], ZTF J2130 [79], ZTF J2055 [80], HD 265435 [81], PTF J2238 [82], LAMOST J1710 [83] and ZTF J0007 [84], for which we also calculate synthetic VIS-band photometry assuming their SED is a blackbody. These stars are located next to corresponding BPASS binary stellar tracks. Specifically, Both

CD -30 11223 and PTF J2238 were found in young stellar population, similar to the environments of type Iax SNe.

2.3 Photometry

2.3.1 Light curve properties

Following discovery, we initiated a photometric campaign to obtain a pan-chromatic lightcurve. We present the bolometric light curve of SN 2024vjm in Extended Data Figure 3. To measure the light curve properties of SN 2024vjm, we interpolate our extinction-corrected multi-band light curve using a custom Gaussian process (GP) fitter based on the `sklearn` [85] Python Package. We present further details on this interpolation in the supplementary material section 4.2. This method resulted in a stable interpolation, which phenomenologically follows the band curves, and allows us to measure the time of maximum light, maximum brightness, and decline rate (ΔM_{15}) for each band. We omit the u -band from this calculation as it is not well sampled, due to the low u -band brightness of SN 2024vjm. We present the measured lightcurve properties in Extended Data Table 1.

Using the interpolated multi-band light curve, we measure the bolometric luminosity of SN 2024vjm by directly integrating it, achieving an almost complete bolometric curve (as SN 2024vjm is not blue and we cover B -band to K -band). Figure 3 panel a shows the bolometric light curve.

With a peak magnitude of $M_B = -12.68 \pm 0.1$, SN 2024vjm is arguably the faintest supernova observed to date. The Type Iax SN 2021fcg [37] may be fainter; however, that event was not well-observed and suffers from high extinction uncertainty. SN 2024vjm occupies a luminosity regime similar to Gap Transients [86]. Notably, ILOT M85 OT2006-1 [87], commonly considered a stellar merger, has also been proposed as a core-collapse SN [88]. Such a scenario would make M85 OT2006-1 a fainter candidate than SN 2024vjm. M85 OT2006-1 is, however, physically different from faint SNe Iax, occurring in an S0 galaxy (rather than the star-forming hosts of SNe Iax) and showing a plateau light curve inconsistent with a thermonuclear explosion.

2.3.2 Explosion time estimate

To estimate the explosion time, we fit a broken power law $f(t) = a \times (t - t_{exp})^n$ to the early q -band light curve. We chose the q -band since it has the earliest data points, as well as a single pre-detection measurement retrieved by the BG forced photometry pipeline. We use both the q -band data from BG and MeerLICHT. Since MeerLICHT has observed SN 2024vjm with a higher cadence, we bin the data points to improve the measurement. Our fit returns an explosion time of $MJD = 60565.58 \pm 0.31$, 6.6 days before B -band maximum with a power law index of $n = 0.91 \pm 0.13$. This result is consistent with those ref. [89], which are based on the GOTO lightcurve.

2.3.3 Slow photometric decline

Figure 4 shows the peak brightness of SN 2024vjm and other SNe Iax [15, 16, 37, 41, 44, 90–93] in absolute peak magnitudes vs its ΔM_{15} value in r-band and B-band.

When compared to other faint SNe Iax we find that SN 2024vjm declines quite slowly 15 days post peak. This effect would be in line with the unusually high t_0 parameter we measure for SN 2024vjm as a slow decline implies a more opaque ejecta.

With the addition of SN 2024vjm, we find two distinct groups of SNe Iax in the absolute magnitude vs decline rate graph. Namely, while bright SNe Iax ($M_r \lesssim -15$) decline more slowly with brightness, the faint group of SNe Iax ($M_r \gtrsim -15$) declines faster the brighter the SN is. This was proposed before [41, 94], though with a marginal statistical significance. With SN 2024vjm being possibly the faintest of this group, it probes a new part of this parameter space, strengthening this correlation (with a linear Pearson correlation coefficient of -0.81 and a p -value of 0.052 , i.e. a $\sim 2\sigma$ correlation).

2.4 Spectroscopy

After classification, we obtained a sequence of 20 additional optical spectra and three near-infrared (NIR) spectra. Optical spectra are presented in Extended Data Figure 4 and the NIR spectra are presented in Extended Data Figure 5.

2.4.1 Spectral Evolution

Our spectral series ranges from -4.22 days to 70.8 days before and after the B -band maximum. SN 2024vjm showed spectroscopic similarity to other faint SNe Iax, sharing most, if not all, spectral features, albeit with lower expansion velocities. A comparison between the spectra of SN 2024vjm and two other faint SNe Iax is shown in Extended Data Figure 6.

The first classification spectrum shows a plethora of narrow absorption lines. Notably, we identify strong low mass elements (LME) and IME such as C II, O I, Mg II, Si II, S II and strong Ca II NIR triplet with P Cygni profiles. From the IGE, we identify relatively few Fe II transitions, while we find no strong evidence for more highly ionized IGEs, such as Fe III. In the NIR, this is even more striking before peak, with only two features identified in the pre-peak X-shooter spectrum being Mg II $\lambda 10927$ in J -band and a weak Fe II $\lambda 16907$ emission line in the H -band. Weak signs of Co II may be present as well; however, it is hard to positively identify them.

After peak, we find more IGE lines developing, as the number of overall lines increases significantly. We find many of those lines to be consistent with Fe II, Cr II, Co II and Ti II. A comprehensive study of a $+12$ days *JWST* IR spectrum, including comprehensive line identification was conducted by ref. [43].

In the NIR, the appearance of Co II lines after peak is striking, as they dominate the H and K bands with distinct P Cygni profiles. We also identify other IGE developing in the J band (for detailed NIR line identification, refer to ref. [43]). The least blended set of Co II transitions (not significantly overlapping with Fe lines) are the 15759, 16064 and 16361 \AA transitions. These lines are usually blended in regular Type Ia SNe, though the low velocity regime of fainter SNe Iax makes these features separate (as seen in the NIR spectra of e.g. SN 2024pxl, [43, 93, 95], SN 2019muj, [92], and SN 2010ae, [15]). The appearance of Co II lines only after peak is intriguing. Our first NIR spectrum was taken about four days after the explosion; therefore, not even half of the Co abundance has been synthesised at the time, as the half-life of ^{56}Ni is

~ 6 days. This later appearance is also consistent with the other faint SNe Iax [15]. Although forbidden Co III is detected in the NIR *JWST* spectrum[43], the lack of permitted Fe III lines in the early spectrum suggests that IGE are not highly ionized in the optically thick ejecta. Therefore, the lack of any Co II lines in the early NIR spectrum is likely the result of optical depth, rather than early abundance, which is suggested by our photometric measurements of optically thick ejecta. The appearance of the Co II lines in the photosphere is somewhat at odds with the slow lightcurve evolution set by the long γ -ray escape time. However, if the ejecta is well-mixed as suggested by the full IR spectrum [43], and as has been suggested for other SNe Iax [46], then ^{56}Ni products should be found in both the outer and inner ejecta, allowing the long γ -ray trapping. We also note that Fe II $\lambda 16907$ is slowly evolving in the NIR spectral series, possibly as a result of ^{56}Co Decay, which would further suggest these Co features are the product of ^{56}Ni decay.

By day +13.83 after *B*-band maximum, the Ca II NIR triplet becomes stronger in emission than absorption, and by day +25.51 we identify forbidden [Ca II] $\lambda\lambda 7291, 7323$. Such an early appearance of forbidden Ca has been seen in SN 2008ha [7, 14], though the feature appears even earlier in SN 2024vjm.

2.4.2 Line Velocities

In Extended Data Figure 7 we show the measured photospheric velocity v_{phot} of several prominent spectral lines. To measure this, we fit an appropriate phenomenological function to each line profile. The results of these fits are shown in Extended Data Figure 8. For C II $\lambda 6578$, Si II $\lambda 6355$, and Fe II $\lambda 5169, \lambda 6257$, we fit a simple negative Gaussian to the line absorption. The reason we chose a simple function is that these lines blend with other lines at later epochs, so complex functions failed to reproduce reliable measurements shortly after the B-band peak. Because of this blending, we only fit the absorption minimum velocity, since the edges are also not well-defined. We visually inspect each fit and remove results that are obviously contaminated by noise or line blending. For the Ca II IR triplet, we fit a double P Cygni profile for the entire structure. This is done as follows: First, we remove a linear continuum. Then we fit 4 Gaussians: 2 are positive and centred at $\lambda 8662$ and $\lambda\lambda 8498, 8542$, representing emission. The other two Gaussians are negative to the blue side of the emission, representing absorption. We use a single set of Gaussians for the blue lines because they are blended. We then measure the absorption minimum of $\lambda 8662$, which is unblended. We find the fits to be more reliable than the absorption method. For the IR Co II 15759, 16064 and 16361Å lines, we fit an individual P Cygni profile to each line. To ensure consistency, we bind the three absorption minima velocity (v_{phot}) and the FWHM velocity to be uniform across the three lines in each epoch. To check our fits, we also run these fits on the *JWST* spectrum from ref. [43], and find our results to be consistent with theirs. Our results show that the early spectra IME lines (Si II and Ca II) and IGE Fe II exhibit a higher expansion velocity ($v_{\text{phot}} \sim 3500 \text{ km s}^{-1}$) than LME C II ($v_{\text{phot}} \sim 2800 \text{ km s}^{-1}$). This early difference could be because these are stronger transitions and hence sample the very outer ejecta early on. Later, however, C II, Si II and IGE lines show consistent velocities, declining to a low expansion

velocity of $v_{\text{phot}} \lesssim 1000 \text{ km s}^{-1}$ by day 30. However, C II declines in velocity much faster, and Ca II remains at a higher velocity ($v \sim 1500 \text{ km s}^{-1}$) for a longer time.

The uniform velocity of LME, IME, and IGE, except Ca, is consistent with the IR spectra presented in [43] and suggests well-mixed ejecta. However, the Ca NIR triplet remains an outlier in that regard. One simple explanation for the high velocity of Ca II is that it has a large optical depth due to its very strong transition. Therefore, it measures the velocity space more thoroughly, representing the fastest ejecta. This ejecta would also be thinner than the inner ejecta represented by the slower-expanding IGE absorption zones.

The appearance of forbidden Ca II at an early epoch also appears to be at odds with the optical depth probed by the slow declining lightcurve and t_0 γ -ray escape time. However, both probes measure the effective optical depth in the Co-rich layers. Therefore, we find further evidence that some Ca lines form further away in a less dense part of the ejecta. If Ca lines only form at the outer ejecta, this could suggest it is richer in IME compared to the inner ejecta. An upper ejecta structure has been seen in other SNe Iax [46]. In some cases, the upper ejecta is optically thick enough to create two ^{56}Ni decay components [45, 96]. In SN 2024vjm we do not find any upper ejecta that affects the lightcurve, possibly due to a low amount of mass or the overall slow velocity regime of the entire ejecta.

2.5 Powering mechanism

SNe Ia are powered by the decay of radioactive nickel [34, 35]. While SNe Iax are thought to arise from the deflagration, rather than detonation of WD material [5], their lightcurves should still follow the same thermonuclear principles. Therefore, to understand the energetics, it is imperative to probe the amount of ^{56}Ni synthesised by the SN explosion. As the SN ejecta become optically thin, we expect the bolometric luminosity to equate the deposited energy by γ -rays and positrons emitted by the decay. These depositions are described by the following set of equations [97, 98]:

$$Q_\gamma(t) = \frac{M_{\text{Ni}56}}{M_\odot} [6.54e^{-\frac{t}{8.76\text{d}}} + 1.38e^{-\frac{t}{111.4\text{d}}}] \times 10^{43} \text{ erg s}^{-1} \quad (1)$$

$$Q_{\text{pos}}(t) = 4.64 \frac{M_{\text{Ni}56}}{M_\odot} [e^{-\frac{t}{111.4\text{d}}} - e^{-\frac{t}{8.76\text{d}}}] \times 10^{41} \text{ erg s}^{-1} \quad (2)$$

Where Q_γ is the γ -ray deposition, Q_{pos} is the positron deposition and $M_{\text{Ni}56}$ is the synthesised Nickel mass.

As the ejecta become optically thin, more γ -ray photons escape, thus reducing the efficiency of γ -ray deposition [99]. The fraction of depositing γ -ray photons f_{dep} scales as $f_{\text{dep}} = 1 - e^{-(\frac{t_0}{t})^2}$ where t_0 is the γ -ray escape time. Therefore, the total deposition is given by:

$$Q_{\text{dep}} = Q_\gamma f_{\text{dep}} + Q_{\text{pos}} \quad (3)$$

To measure the Nickel mass of SN 2024vjm, we fit Eq. (3) to the late bolometric lightcurve ($t > 45$ days after explosion) and up to the our last B -band measurement (57 days after explosion), corresponding to a time where the SN should be optically

thin and we have good photometric coverage. We find the best fit to the lightcurve to be $M_{^{56}\text{Ni}} = 3.67_{-0.45}^{+0.1} \times 10^{-3} \text{ M}_\odot$ in line with other faint SNe Iax [37]. We further find the best fit for t_0 to be ≈ 70 days. To confirm this, we probe the t_0 parameter using another method, using the entire lightcurve, including its peak. The internal energy of the low mass ejecta, having gone through significant adiabatic losses (since the progenitor is compact), is negligible compared to the contribution of radioactive decay energy. Therefore, one can measure the t_0 parameter independently from the nickel mass, using conservation of energy and based on the Katz integral [36, 100], whereby:

$$\frac{L(t)}{\int_0^t L(t')t'dt} = \frac{Q(t)}{\int_0^t Q(t', t_0)t'dt} \quad (4)$$

This equation holds for the late lightcurve, where opacity effects are averaged out. This is seen in Figure 3 panel c, as the convergence of both the nominators and denominators in both sides of equation (4) reaching unity.

We solve Eq. (4) for 57 days, and find the best fit t_0 to be 83.05 days. We then probe the parameter space by running a basic 1-d Markov chain Monte Carlo (MCMC) algorithm using the inferred bolometric lightcurve error. We find a median value of $t_0 = 83.05_{-15.71}^{+14.93}$ days (1σ errors) days and that $t_0 > 48.2$ days with a 3σ confidence. This confirms that SN 2024vjm has an unusually high γ -ray escape time, suggesting the SN ejecta remains optically thick to γ -rays for a long duration after explosion. We further find that ^{56}Ni accounts for 99.98% of the SN luminosity for the best fit t_0 value, ruling out any additional energy source.

We find that the low ejecta expansion velocity (as measured by slow photospheric velocities) provides a good explanation to the slow lightcurve evolution. The γ -ray escape time, t_γ , beyond which γ -ray deposition becomes inefficient is determined by the plasma column density Σ (i.e the ejecta density at the line-of-sight) and an effective γ -ray opacity $\kappa_\gamma \approx 0.025$ that has very weak dependence on chemical composition [42]. This dependence is given by:

$$t_\gamma = \sqrt{\kappa_\gamma \Sigma(t) t^2} \quad (5)$$

Where t is the time since explosion. For a homologous expanding ejecta, Σ is given by:

$$\Sigma(t) = \frac{M_{ej}}{4\pi v_{ej} t^2} \quad (6)$$

Where M_{ej} is the ejecta mass and v_{ej} is the ejecta velocity. Therefore, the ejecta mass ejected by a thermonuclear explosion can be assessed as:

$$M_{ej} = \frac{4\pi t_\gamma^2 v_{ej}^2}{\kappa_\gamma} \quad (7)$$

For $t_\gamma = 80$ days as inferred from the Katz integral method and an ejecta velocity of $v \approx 1,000 \text{ km s}^{-1}$ we find that an ejecta mass of $M_{ej} \approx 0.12 \text{ M}_\odot$ is produced.

To check that the ejecta mass is consistent with other measurements, we assess it using its bolometric rise time. This provides an independent measurement of the ejecta mass. The ejecta mass of a thermonuclear explosion can be assessed using a scaling relation[14, 101]:

$$M_{ej} = 0.16 \left(\frac{t_r}{10 \text{ days}} \right) \left(\frac{0.1 \text{ cm}^2 \text{ g}^{-1}}{\kappa_{\text{opt}}} \right) \left(\frac{v_{ej}}{2 \times 10^8 \text{ cm}} \right) M_{\odot} \quad (8)$$

where t_r is the bolometric rise time and κ_{opt} is the optical opacity. For SN 2024vjm we measure a rise time of $t_r \approx 11.3$ days. Assuming an opacity of $0.1 \text{ cm}^2 \text{ g}^{-1}$, we find the ejecta mass to be $M_{ej} \approx 0.1 M_{\odot}$. While detailed modelling is needed to precisely calculate the ejecta mass, the agreement between these two assessments strengthens the hypothesis that the slow-expanding ejecta is the source of long γ -ray escape time duration, and hence its slow bolometric decline.

2.5.1 Bound remnant and late-time lightcurve

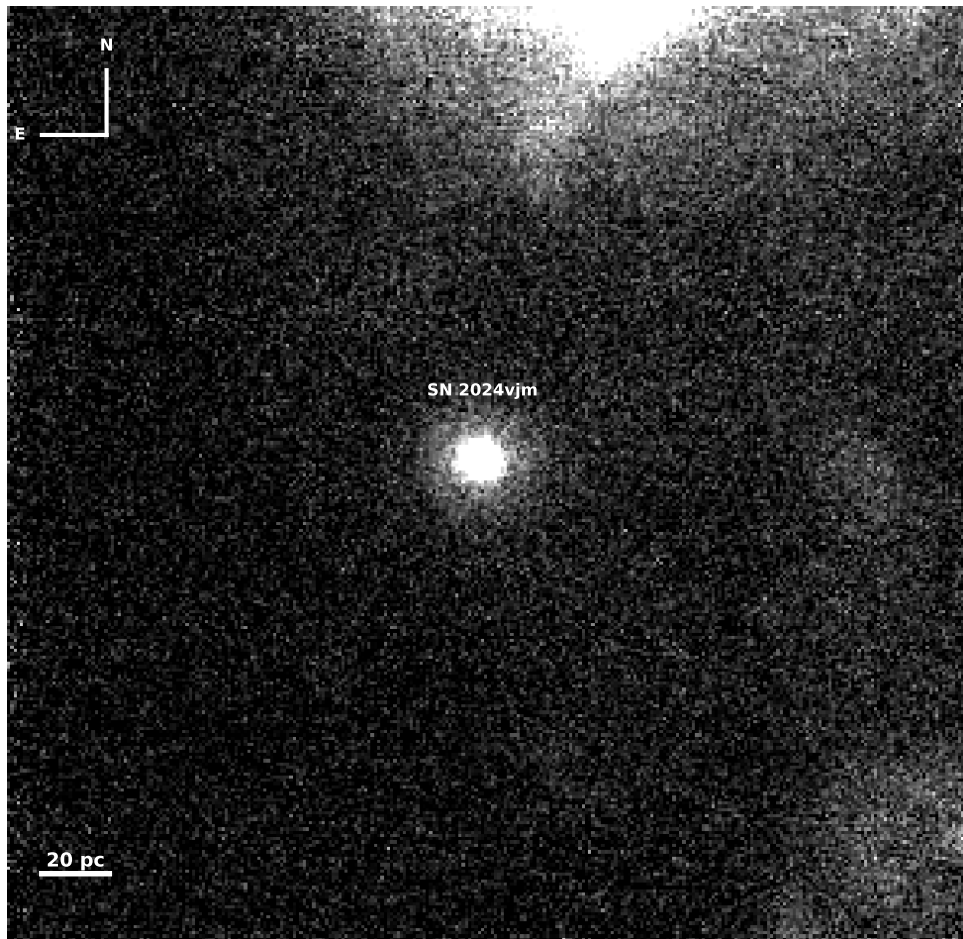
Type SNe Iax often display a late-time luminosity excess exceeding that of pure thermonuclear explosion models [45, 96]. This excess is often found to begin > 50 days past their explosion, and can potentially last for years [9, 22, 102]. A gravitationally bound remnant, left behind the weak explosion, is often credited to create this discrepancy, possibly due to ^{56}Ni deep within the bound remnant or secondary ejecta produced by it [46]. Due to the faintness and since SN 2024vjm's field was setting, our multiband lightcurve coverage ended too early to find any discrepancy from a single thermonuclear explosion.

However, as the field with SN 2024vjm became observable again, we obtained further observations of SN 2024vjm. Interestingly, SN 2024vjm was not detected in bands other than i -band in regular LCO images, while deep images taken with EFOSC2 and Magellen/IMACS provided detections in the z , r and g -bands as well. In all cases, the i -band was significantly brighter than the other bands. This is likely caused by strong lines in the SN spectra, which can be attributed to the forbidden Ca II NIR doublet. Interestingly, at no late epoch did the optical bands (redder than i -band) cover more than 10% of the total luminosity predicted by Nickel decay, when integrated together and compared to the expected luminosity from ^{56}Ni decay. This means that at late times, most of the luminosity released by SN 2024vjm is emitted in the IR. To confirm this, we integrate the flux from a *JWST* spectrum obtained at +194 days post-peak, covering $0.7\text{--}13 \mu\text{m}$, obtained through a director discretionary program (PI: Baron). We find that more than 50% of the flux is emitted at wavelengths longer than $2 \mu\text{m}$ at this epoch. This suggests the SN 2024vjm caused dust formation at these later epochs, shifting the SED to the infrared.

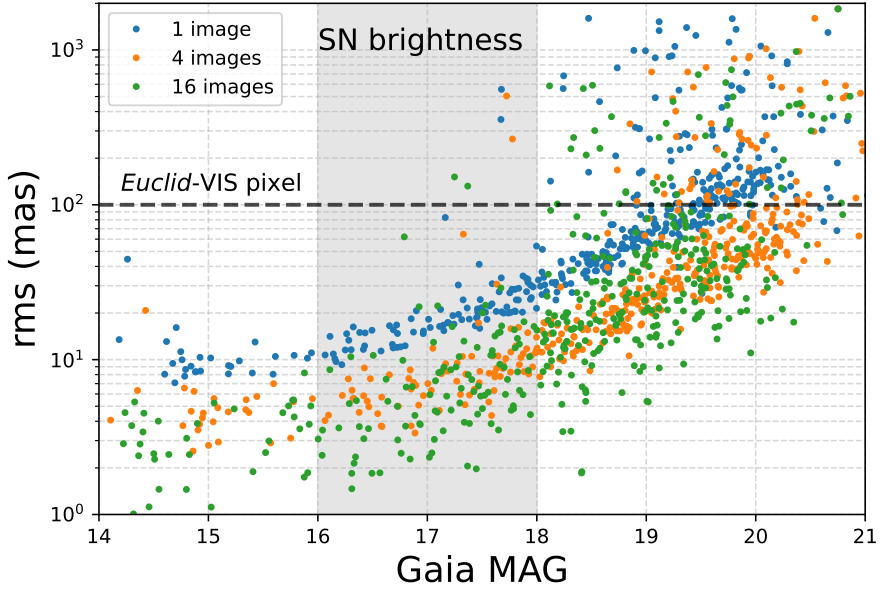
Using late-time data, we find no additional emission from the bound remnant. The flux from the *JWST* spectrum matches the expected flux from the late-time ^{56}Ni decay tail. Furthermore, by correcting the late i -band assuming they account 6% of the SN 2024vjm flux, we can reconstruct a lightcurve that follows the ^{56}Ni deposition tail. Since the i -band decline rate follows that of a single ^{56}Ni tail, it confirms that no excess energy source exists at these epochs for SN 2024vjm. It should be noted, however, that

at later epochs this correction fails, as expected if the temperature further drops or the effects of dust formation accumulate, decreasing the i -band fraction of the total flux. We therefore cannot construct the decline rate longer than 209 days, such that excess flux from the remnant would be possible at these later epochs. Regardless, such flux is only expected in the deep IR, necessitating further *JWST* observations to detect.

2.6 Extended Data Figure



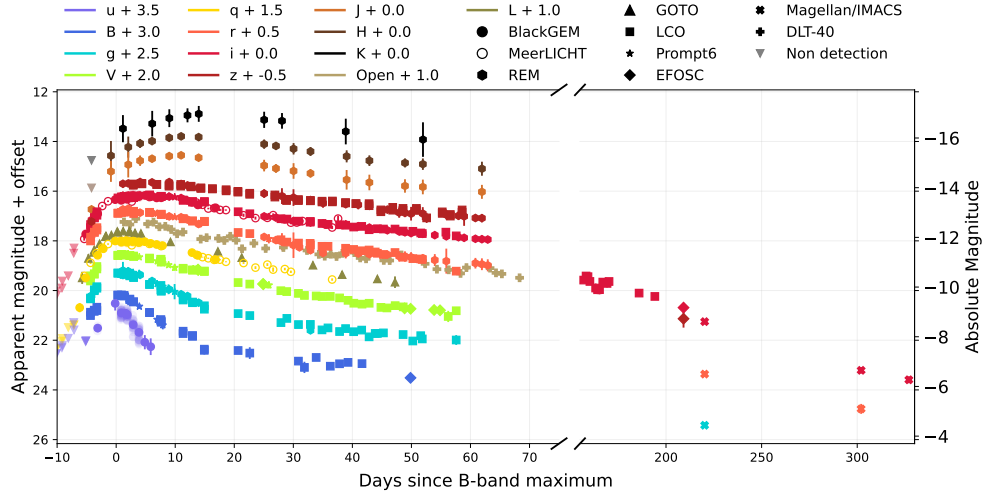
Extended Data Figure 1: SN 2024vjm is surrounded by star-formation. The host redshifted H α slice of the MUSE datacube is shown. SN 2024vjm is clearly visible at the centre and is marked by its name. The edges of two large star-forming regions are seen to the north (~ 80 pc) and south-west (~ 140 pc) of the SN. However, the SN lies away from large star-forming regions. The emission lines produced by the northern star-forming region are consistent with a solar abundance of metals.



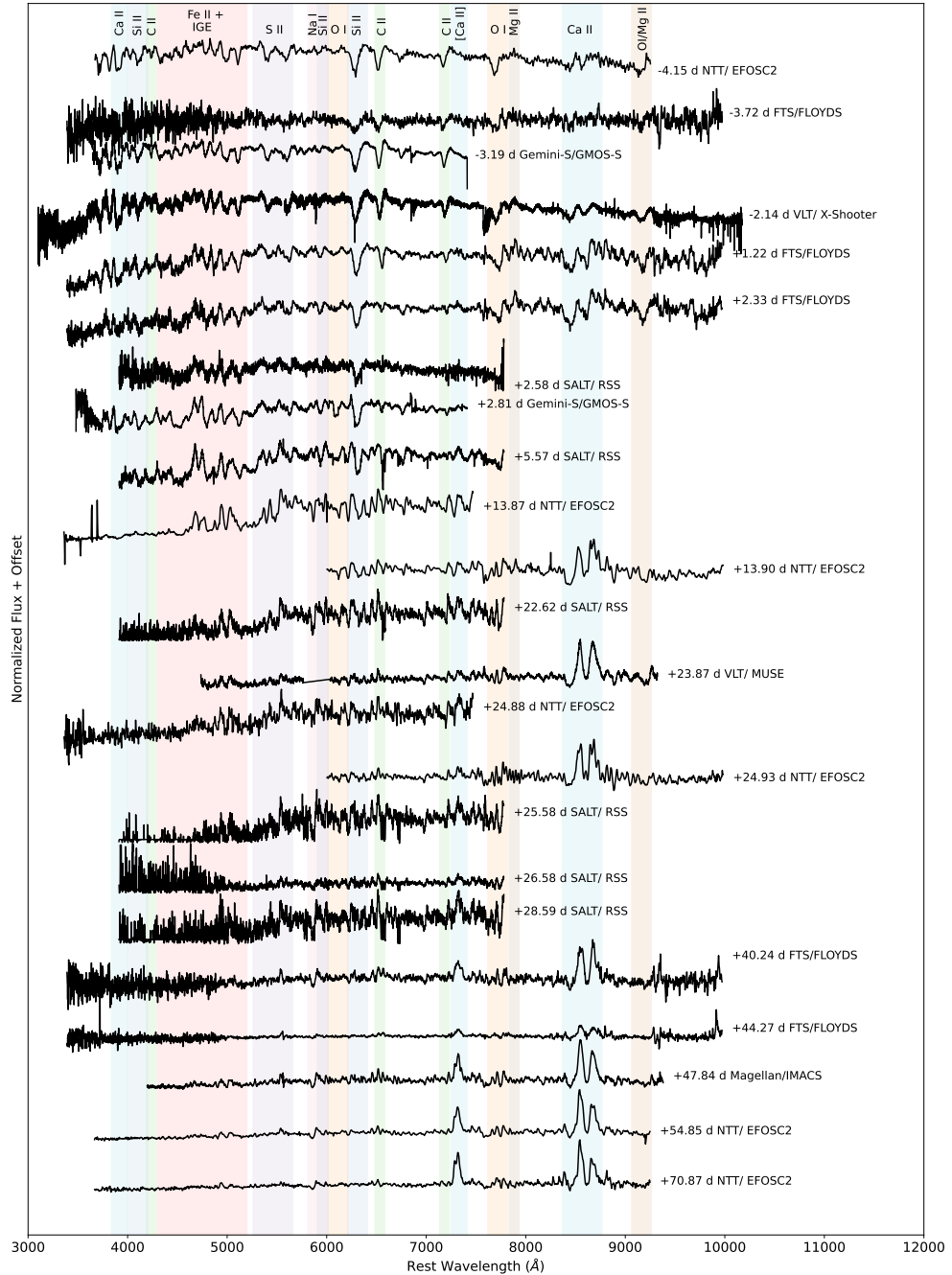
Extended Data Figure 2: Binning seeing-limited BG images improves the astrometric accuracy. Median astrometric position of identified Gaia sources within BG *i*-band images in single images (blue), four binned images (orange) and sixteen binned images (green). By combining more images the astrometric noise decreases by roughly the square root of the number of images. This demonstrates that the mean astrometric points are largely independent, and therefore, averaging multiple data points can achieve better accuracy. A single *Euclid*-VIS pixel is marked at $0.1''$ with a striped line. The brightness of SN 2024vjm within the *i*-band images is marked with a shaded grey region.

Extended Data Table 1: Lightcurve parameters of SN 2024vjm. All values are extinction extinction corrected. SN 2024vjm is possibly the faintest SN observed to date. The errors are of 1σ .

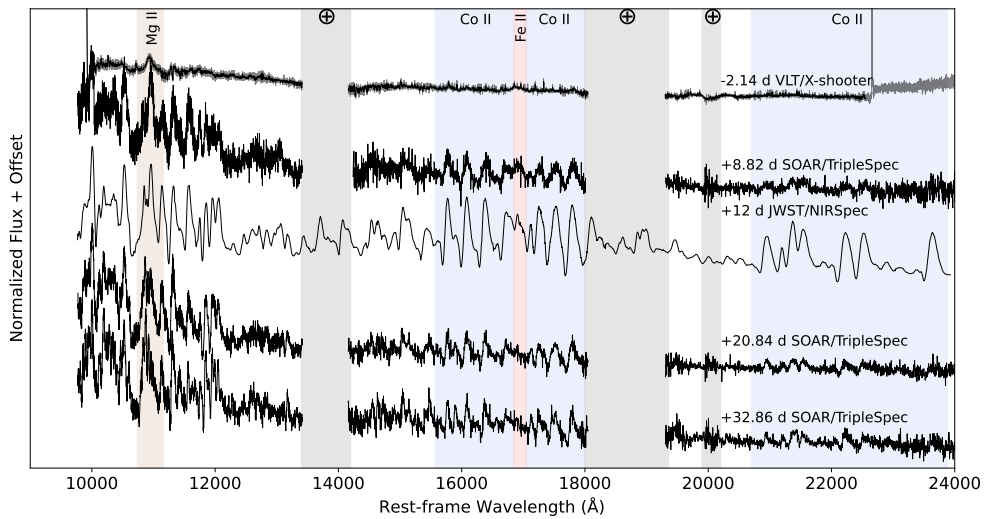
Filter	Maximum light (MJD)	Peak apparent magnitude	Peak absolute magnitude	ΔM_{15}
u (BG)	60572.64 ± 0.41	17.39 ± 0.10	-12.47 ± 0.14	1.15 ± 0.56
B	60572.29 ± 0.17	17.18 ± 0.03	-12.68 ± 0.10	1.85 ± 0.05
g	60572.50 ± 0.03	16.80 ± 0.02	-13.06 ± 0.10	1.32 ± 0.04
V	60573.23 ± 0.14	16.56 ± 0.01	-13.30 ± 0.10	0.74 ± 0.06
q	60573.74 ± 0.04	16.53 ± 0.04	-13.33 ± 0.11	0.71 ± 0.04
r	60574.43 ± 0.07	16.33 ± 0.01	-13.53 ± 0.10	0.58 ± 0.13
i	60577.63 ± 0.21	16.17 ± 0.01	-13.69 ± 0.10	0.57 ± 0.02
z	60576.86 ± 0.34	16.20 ± 0.01	-13.66 ± 0.10	0.31 ± 0.03
J	60582.35 ± 0.83	14.61 ± 0.10	-15.25 ± 0.14	0.38 ± 0.14
H	60583.40 ± 0.22	13.83 ± 0.07	-16.03 ± 0.12	0.32 ± 0.11
K	60586.31 ± 0.15	13.04 ± 0.19	-16.82 ± 0.22	0.20 ± 0.29



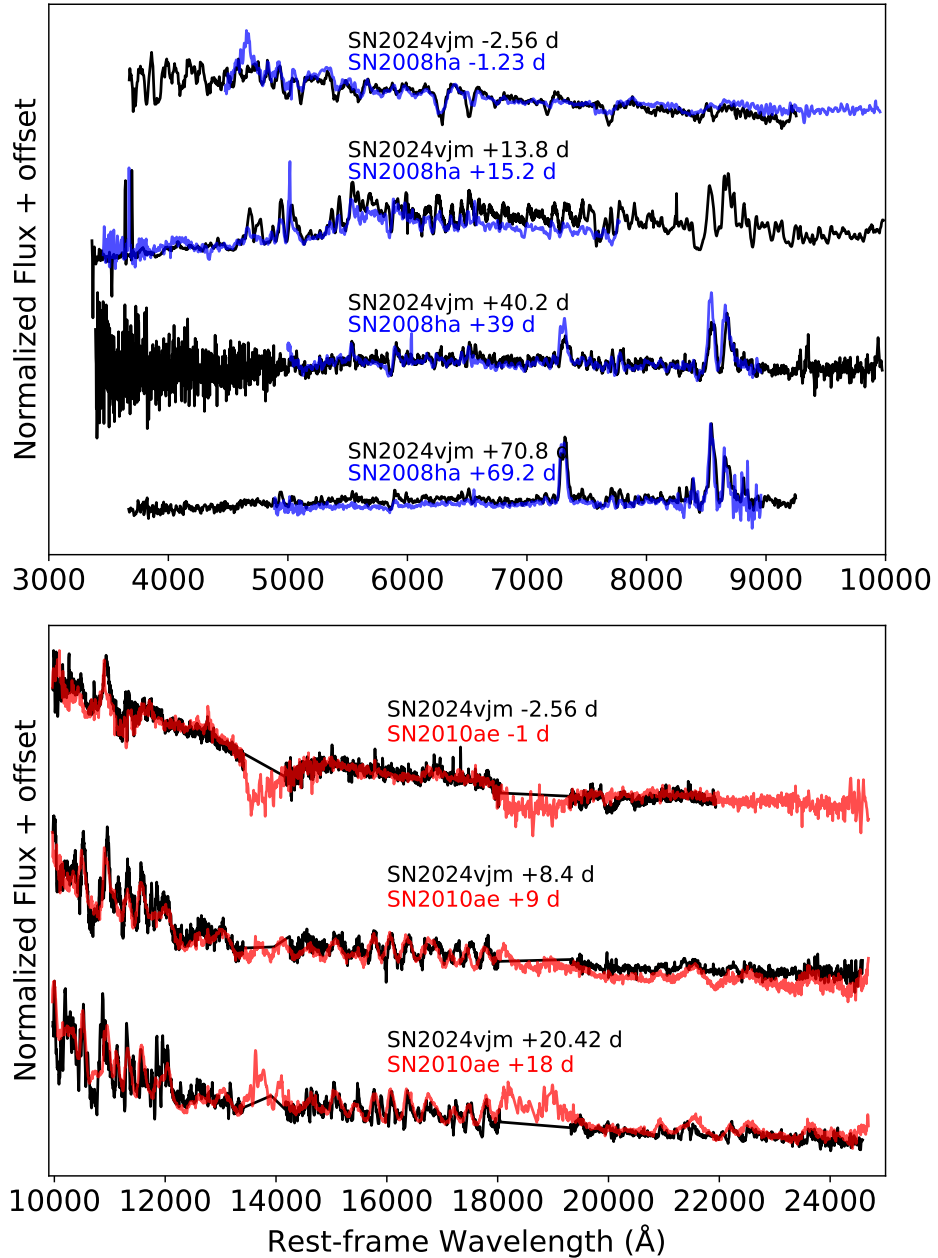
Extended Data Figure 3: Multi-band lightcurve of SN 2024vjm. Different filter bands are plotted with vertical offsets for clarity. $BVJHK$ bands are shown in the Vega magnitude system following convention, while all other bands are in the AB magnitude system. We show non-detections up to the first detection in each band in triangles. Individual unbinned measurements are shown with semi-transparent markers, while binned data points are shown in opaque markers. All other data are displayed with marker styles and colours corresponding to their respective telescope and band. The gap in observations is due to the field setting behind the sun. Error bars represent 1σ uncertainties.



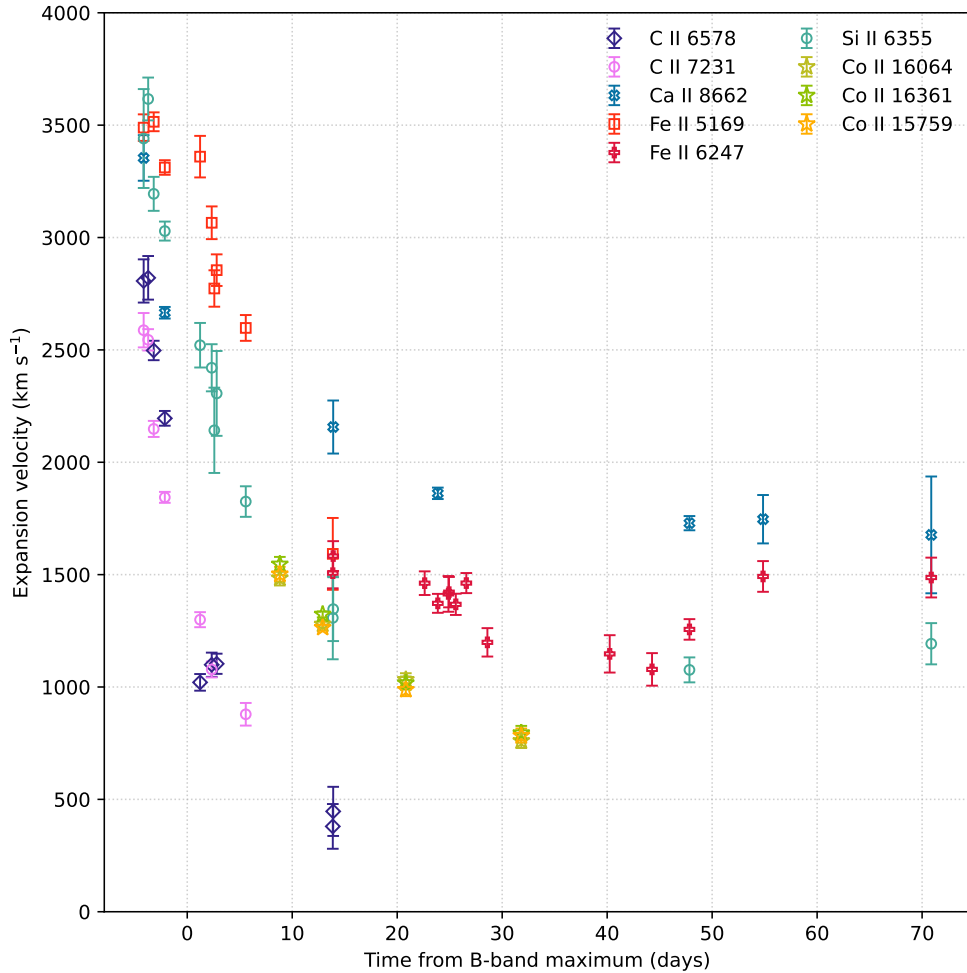
Extended Data Figure 4: Optical spectra of SN 2024vjm. The spectra are ordered in phase from *B*-band maximum and are corrected for extinction. Prominent features are marked in shaded colour.



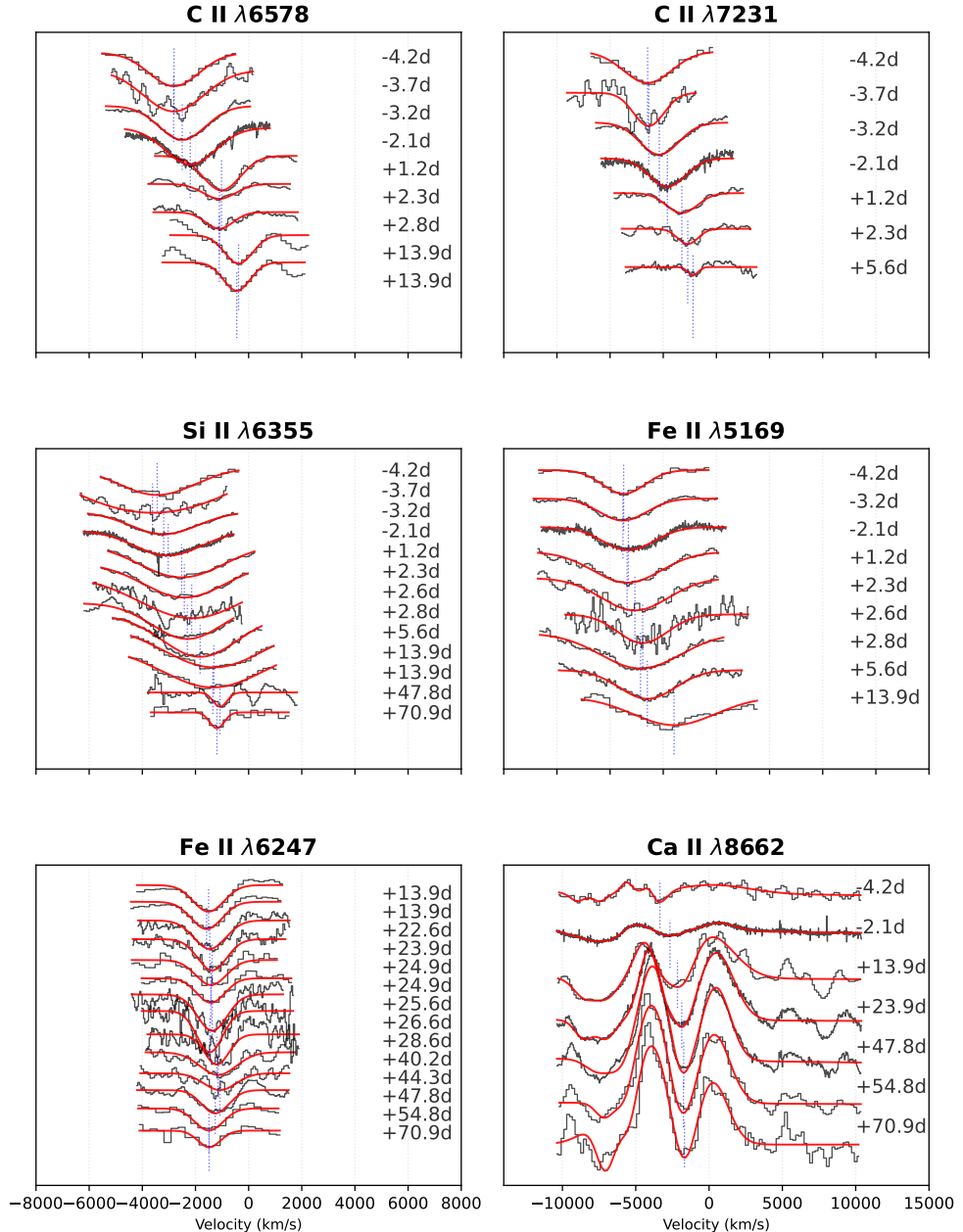
Extended Data Figure 5: NIR Spectra of SN 2024vjm. The NIR section of the +12 d *JWST* spectrum from [43] is shown along with spectra obtained for this study. While early on the spectrum is almost featureless, barring Mg II and a possible single Fe II line, later epochs show striking Co II P Cygni profiles throughout the H and K band.



Extended Data Figure 6: SN 2024vjm shows spectral similarity to other faint SNe Iax. We compare the normalised spectra of SN 2024vjm to faint SNe Iax SN 2008ha (blue, optical) and SN 2010ae (red, NIR). The spectral evolution of SN 2024vjm is similar to the other faint SNe Iax per epoch, although its expansion velocity is smaller than the other two faint SNe.



Extended Data Figure 7: The ejecta of SN 2024vjm was slowly expanding. Absorption line velocities from SN 2024vjm's spectra are shown in different phases. Different lines are marked with distinct colours. We initially measure similar velocities in all lines; however, we find that Ca diverges from the IGE at later epochs, maintaining a larger expansion velocity. Error bars represent 1σ uncertainties.



Extended Data Figure 8: Velocity fits to prominent spectral lines of SN 2024vjm. The fit (red) to the original spectral data (black) shows that the fits match the original shape well. The absorption minima of the different lines are marked (blue-striped line), showing that all spectral features decline in early epochs.

3 Declarations

Supplementary information. Supplementary Information is available for this paper.

Correspondence. Correspondence and requests for materials should be addressed to Erez A. Zimmerman (email: erezimm@gmail.com).

Acknowledgements. We thank Dr. Amir Sharon, Prof. Boaz Katz, Prof. Doron Kushnir and Prof. Eli Waxmann for meaningful discussions. Based on observations with the BlackGEM telescope array. BlackGEM has been made possible with financial aid from Radboud University, the Netherlands Research School for Astronomy (NOVA), the KU Leuven Department of Physics and Astronomy, the Netherlands Organization for Scientific Research (NWO), the Research Foundation Flanders (FWO) under grant agreement G0A2917N (BlackGEM, with PIs C. Aerts & G. Raskin and personnel C. Johnston and P. Ranaivomanana), the European Research Council. BlackGEM is a collaboration between NOVA, Radboud University, KU Leuven and the Universities of Manchester, Warwick, Hamburg, Potsdam, Barcelona, Durham, Tel Aviv and Valparaiso, and the Armagh Observatory and Planetarium, the University of California at Davis, the Danish Technical University, Texas Tech University, the Weizmann Institute, Las Cumbres Observatory, and the Hebrew University of Jerusalem. BlackGEM is hosted at the La Silla Observatory of the European Southern Observatory. Based on observations with the MeerLICHT telescope. The MeerLICHT telescope is operated at the SAAO Sutherland site and supported by a consortium consisting of Radboud University, the University of Cape Town, the University of Oxford, the University of Manchester, the University of Amsterdam and the South African Astronomical Observatory, on behalf of the National Science Foundation of South Africa. Based on observations collected at the European Southern Observatory under ESO programmes 1112.D-0334, 113.26B1, 114.28GZ and 1103.D-0328. This work makes use of observations from the Las Cumbres Observatory network. The LCO team is supported by NSF grants AST-2308113 and AST-1911151. This research is based in part on data collected at the international Gemini Observatory within the framework of Subaru-Gemini time exchange program (S24B-041, GS-2024B-Q-101, GS-2024B-Q-102: PI, K. Maeda). We are honored and grateful for the opportunity of observing the Universe from Maunakea, which has the cultural, historical and natural significance in Hawaii. This paper includes data gathered with the 6.5 meter Magellan Telescopes located at Las Campanas Observatory, Chile. REM data were obtained under the program: REM AOT47-37 (ID 49337), "Characterising the elusive interacting transients", (PI: G. Valerin) The Prompt telescopes belong to 'The Skynet Robotic Telescope Network which operates out of the University of North Carolina at Chapel Hill. Supported by the National Science Foundation, North Carolina Space Grant, and the Mount Cuba Astronomical Foundation.' This work has made use of the Early Release Observations (ERO) data from the *Euclid* mission of the European Space Agency (ESA), 2024, <https://doi.org/10.57780/esa-qmocze3>. Euclid is a fully European mission, built and operated by ESA, with contributions from NASA. The Euclid Consortium is responsible for providing the scientific instruments and scientific data analysis. ESA selected Thales Alenia Space as prime contractor for the construction of

the satellite and its Service Module, with Airbus Defence and Space chosen to develop the Payload Module, including the telescope. NASA provided the near-infrared detectors of the NISP instrument. Euclid is a medium-class mission in ESA’s Cosmic Vision Programme. This work is based in part on observations made with the NASA/ESA/CSA James Webb Space Telescope. The data were obtained from the Mikulski Archive for Space Telescopes at the Space Telescope Science Institute, which is operated by the Association of Universities for Research in Astronomy, Inc., under NASA contract NAS 5-03127 for JWST. These observations are associated with program #DD9231. The authors acknowledge the team led by coPIs Eddie Baron and James M. DerKacy for developing their observing program with a zero-exclusive-access period. This research made use of Photutils, an Astropy package for detection and photometry of astronomical sources (Bradley et al. 2025) PJG is supported by NRF SARCHI grant 111692. S.V. and the UC Davis time-domain research team acknowledge support by NSF grants AST-2407565. PC acknowledges the support from the Zhejiang provincial top-level research support program. Time-domain research by the University of Arizona team and D.J.S. is supported by National Science Foundation (NSF) grants 2108032, 2308181, 2407566, and 2432036 and the Heising-Simons Foundation under grant #2020-1864. GL and SdW were supported by a research grant (VIL60862) from VILLUM FONDEN This research was supported by Deutsche Forschungsgemeinschaft (DFG, German Research Foundation) under Germany’s Excellence Strategy - EXC 2121 ”Quantum Universe” – 390833306. Co-funded by the European Union (ERC, CompactBINARIES, 101078773). Views and opinions expressed are however those of the author(s) only and do not necessarily reflect those of the European Union or the European Research Council. Neither the European Union nor the granting authority can be held responsible for them. N.B. acknowledges financial support from grant CEX2024-001451-M, funded by MICIU/AEI/10.13039/501100011033. N.B. acknowledges funding from the European Union (ERC, CET-3PO, 101042610). Views and opinions expressed are however those of the author(s) only and do not necessarily reflect those of the European Union or the European Research Council Executive Agency. Neither the European Union nor the granting authority can be held responsible for them. LAK is supported by NASA through a Hubble Fellowship grant No. HF2-51579.001-A awarded by the Space Telescope Science Institute (STScI), which is operated by the Association of Universities for Research in Astronomy, Inc., for NASA, under contract NAS5-26555. KM acknowledges funding from Horizon Europe ERC grant no. 101125877 M.A. is supported by NSF grant AST-2308113 K.M. acknowledges support from JSPS KAKENHI grant (JP24KK0070, JP24H01810) and JSPS Bilateral Joint Research Projects (JPJSBP120229923). H.K. was funded by the Research Council of Finland projects 324504, 328898, and 353019. SM is funded by Leverhulme Trust grant RPG-2023-240. AR acknowledges financial support from the GRAWITA Large Program Grant (PI P. D’Avanzo) and from the PRIN-INAF 2022 ”Shedding light on the nature of gap transients: from the observations to the models”. AM gratefully acknowledges support from an STFC PhD studentship and the Faculty of Science and Technology at Lancaster University. T.-W.C. acknowledges the financial support from the Yushan Fellow Program by the Ministry of Education, Taiwan (MOE-111-YSFMS-0008-001-P1) and the National Science and Technology Council,

Taiwan (NSTC grant 114-2112-M-008-021-MY3). W.Z. acknowledges support by the National Natural Science Foundation of China (Grant No. 12133005).

Declarations

Author Contribution.

- **Paper Writing** — E. A. Zimmerman, A. Gal-Yam
- **Discussion and Interpretation** — All authors contributed to discussions and interpretation.
- **Discovery of SN 2024vjm** — P. J. Groot
- **Data analysis** — E. A. Zimmerman, E. O. Ofek
- **Observations and Data Reduction** — E. A. Zimmerman, A. Pastorello, S. Valenti, A. P. Ravi, P. Chen, N. Blagorodnova, M. Wavasseur, M. A. Gómez-Muñoz, P. M. Vreeswijk, S. de Wet, L. A. Kwok, M. Schwab, S. W. Jha, D. Hiramatsu, J. Li, H. Kuncarayakti, K. Maeda, G. Pignata, A. Reguitti, G. Valerin, W. Zang
- **BlackGEM Collaboration** — P. J. Groot, J. van Roestel, E. A. Zimmerman, A. Gal-Yam, S. Valenti, A. P. Ravi, N. Blagorodnova, M. Wavasseur, M. A. Gómez-Muñoz, H. Tranin, P. M. Vreeswijk, S. de Wet, G. Leloudas, E. Stringer, T. Kupfer, S. Bloemen, D. L. A. Pieterse, F. Stoppa
- **ePESSTO+ Collaboration** — A. Pastorello, J. P. Anderson, T. -W. Chen, K. Maguire, M. Della Valle, G. Dimitriadis, M. Gromadzki, J. H. Gillanders, J. D. Lyman, M. R. Magee, A. Milligan, G. Pignata, A. Reguitti, R. P. Santos, S. Srivastav, G. Valerin
- **LCO Collaboration** — D. A. Howell, S. W. Jha, M. Schwab, M. Andrews, D. Hiramatsu, S. Moran, Y. Ni, X. Wang, J. R. Farah, K. Wynn
- **DLT-40 Collaboration** — D. J. Sand, S. Valenti, A. P. Ravi, J. Pearson, Y. Dong, M. Shrestha, K. A. Bostroem, N. M. Retamal, D. Janzen, D. E. Reichart, B. Subrayan, E. Hoang, J. Andrews, D. Mehta

Competing Interests. The authors declare that they have no competing financial interests.

Data Availability Statement. Photometry and spectra used in this study will be made available on WISEREP[103]. A log of the available spectra can be found in Supplementary Table 1.

Code Availability Statement. All scripts used to conduct the analyses presented in this paper are available from the corresponding author upon request. Relevant software sources have been provided in the text, web locations provided as references, and are publicly available.

4 Supplementary Methods

4.1 Photometric reductions

Data was obtained with the facilities listed below:

- BlackGEM and MeerLICHT – BG photometry in uqi bands was obtained by the BG LTS and fast-synoptic survey, with an intra-night cadence. Additional uqi images were obtained by MeerLICHT (ML), which is the BG sister project at the South African Astronomical Observatory (SAAO). Observations were performed until the SN field began setting. The photometry was reduced by the BlackGEM `BlackBOX` pipeline [104], which performs the astrometric and photometric calibration based on Gaia DR3 data [71, 72], determines the PSF as a function of pixel position, and performs image subtraction with respect to a pre-built reference image closely following `ZOGY` [105], which includes an estimate of the transient PSF photometry. Using the so-called Scorr (significance) image, objects with $S/N \geq 6$ are selected as transient candidates. To identify detections with a lower $S/N > 3$ directly at the SN location, we ran a forced-photometry pipeline on the BG images. This resulted in a single (5σ) pre-discovery q -band detection at an absolute magnitude of $M_q = -9.56 \pm 0.61$ mag (apparent $m_q = 19.92 \pm 0.19$ mag) a day before detection ($MJD = 60566.00$).
- LCO – $BVgriz$ photometry was obtained by the Global Supernova Project (GSP) through the Las Cumbres Observatory [LCO; 106] 1 meter telescope network. We performed PSF photometry with the `daophot` task in `IRAF` on the reduced images with the LCOGT/BANZAI pipeline [107] without image subtraction. We utilize the ATLAS All-sky Stellar Reference Catalog (ATLAS-REFCAT2; Tonry et al. 108) to derive the photometric zero-point. Before being used for photometric calibrations of our target, the ATLAS-REFCAT2 magnitudes of the reference stars in the fields are first converted into Johnson BV and Sloan- $griz$ bands adopting the following transformations given in [109]. We also performed image subtraction on some selected images in the r band using the image taken on 5 June 2025 as a template image, then obtained PSF photometry on the subtracted images. We obtained photometry results consistent with those without image subtraction, confirming that image subtraction is not necessary for LCOGT images due to a relatively faint and smooth host galaxy background. All these photometry procedures were performed using the `pmpyeasy` pipeline [110].
- REM – Additional photometry was obtained by the 60-cm Rapid Eye Mount (REM) telescope hosted in the La-Silla observatory. Thanks to a dichroic, simultaneous optical ($griz$) and near-infrared (JHK) observations can be obtained using two cameras, ROSS2 for the optical and REMIR for the NIR. REM/ROSS2 images were treated with standard reduction steps, such as bias and flat field corrections, and final trimming. Individual images were then combined in a single (stacked) image to increase the signal-to-noise ratio. For the REM/REMIR images, pre-reduction only consisted in the subtraction of a sky frame before combining the images to obtain a final stack.

Photometric measurements were performed using the `ECsnoopy` pipeline¹. `ECsnoopy` allows the user to perform an accurate astrometric calibration of the stacked images and to measure the instrumental PSF-fitting photometry of the target. For the optical images, the magnitude measurements were performed after the subtraction of a host galaxy template². No template subtraction was applied to the near-infrared images, given the modest host galaxy contamination in the SN region. The final photometric calibration was performed accounting for the zero point and colour-term corrections for each instrumental configuration, and making use of secondary standards from the Skymapper (*griz*) and the 2MASS (JHK) catalogues.

The first epoch of data was obtained through OPTICON program 24B042 (PI: Blagorodnova), while the rest of the data were obtained through REM program AOT47-37 (ID 49337; PI: G. Valerin).

- Prompt-6 – Further *BVgriz* photometry was obtained by the 0.41m Prompt-6 telescope hosted at the Cerro-Tololo Inter-American Observatory (CTIO; Chile) equipped with an FLI CCD. The data were taken under the CNTAC (Chilean National Telescope Allocation Committee) time and were pre-reduced for bias and flats. The images were reduced using the `ECsnoopy` software in a similar fashion to that of the REM photometry. To construct a magnitude catalogue with secondary standards in the Johnson-Bessell system, we transformed Skymapper *griz* magnitudes into Johnson-Bessell ones using the transformation relations of [111].
- DLT 40 – Follow up photometry was taken by the DLT 40 [112] survey using the PROMPT 0.4 m telescope at the Cerro Tololo Inter-American Observatory (CTIO), Chile. The observations were taken with no filter, and were calibrated to the APASS r-band catalogue [112]. The observations were grouped into one-day bins to improve the signal.
- GOTO – Data from The Gravitational-wave Optical Transient Observer (GOTO) [113] were obtained in the primary GOTO-L filter ($\sim 400 - 700$ nm). Following discovery announcement by the BlackGEM collaboration, a recent detection in GOTO’s regular all-sky survey was found, and nightly-cadence observations scheduled to capture the rise and peak of SN 2024vjm. Images had CCD reduction, calibration and photometry performed in real-time using the GOTO transient pipeline detailed in ref. [114]. Astrometric and photometric calibration were performed using Gaia DR3 data [71, 72] and ATLAS REFCAT2 [115]. Difference image analysis was performed by a multi-threaded version of HOTPANTS [116], using historical templates taken by GOTO of the same region of sky. Forced aperture photometry at the position of SN 2024vjm was performed to recover the final GOTO light curve.
- NTT/EFOSC2 – The aquisition images taken before obtaining NTT/EFOSC2 spectra were reduced using the `ECsnoopy` pipeline in a similar fashion to that of the REM images described above. Additional late-time photometry was reduced using *AstroPack/MAATv2* using the DELVE DR2 star-catalog [117] as reference.

¹`ECsnoopy` is a package for supernova photometry using PSF fitting and/or template subtraction developed by E. Cappellaro. A package description can be found at the website: <http://sngroup.oapd.inaf.it/ecECsnoopy.html>

²Skymapper *griz* templates were adopted.

4.2 Lightcurve interpolation

As described in *Extended Data 2.3*, to compute the lightcurve properties, we interpolated the different filter-band curves using a custom GP fitter based on the `sklearn` [85] Python Package. We run this interpolation in flux-space. To instigate a rising interpolation function in the early data, we added 0 flux “ghost points” at the inferred explosion time. This anchors the GP to zero flux before the explosion and prevents unphysical extrapolation to pre-explosion time. Because the temporal behavior of the light curve differs between the rapid rise to maximum and the smoother post-maximum decline, we employ two distinct GP kernels. For the early data (up to \sim 10 days after explosion), we use `Matern` kernel (with a parameter of $\nu = 2.5$), and a short characteristic length scale (of 2–12 days), allowing the GP flexibility during the rise time. For later epochs, we use a long-scale squared-exponential (RBF) component (with a fixed 10 day kernel) plus a linear `DotProduct` component. To ensure continuity, the early- and late-phase GPs are blended smoothly using a logistic transition function centred at 10 d after explosion. The final interpolant is the weighted combination of the two GP predictions, with uncertainties propagated in quadrature. To mitigate GP overconfidence in sparsely sampled parts of the data, we further inflate the effective GP noise wherever a temporal gap of > 3 days exists. This prevents the GP from artificially shrinking its posterior variance in poorly constrained regions of the light curve. We present the result of this interpolation in Supplementary Data Figure 1, showing an excellent fit to the data in each band.

4.3 Spectroscopic reductions

We obtained spectra using the facilities and spectrographs listed below:

- **NTT/EFOSC2** – A first classification spectrum was taken with the ESO Faint Object Spectrograph and Camera 2 (EFOSC2) spectrograph mounted on the 3.58 m New Technology Telescope (NTT) in the ESO observatory at La Silla, Chile. The spectrum was taken during a test run for the Son of X-shooter (SoXS) spectrograph scheduler [118] with the EFOSC2 spectrograph. The spectrum was uploaded to the Transient Name Server[119] (TNS) and was made public. An additional four epochs of EFOSC2 spectra were taken through the European Southern Observatory Spectroscopic Survey of Transient Objects (ePESSTO+) collaboration and were reduced using the standard PESSTO pipeline [120].
- **Gemini-S/GMOS** – We used the Gemini Multi-Object Spectrograph (GMOS) [121, 122] attached to the Gemini South telescope in long-slit mode to observe SN 2024vjm on 2024-09-16 and 2024-09-21, with total exposure times of 1200 s in each epoch. With the B480 grating centred at 540/545 nm, and 2x2 binning, the observations covered 380–750 nm at spectral resolution around 1300. The Gemini DRAGONS software package [123] was used to reduce the data following standard procedure, to obtain the reduced spectra calibrated in wavelength and flux.
- **FTS/FLOYDS** – Additional five spectra were obtained by the GSP with the FLOYDS spectrograph mounted on the LCO 2m telescope in the Sliding Springs Observatory in Australia. The spectra were reduced using the LCO `floydsspec`

pipeline, which deals with cosmic ray removal, flagging, spectrum extraction and calibration [124].

- **VLT/X-shooter** – We obtained a single epoch of spectroscopy using the X-shooter wide-band echelle spectrograph [125] mounted on the 8.2m Very Large Telescope (VLT) in ESO’s Paranal Observatory, Chile. The observations were performed under the program 113.26B1 (PI: Blagorodnova). The SN was obtained near the parallactic angle using a stare mode with slit sizes of 1, 0.9, and 0.6 arcsec for the UBV, VIS, and NIR channels, respectively. The data were reduced using the ESO pipeline `EsoRex` v.3.13.7 together with the standard X-shooter slit spectrograph pipeline v.3.6.3. Bias frames were taken five days before the observation, and the flat fields five to 15 days before the observation. Telluric absorption correction was applied to the VIS arm using a standard template.
As SN 2024vjm was yet to be classified during the observation, the data were taken to optimize the signal in the optical UBV and VIS bands. Hence, the stare mode was chosen, leading to decreased quality in the NIR band, as telluric emission lines could not be subtracted from adjacent pixels. Additionally, to increase the exposure time, no telluric star observations were taken at a similar airmass to allow telluric subtraction. To mitigate this, since much of the telluric noise in the NIR originates from strong emission lines, we employed a sigma clipping method to subtract strong telluric spikes in the X-shooter NIR spectrum. To achieve decent quality reductions, we used a window of 21 flux entries corresponding to 12.6 Å bins. We then calculate the mean value of each window and remove any residual flux values that are more than 5σ from the mean. We run this process iteratively seven times until no more residuals are found by the algorithm, after which a cleaner spectrum is left for which we can identify SNe features similar to other early Type Iax NIR spectra (see *Extended Data 2.4*).
- **SALT/RSS** – SN 2024vjm spectra, obtained by SALT/RSS were observed with a 1.5'' wide long-slit, and the PG0900 grism in two tilt positions. The data was reduced using a custom pipeline, called `RUSALT`, based on the `PySALT` package [126] and standard `Pyraf` [127] spectral reduction routines.
- **Magellan/IMACS** – We obtained one optical spectrum of SN 2024vjm on 2024-11-06 using the Inamori Magellan Areal Camera and Spectrograph [IMACS; 128] mounted on the 6.5-m Magellan-Baade telescope under decent conditions ($\sim 0.8''$). The observations consist of three 600-second exposures with a 300 lines/mm grating, resulting in a spectral resolution $R \sim 1000$. The spectra were reduced with `IRAF`, including basic data processing (bias subtraction, flat fielding), cosmic-ray removal, wavelength calibration (using arc lamp frames taken immediately after the target observation), and relative flux calibration with a spectroscopic standard observed the same night as the science object.
- **SOAR/ TripleSpec** – We obtained three NIR spectra of SN 2024vjm on 2024-09-28, 2024-10-10, and 2024-10-21 using the TripleSpec spectrograph on the SOAR telescope. All spectra were taken in the cross-dispersed mode through AEON queue observations (NOIRLab Program ID: 2024B-237887; PI: Aravind P. Ravi) using a 1.1 arcsec longslit. Data were reduced using the TripleSpec-specific modification [129, 130] of the commonly used NIR spectral reduction package, `Spextool` [131].

Both the science and the adjacent (in airmass) A0V standard targets were observed in an ABBA dithering pattern and the latter were used for telluric correction following the standard procedure as described in Vacca et al. [132].

To improve upon the original telluric reduction, we apply the same sigma-clipping method applied to the X-shooter spectrum to the SOAR spectra. This marginally improves the quality of the spectra by removing residual telluric spikes from the spectra.

4.4 MUSE reduction

The observations were reduced using the ESO MUSE pipeline [133] run automatically by ESO and uploaded to the ESO archive. We then post-reduce excess sky emission using the Zurich Atmosphere Purge [ZAP; 134] code using its Python implementation. The original astrometric solution derived by the pipeline was offset, likely due to the lack of point sources in the MUSE field of view. We therefore recalibrated the astrometric solution by pegging SN 2024vjm’s coordinates to its centre of light spaxel in the MUSE data.

Alongside spectra of the nearby star-forming regions (see Section 2.1), we have extracted a spectrum of SN 2024vjm from the MUSE datacube, presented in Extended Data Figure 4 alongside the other optical spectra taken for this study. Additionally, we obtained a spectrum from our single VLT/MUSE observation described in *Supplementary Material 4.4*.

5 Supplementary Data Items

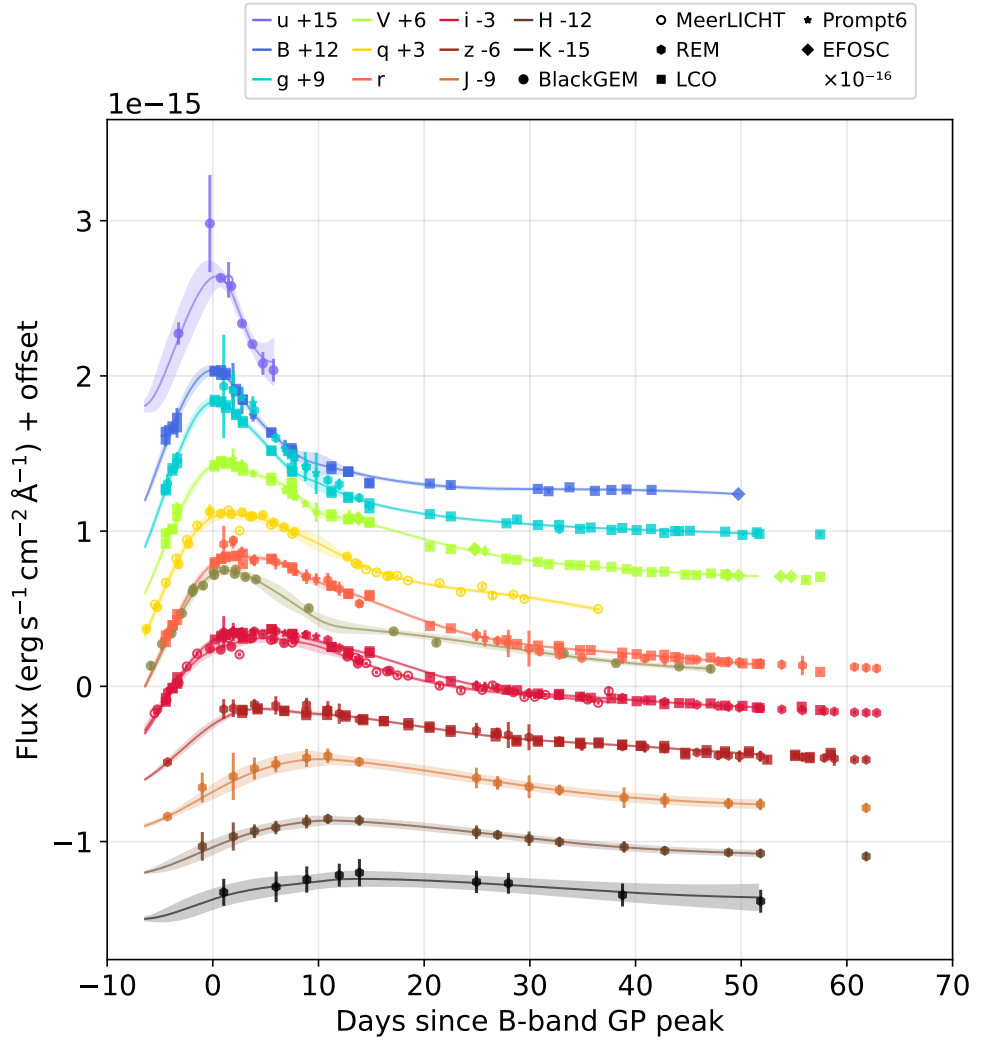
Supplementary Material Table 1: Log of spectra

Telescope/Instrument	Observation time (UTC)	Phase (days)	Grating	Slit (arcsec)	Exposure time (s)
NTT/ EFOSC2	2024-09-15T00:40:56.00	-4.32	gr13	—	2700
FTS/ FLOYDS	2024-09-15T10:59:34.538	-3.89	red/blu	2.0	3600.153
Gemini/ GMOS-S	2024-09-15T23:40:54.650	-3.19	B480	1.0	300
VLT/ X-Shooter	2024-09-17T01:03:12.890	-2.31	UVB	1.0	2850
VLT/ X-Shooter	2024-09-17T01:03:18.050	-2.31	VIS	0.9	2880
VLT/ X-Shooter	2024-09-17T01:03:21.1465	-2.31	NIR	0.6	3000
FTS/ FLOYDS	2024-09-20T09:40:02.792	1.05	red/blu	2.0	3600.145
FTS/ FLOYDS	2024-09-21T12:17:05.117	2.16	red/blu	2.0	3600.026
SALT/ RSS	2024-09-21T18:13:18.330	2.41	PG0900	—	1133.290
Gemini/ GMOS-S	2024-09-21T23:38:26.2	2.58	B480	1.0	1200
SALT/ RSS	2024-09-24T18:06:51.693	5.40	PG0900	—	1533.287
SOAR/ TripleSpec	2024-09-28T00:06:35.427	8.4	—	1.1	266.873
NTT/ EFOSC2	2024-10-03T01:58:23.00	13.73	Gr16	—	2699
SOAR/ TripleSpec	2024-10-10T00:25:31.077	20.42	—	1.1	200.
SALT/ RSS	2024-10-11T19:07:49.104	22.45	PG0900	—	1945.238
VLT/ MUSE	2024-10-13T01:10:42.118	23.70	—	—	2827.889
NTT/ EFOSC2	2024-10-14T02:41:48.00	24.76	Gr16	—	2699
SALT/ RSS	2024-10-14T18:17:13.196	25.41	PG0900	—	2000.285
SALT/ RSS	2024-10-15T18:19:32.107	26.41	PG0900	—	2000.278
SALT/ RSS	2024-10-17T18:31:33.722	28.42	PG0900	—	2000.283
SOAR/ TripleSpec	2024-10-22T01:01:26.277	32.44	—	1.1	200.
FTS/ FLOYDS	2024-10-29T10:09:31.254	40.07	red/blu	2.0	3000.179
FTS/ FLOYDS	2024-11-02T10:54:34.597	44.10	red/blu	2.0	3600.186
Magellan/ IMACS	2024-11-06T00:27:45	47.67	Gri-300	1.0	1800
NTT/ EFOSC2	2024-11-13T00:41:40.00	54.68	Gr13	—	2699
NTT/ EFOSC2	2024-11-29T01:13:41.00	70.70	Gr13	—	1799

Supplementary Material Table 2:

Measured emission line fluxes for the star-forming region

Line	Flux (10^{-16} erg s $^{-1}$ cm $^{-2}$)
H α	19.13 ± 0.86
H β	5.27 ± 1.14
[O III] $\lambda 5008$	2.46 ± 1.09
[N II] $\lambda 6583$	7.16 ± 0.39
[S II] $\lambda 6716$	4.94 ± 0.41
[S II] $\lambda 6732$	3.15 ± 0.37



References

- [1] Maoz, D., Mannucci, F., Nelemans, G.: Observational Clues to the Progenitors of Type Ia Supernovae. *ARA&A* **52**, 107–170 (2014) <https://doi.org/10.1146/annurev-astro-082812-141031> [arXiv:1312.0628](https://arxiv.org/abs/1312.0628) [astro-ph.CO]
- [2] Jha, S.W., Maguire, K., Sullivan, M.: Observational properties of thermonuclear supernovae. *Nature Astronomy* **3**, 706–716 (2019) <https://doi.org/10.1038/s41550-019-0858-0> [arXiv:1908.02303](https://arxiv.org/abs/1908.02303) [astro-ph.HE]
- [3] Jha, S.W.: Type Iax Supernovae. In: Alsabti, A.W., Murdin, P. (eds.) *Handbook of Supernovae*, p. 375 (2017). https://doi.org/10.1007/978-3-319-21846-5_42
- [4] McCully, C., Jha, S.W., Foley, R.J., Bildsten, L., Fong, W.-F., Kirshner, R.P., Marion, G.H., Riess, A.G., Stritzinger, M.D.: A luminous, blue progenitor system for the type Iax supernova 2012Z. *Nature* **512**(7512), 54–56 (2014) <https://doi.org/10.1038/nature13615> [arXiv:1408.1089](https://arxiv.org/abs/1408.1089) [astro-ph.SR]
- [5] Fink, M., Kromer, M., Seitenzahl, I.R., Ciaraldi-Schoolmann, F., Röpke, F.K., Sim, S.A., Pakmor, R., Ruiter, A.J., Hillebrandt, W.: Three-dimensional pure deflagration models with nucleosynthesis and synthetic observables for Type Ia supernovae. *MNRAS* **438**(2), 1762–1783 (2014) <https://doi.org/10.1093/mnras/stt2315> [arXiv:1308.3257](https://arxiv.org/abs/1308.3257) [astro-ph.SR]
- [6] Kromer, M., Ohlmann, S.T., Pakmor, R., Ruiter, A.J., Hillebrandt, W., Marquardt, K.S., Röpke, F.K., Seitenzahl, I.R., Sim, S.A., Taubenberger, S.: Deflagrations in hybrid CONe white dwarfs: a route to explain the faint Type Iax supernova 2008ha. *MNRAS* **450**(3), 3045–3053 (2015) <https://doi.org/10.1093/mnras/stv886> [arXiv:1503.04292](https://arxiv.org/abs/1503.04292) [astro-ph.HE]
- [7] Valenti, S., Pastorello, A., Cappellaro, E., Benetti, S., Mazzali, P.A., Manteca, J., Taubenberger, S., Elias-Rosa, N., Ferrando, R., Harutyunyan, A., Hentunen, V.P., Nissinen, M., Pian, E., Turatto, M., Zampieri, L., Smartt, S.J.: A low-energy core-collapse supernova without a hydrogen envelope. *Nature* **459**(7247), 674–677 (2009) <https://doi.org/10.1038/nature08023> [arXiv:0901.2074](https://arxiv.org/abs/0901.2074) [astro-ph.SR]
- [8] Moriya, T., Tominaga, N., Tanaka, M., Nomoto, K., Sauer, D.N., Mazzali, P.A., Maeda, K., Suzuki, T.: Fallback Supernovae: A Possible Origin of Peculiar Supernovae with Extremely Low Explosion Energies. *ApJ* **719**(2), 1445–1453 (2010) <https://doi.org/10.1088/0004-637X/719/2/1445> [arXiv:1006.5336](https://arxiv.org/abs/1006.5336) [astro-ph.HE]
- [9] Foley, R.J., McCully, C., Jha, S.W., Bildsten, L., Fong, W.-f., Narayan, G., Rest, A., Stritzinger, M.D.: Possible Detection of the Stellar Donor or Remnant for the Type Iax Supernova 2008ha. *ApJ* **792**(1), 29 (2014) <https://doi.org/10.1088/0004-637X/792/1/29> [arXiv:1408.1091](https://arxiv.org/abs/1408.1091) [astro-ph.HE]

[10] Phillips, M.M.: The Absolute Magnitudes of Type IA Supernovae. *ApJ* **413**, 105 (1993) <https://doi.org/10.1086/186970>

[11] Groot, P.J., Bloemen, S., Vreeswijk, P.M., van Roestel, J.C.J., Jonker, P.G., Nelemans, G., Klein-Wolt, M., Lepoole, R., Pieterse, D.L.A., Rodenhuis, M., Boland, W., Havercorn, M., Aerts, C., Bakker, R., Balster, H., Bekema, M., Dijkstra, E., Dolron, P., Elswijk, E., van Elteren, A., Engels, A., Fokker, M., de Haan, M., Hahn, F., ter Horst, R., Lesman, D., Kragt, J., Morren, J., Nillissen, H., Pessemier, W., Raskin, G., de Rijke, A., Scheers, L.H.A., Schuil, M., Timmer, S.T., Antunes Amaral, L., Arancibia-Rojas, E., Arcavi, I., Blagorodnova, N., Biswas, S., Breton, R.P., Dawson, H., Dayal, P., De Wet, S., Duffy, C., Faris, S., Fausnaugh, M., Gal-Yam, A., Geier, S., Horesh, A., Johnston, C., Katusiime, G., Kelley, C., Kosakowski, A., Kupfer, T., Leloudas, G., Levan, A., Modiano, D., Mogawana, O., Munday, J., Paice, J., Patat, F., Pelisoli, I., Ramsay, G., Ranaivomanana, P.T., Ruiz-Carmona, R., Schaffenroth, V., Scaringi, S., Stoppa, F., Street, R., Tranin, H., Uzundag, M., Valenti, S., Veresvarska, M., Vucković, M., Wichern, H.C.I., Wijers, R.A.M.J., Wijnands, R.A.D., Zimmerman, E.: The BlackGEM Telescope Array. I. Overview. *PASP* **136**(11), 115003 (2024) <https://doi.org/10.1088/1538-3873/ad8b6a> arXiv:2405.18923 [astro-ph.IM]

[12] Asquini, L., Landoni, M., Campana, S., Reguitti, A., Benetti, S., Farias, C.: Spectroscopic classification of AT 2024vjm and other optical transients during the tests of the SOXS Scheduler. *Transient Name Server AstroNote* **258**, 1 (2024)

[13] Srivastav, S., Smartt, S.J., Fulton, M., Smith, K.W., Young, D.R., Gillanders, J., Stoppa, F., Chen, T.W., Schmidt, B.P.: Reclassification of SN 2024vjm as a faint Iax supernova. *Transient Name Server AstroNote* **265**, 1 (2024)

[14] Foley, R.J., Chornock, R., Filippenko, A.V., Ganeshalingam, M., Kirshner, R.P., Li, W., Cenko, S.B., Challis, P.J., Friedman, A.S., Modjaz, M., Silverman, J.M., Wood-Vasey, W.M.: SN 2008ha: An Extremely Low Luminosity and Exceptionally Low Energy Supernova. *AJ* **138**(2), 376–391 (2009) <https://doi.org/10.1088/0004-6256/138/2/376> arXiv:0902.2794 [astro-ph.CO]

[15] Stritzinger, M.D., Hsiao, E., Valenti, S., Taddia, F., Rivera-Thorsen, T.J., Leloudas, G., Maeda, K., Pastorello, A., Phillips, M.M., Pignata, G., Baron, E., Burns, C.R., Contreras, C., Folatelli, G., Hamuy, M., Höflich, P., Morrell, N., Prieto, J.L., Benetti, S., Campillay, A., Haislip, J.B., LaClutze, A.P., Moore, J.P., Reichart, D.E.: Optical and near-IR observations of the faint and fast 2008ha-like supernova 2010ae. *A&A* **561**, 146 (2014) <https://doi.org/10.1051/0004-6361/201322889> arXiv:1311.4525 [astro-ph.HE]

[16] Srivastav, S., Smartt, S.J., Leloudas, G., Huber, M.E., Chambers, K., Malesani, D.B., Hjorth, J., Gillanders, J.H., Schultz, A., Sim, S.A., Auchettl, K., Fynbo, J.P.U., Gall, C., McBrien, O.R., Rest, A., Smith, K.W., Wojtak, R., Young, D.R.: The Lowest of the Low: Discovery of SN 2019gsc and the Nature of Faint

Iax Supernovae. *ApJ* **892**(2), 24 (2020) <https://doi.org/10.3847/2041-8213/ab76d5> arXiv:2001.09722 [astro-ph.HE]

- [17] Tomasella, L., Stritzinger, M., Benetti, S., Elias-Rosa, N., Cappellaro, E., Kankare, E., Lundqvist, P., Magee, M., Maguire, K., Pastorello, A., Prenite, S., Reguitti, A.: Observations of the low-luminosity Type Iax supernova 2019gsc: a fainter clone of SN 2008ha? *MNRAS* **496**(2), 1132–1143 (2020) <https://doi.org/10.1093/mnras/staa1611> arXiv:2002.00393 [astro-ph.SR]
- [18] Euclid Collaboration, Mellier, Y., Abdurro'uf, Acevedo Barroso, J.A., Achúcarro, A., Adamek, J., Adam, R., Addison, G.E., Aghanim, N., Aguena, M., Ajani, V., Akrami, Y., Al-Bahlawan, A., Alavi, A., Albuquerque, I.S., Alestas, G., Alguero, G., Allaoui, A., Allen, S.W., Allevato, V., Alonso-Tetilla, A.V., Altieri, B., Alvarez-Candal, A., Alvi, S., Amara, A., Amendola, L., Amiaux, J., Andika, I.T., Andreon, S., Andrews, A., Angora, G., Angulo, R.E., Annibali, F., Anselmi, A., Anselmi, S., Arcari, S., Archidiacono, M., Aricò, G., Arnaud, M., Arnouts, S., Asgari, M., Asorey, J., Atayde, L., Atek, H., Atrio-Barandela, F., Aubert, M., Aubourg, E., Auphan, T., Auricchio, N., Aussel, B., Aussel, H., Avelino, P.P., Avgoustidis, A., Avila, S., Awan, S., Azzollini, R., Baccigalupi, C., Bachelet, E., Bacon, D., Baes, M., Bagley, M.B., Bahr-Kalus, B., Balaguera-Antolinez, A., Balbinot, E., Balcells, M., Baldi, M., Baldry, I., Balestra, A., Ballardini, M., Ballester, O., Balogh, M., Bañados, E., Barbier, R., Bardelli, S., Baron, M., Barreiro, T., Barrena, R., Barriere, J.-C., Barros, B.J., Barthelemy, A., Bartolo, N., Basset, A., Battaglia, P., Battisti, A.J., Baugh, C.M., Baumont, L., Bazzanini, L., Beaulieu, J.-P., Beckmann, V., Belikov, A.N., Bel, J., Bellagamba, F., Bella, M., Bellini, E., Benabed, K., Bender, R., Benevento, G., Bennett, C.L., Benson, K., Bergamini, P., Bermejo-Climent, J.R., Bernardeau, F., Bertacca, D., Berthe, M., Berthier, J., Bethermin, M., Beutler, F., Bevillon, C., Bhargava, S., Bhatawdekar, R., Bianchi, D., Bisigello, L., Biviano, A., Blake, R.P., Blanchard, A., Blazek, J., Blot, L., Bosco, A., Bodendorf, C., Boenke, T., Böhringer, H., Boldrini, P., Bolzonella, M., Bonchi, A., Bonici, M., Bonino, D., Bonino, L., Bonvin, C., Bon, W., Booth, J.T., Borgani, S., Borlaff, A.S., Borsato, E., Bose, B., Botticella, M.T., Boucaud, A., Bouche, F., Boucher, J.S., Boutigny, D., Bouvard, T., Bouwens, R., Bouy, H., Bowler, R.A.A., Bozza, V., Bozzo, E., Branchini, E., Brando, G., Brau-Nogue, S., Brekke, P., Bremer, M.N., Brescia, M., Breton, M.-A., Brinchmann, J., Brinckmann, T., Brockley-Blatt, C., Brodwin, M., Brouard, L., Brown, M.L., Bruton, S., Bucko, J., Buddelmeijer, H., Buenadicha, G., Buitrago, F., Burger, P., Burigana, C., Busillo, V., Busonero, D., Cabanac, R., Cabayol-Garcia, L., Cagliari, M.S., Caillat, A., Caillat, L., Calabrese, M., Calabro, A., Calderone, G., Calura, F., Camacho Quevedo, B., Camera, S., Campos, L., Cañas-Herrera, G., Candini, G.P., Cantiello, M., Capobianco, V., Cappellaro, E., Cappelluti, N., Cappi, A., Caputi, K.I., Cara, C., Carbone, C., Cardone, V.F., Carella, E., Carlberg, R.G., Carle, M., Carminati, L., Caro, F., Carrasco, J.M., Carretero, J., Carrilho, P., Carron Duque, J., Carry, B.: Euclid: I. Overview of the Euclid mission. *A&A* **697**, 1 (2025) <https://doi.org/10.1051/0004-6361/202450810> arXiv:2405.13491 [astro-ph.CO]

[19] Hunt, L.K., Annibali, F., Cuillandre, J.-C., Ferguson, A.M.N., Jablonka, P., Larsen, S.S., Marleau, F.R., Schinnerer, E., Schirmer, M., Stone, C., Tortora, C., Saifollahi, T., Lançon, A., Bolzonella, M., Gwyn, S., Kluge, M., Laureijs, R., Carollo, D., Collins, M.L.M., Dimauro, P., Duc, P.-A., Erkal, D., Howell, J.M., Nally, C., Saremi, E., Scaramella, R., Belokurov, V., Conselice, C.J., Knapen, J.H., McConnachie, A.W., McDonald, I., Miro Carretero, J., Roman, J., Sauvage, M., Sola, E., Aghanim, N., Altieri, B., Andreon, S., Auricchio, N., Awan, S., Azzollini, R., Baldi, M., Balestra, A., Bardelli, S., Basset, A., Bender, R., Bonino, D., Branchini, E., Brescia, M., Brinchmann, J., Camera, S., Candini, G.P., Capobianco, V., Carbone, C., Carretero, J., Casas, S., Castellano, M., Cavuoti, S., Cimatti, A., Congedo, G., Conversi, L., Copin, Y., Corcione, L., Courbin, F., Courtois, H.M., Cropper, M., Da Silva, A., Degaudenz, H., De Lucia, G., Di Giorgio, A.M., Dinis, J., Dubath, F., Dupac, X., Dusini, S., Farina, M., Farrens, S., Ferriol, S., Fosalba, P., Frailis, M., Franceschi, E., Fumana, M., Galeotta, S., Garilli, B., George, K., Gillard, W., Gillis, B., Giocoli, C., Gómez-Alvarez, P., Granett, B.R., Grazian, A., Grupp, F., Guzzo, L., Haugan, S.V.H., Hoar, J., Hoekstra, H., Holliman, M.S., Holmes, W., Hook, I., Hormuth, F., Hornstrup, A., Hudelot, P., Jahnke, K., Keihänen, E., Kermiche, S., Kiessling, A., Kilbinger, M., Kitching, T., Kohley, R., Kubik, B., Kuijken, K., Kümmel, M., Kunz, M., Kurki-Suonio, H., Lahav, O., Le Mignant, D., Lilje, P.B., Lindholm, V., Lloro, I., Maiorano, E., Mansutti, O., Marggraf, O., Markovic, K., Martinet, N., Marulli, F., Massey, R., Maurogordato, S., McCracken, H.J., Medinaceli, E., Mei, S., Mellier, Y., Meneghetti, M., Merlin, E., Meylan, G., Moresco, M., Moscardini, L., Munari, E., Nakajima, R., Nichol, R.C., Niemi, S.-M., Nightingale, J.W., Padilla, C., Paltani, S., Pasian, F., Pedersen, K., Percival, W.J., Pettorino, V., Pires, S., Polenta, G., Poncet, M., Popa, L.A., Pozzetti, L., Racca, G.D., Raison, F., Rebolo, R., Refregier, A., Renzi, A., Rhodes, J., Riccio, G., Romelli, E., Roncarelli, M., Rossetti, E., Saglia, R., Sapone, D., Sartoris, B., Schneider, P., Schrabback, T., Scodéggi, M., Secroun, A., Seidel, G., Serrano, S., Sirignano, C., Sirri, G., Skottfelt, J., Stanco, L., Tallada-Crespí, P., Tavagnacco, D., Taylor, A.N., Teplitz, H.I., Tereno, I., Toledo-Moreo, R., Torradeflot, F., Tutusaus, I., Valentijn, E.A., Valenziano, L., Vassallo, T., Verdoes Kleijn, G., Veropalumbo, A., Wang, Y., Weller, J., Williams, O.R., Zamorani, G., Zucca, E., Burigana, C., Scottez, V., Miluzio, M., Simon, P., Mora, A., Martín-Fleitas, J., Scott, D.: Euclid: Early Release Observations – Deep anatomy of nearby galaxies. *A&A* **697**, 9 (2025) <https://doi.org/10.1051/0004-6361/202450781> arXiv:2405.13499 [astro-ph.GA]

[20] Euclid Early Release Observations <https://doi.org/10.57780/esa-qmocze3> (2024)

[21] Cuillandre, J.-C., Bertin, E., Bolzonella, M., Bouy, H., Gwyn, S., Isani, S., Kluge, M., Lai, O., Lançon, A., Lang, D.A., Laureijs, R., Saifollahi, T., Schirmer, M., Stone, C., Abdurro'uf, Aghanim, N., Altieri, B., Annibali, F., Atek, H., Awad, P., Baes, M., Bañados, E., Barrado, D., Belladitta, S., Belokurov, V., Boselli, A., Bournaud, F., Bovy, J., Bowler, R.A.A., Buenadicha, G., Buitrago, F., Cantiello,

M., Carollo, D., Codis, S., Collins, M.L.M., Congedo, G., Dalessandro, E., de Lapparent, V., De Paolis, F., Diego, J.M., Dimauro, P., Dinis, J., Dole, H., Duc, P.-A., Erkal, D., Ezziati, M., Ferguson, A.M.N., Ferré-Mateu, A., Franco, A., Gavazzi, R., George, K., Gillard, W., Golden-Marx, J.B., Goldman, B., Gonzalez, A.H., Habas, R., Hartley, W.G., Hatch, N.A., Kohley, R., Hoar, J., Howell, J.M., Hunt, L.K., Jablonka, P., Jauzac, M., Kang, Y., Knapen, J.H., Kneib, J.-P., Kuzma, P.B., Larsen, S.S., Marchal, O., Martín-Fleitas, J., Marcos-Arenal, P., Marleau, F.R., Martín, E.L., Massari, D., McConnachie, A.W., Meneghetti, M., Miluzio, M., Miro Carretero, J., Miyatake, H., Mondelin, M., Montes, M., Mora, A., Müller, O., Nally, C., Noeske, K., Nucita, A.A., Oesch, P.A., Oguri, M., Peletier, R.F., Poulain, M., Quilley, L., Racca, G.D., Rejkuba, M., Rhodes, J., Roccia, P.-F., Román, J., Sacquegna, S., Saremi, E., Scaramella, R., Schinnerer, E., Serjeant, S., Sola, E., Sorce, J.G., Tarsitano, F., Tereno, I., Toft, S., Tortora, C., Urbano, M., Venhola, A., Voggel, K., Weaver, J.R., Xu, X., Žerjal, M., Zöller, R., Andreon, S., Auricchio, N., Baccigalupi, C., Baldi, M., Balestra, A., Bardelli, S., Basset, A., Bender, R., Bodendorf, C., Branchini, E., Brau-Nogue, S., Brescia, M., Brinchmann, J., Camera, S., Capobianco, V., Carbone, C., Carretero, J., Casas, S., Castander, F.J., Castellano, M., Cavuoti, S., Cimatti, A., Conselice, C.J., Conversi, L., Copin, Y., Courbin, F., Courtois, H.M., Cropper, M., Cuby, J.-G., Da Silva, A., Degaudenzi, H., Di Giorgio, A.M., Douspis, M., Duncan, C.A.J., Dupac, X., Dusini, S., Fabricius, M., Farina, M., Farrens, S., Ferriol, S., Fosalba, P., Fotopoulou, S., Frailis, M., Franceschi, E., Galeotta, S., Garilli, B., Gillis, B., Giocoli, C., Gómez-Alvarez, P., Grazian, A., Grupp, F., Guzzo, L., Haugan, S.V.H., Hoekstra, H., Holmes, W., Hook, I., Hormuth, F., Hornstrup, A., Hudelot, P., Jahnke, K., Jhabvala, M., Keihänen, E., Kermiche, S., Kiessling, A., Kilbinger, M., Kitching, T., Kubik, B., Kuijken, K., Kümmel, M., Kunz, M., Kurki-Suonio, H., Lahav, O., Liebing, P., Ligori, S., Lilje, P.B., Lindholm, V., Lloro, I., Maino, D., Maiorano, E., Mansutti, O., Marggraf, O., Markovic, K., Martinet, N., Marulli, F., Massey, R.: Euclid: Early Release Observations – Programme overview and pipeline for compact- and diffuse-emission photometry. *A&A* **697**, 6 (2025) <https://doi.org/10.1051/0004-6361/202450803> [arXiv:2405.13496](https://arxiv.org/abs/2405.13496) [astro-ph.IM]

- [22] Schwab, M., Kwok, L.A., Jha, S.W., McCully, C., Graur, O., Foley, R.J., Camacho-Neves, Y., Newman, M.J.B., Larison, C., Sears, H.: The Remarkable Late-Time Flux Excess in Hubble Space Telescope Observations of the Type Iax Supernova 2012Z. *arXiv e-prints*, 2504-01063 (2025) <https://doi.org/10.48550/arXiv.2504.01063> [arXiv:2504.01063](https://arxiv.org/abs/2504.01063) [astro-ph.HE]
- [23] Kato, M., Hachisu, I.: V445 Puppis: Helium Nova on a Massive White Dwarf. *ApJ* **598**(2), 107–110 (2003) <https://doi.org/10.1086/380597> [arXiv:astro-ph/0310351](https://arxiv.org/abs/astro-ph/0310351) [astro-ph]
- [24] Foley, R.J., Van Dyk, S.D., Jha, S.W., Clubb, K.I., Filippenko, A.V., Mauerhan, J.C., Miller, A.A., Smith, N.: On the Progenitor System of the Type Iax Supernova 2014dt in M61. *ApJ* **798**(2), 37 (2015) <https://doi.org/10.1088/2041-8205/>

- [25] Eldridge, J.J., Stanway, E.R., Xiao, L., McClelland, L.A.S., Taylor, G., Ng, M., Greis, S.M.L., Bray, J.C.: Binary Population and Spectral Synthesis Version 2.1: Construction, Observational Verification, and New Results. *PASA* **34**, 058 (2017) <https://doi.org/10.1017/pasa.2017.51> arXiv:1710.02154 [astro-ph.SR]
- [26] Stanway, E.R., Eldridge, J.J.: Re-evaluating old stellar populations. *MNRAS* **479**(1), 75–93 (2018) <https://doi.org/10.1093/mnras/sty1353> arXiv:1805.08784 [astro-ph.GA]
- [27] Bacon, R., Accardo, M., Adjali, L., Anwand, H., Bauer, S., Biswas, I., Blaizot, J., Boudon, D., Brau-Nogue, S., Brinchmann, J., Caillier, P., Capoani, L., Carollo, C.M., Contini, T., Couderc, P., Daguisé, E., Deiries, S., Delabre, B., Dreizler, S., Dubois, J., Dupieux, M., Dupuy, C., Emsellem, E., Fechner, T., Fleischmann, A., François, M., Gallou, G., Gharsa, T., Glindemann, A., Gojak, D., Guiderdoni, B., Hansali, G., Hahn, T., Jarno, A., Kelz, A., Koehler, C., Kosmalski, J., Laurent, F., Le Floch, M., Lilly, S.J., Lizon, J.-L., Loupias, M., Manescau, A., Monstein, C., Nicklas, H., Olaya, J.-C., Pares, L., Pasquini, L., Pécontal-Rousset, A., Pelló, R., Petit, C., Popow, E., Reiss, R., Remillieux, A., Renault, E., Roth, M., Rupprecht, G., Serre, D., Schaye, J., Souail, G., Steinmetz, M., Streicher, O., Stuik, R., Valentin, H., Vernet, J., Weilbacher, P., Wisotzki, L., Yerle, N.: The MUSE second-generation VLT instrument. In: McLean, I.S., Ramsay, S.K., Takami, H. (eds.) *Ground-based and Airborne Instrumentation for Astronomy III*. Society of Photo-Optical Instrumentation Engineers (SPIE) Conference Series, vol. 7735, p. 773508 (2010). <https://doi.org/10.1117/12.856027>
- [28] Camacho-Neves, Y., Jha, S.W., Barna, B., Dai, M., Filippenko, A.V., Foley, R.J., Hosseinzadeh, G., Howell, D.A., Johansson, J., Kelly, P.L., Kerzendorf, W.E., Kwok, L.A., Larison, C., Magee, M.R., McCully, C., O'Brien, J.T., Pan, Y.-C., Pandya, V., Singhal, J., Stahl, B.E., Szalai, T., Wieber, M., Williamson, M.: Over 500 Days in the Life of the Photosphere of the Type Iax Supernova SN 2014dt. *ApJ* **951**(1), 67 (2023) <https://doi.org/10.3847/1538-4357/acd558> arXiv:2302.03105 [astro-ph.HE]
- [29] Sander, A.A.C., Hamann, W.-R., Todt, H., Hainich, R., Shenar, T., Ramachandran, V., Oskinova, L.M.: The Galactic WC and WO stars. The impact of revised distances from Gaia DR2 and their role as massive black hole progenitors. *A&A* **621**, 92 (2019) <https://doi.org/10.1051/0004-6361/201833712> arXiv:1807.04293 [astro-ph.GA]
- [30] Piersanti, L., Yungelson, L.R., Bravo, E.: Expected evolution of the binary system PTF J2238+743015.1. *A&A* **689**, 287 (2024) <https://doi.org/10.1051/0004-6361/202450008> arXiv:2405.17896 [astro-ph.SR]
- [31] Heber, U.: Hot Subdwarf Stars. arXiv e-prints, 2410–11663 (2024) <https://doi.org/10.48550/arXiv.2410.11663> arXiv:2410.11663 [astro-ph.SR]

- [32] Hillman, Y., Michaelis, A., Perets, H.B.: Helium Accumulation and Thermonuclear Instabilities on Accreting White Dwarfs: From Recurring Helium Novae to Type Ia Supernovae. arXiv e-prints, 2503–12586 (2025) <https://doi.org/10.48550/arXiv.2503.12586> arXiv:2503.12586 [astro-ph.SR]
- [33] Rajamuthukumar, A.S., Bauer, E.B., Justham, S., Pakmor, R., de Mink, S.E., Neunteufel, P.: Evolution of binaries containing a hot subdwarf and a white dwarf to double white dwarfs, and double detonation supernovae with hypervelocity runaway stars. *A&A* **704**, 82 (2025) <https://doi.org/10.1051/0004-6361/202554452> arXiv:2411.08099 [astro-ph.SR]
- [34] Arnett, W.D.: On the theory of type I supernovae. *ApJ* **230**, 37–40 (1979) <https://doi.org/10.1086/182957>
- [35] Arnett, W.D.: Type I supernovae. I - Analytic solutions for the early part of the light curve. *ApJ* **253**, 785–797 (1982) <https://doi.org/10.1086/159681>
- [36] Katz, B., Kushnir, D., Dong, S.: An exact integral relation between the Ni56 mass and the bolometric light curve of a type Ia supernova. arXiv e-prints, 1301–6766 (2013) <https://doi.org/10.48550/arXiv.1301.6766> arXiv:1301.6766 [astro-ph.HE]
- [37] Karambelkar, V.R., Kasliwal, M.M., Maguire, K., Anand, S.G., Andreoni, I., De, K., Drake, A., Duev, D.A., Graham, M.J., Kool, E.C., Laher, R.R., Magee, M.R., Mahabal, A.A., Medford, M.S., Perley, D., Rigault, M., Rusholme, B., Schulze, S., Sharma, Y., Sollerman, J., Tzanidakis, A., Walters, R., Yao, Y.: Faintest of Them All: ZTF 21aaoryiz/SN 2021fcg-Discovery of an Extremely Low Luminosity Type Iax Supernova. *ApJ* **921**(1), 6 (2021) <https://doi.org/10.3847/2041-8213/ac2e90> arXiv:2110.04306 [astro-ph.HE]
- [38] Stritzinger, M., Mazzali, P.A., Sollerman, J., Benetti, S.: Consistent estimates of ^{56}Ni yields for type Ia supernovae. *A&A* **460**(3), 793–798 (2006) <https://doi.org/10.1051/0004-6361:20065514> arXiv:astro-ph/0609232 [astro-ph]
- [39] Wygoda, N., Elbaz, Y., Katz, B.: Type Ia supernovae have two physical width-luminosity relations and they favour sub-Chandrasekhar and direct collision models - II. Colour evolution. *MNRAS* **484**(3), 3951–3967 (2019) <https://doi.org/10.1093/mnras/stz146> arXiv:1805.06907 [astro-ph.HE]
- [40] Sharon, A., Kushnir, D.: The γ -ray deposition histories of core-collapse supernovae. *MNRAS* **496**(4), 4517–4545 (2020) <https://doi.org/10.1093/mnras/staa1745> arXiv:2004.07244 [astro-ph.HE]
- [41] Singh, M., Sahu, D.K., Dastidar, R., Barna, B., Misra, K., Gangopadhyay, A., Howell, D.A., Jha, S.W., Im, H., Taggart, K., Andrews, J., Hiramatsu, D., Teja, R.S., Pellegrino, C., Foley, R.J., Joshi, A., Anupama, G.C., Bostroem, K.A., Burke, J., Camacho-Neves, Y., Dutta, A., Kwok, L.A., McCully, C., Pan, Y.-C.,

Siebert, M., Srivastav, S., Szalai, T., Swift, J.J., Yang, G., Zhou, H., DiLullo, N., Scheer, J.: Observational Properties of a Bright Type Iax SN 2018cni and a Faint Type Iax SN 2020kyg. *ApJ* **953**(1), 93 (2023) <https://doi.org/10.3847/1538-4357/acd559> arXiv:2305.12713 [astro-ph.HE]

[42] Guttman, O., Shenhar, B., Sarkar, A., Waxman, E.: The thermalization of γ -rays in radioactive expanding ejecta: a simple model and its application for Kilonovae and Ia SNe. *MNRAS* **533**(1), 994–1011 (2024) <https://doi.org/10.1093/mnras/stae1795> arXiv:2403.08769 [astro-ph.HE]

[43] Kwok, L.A., Singh, M., Jha, S.W., Blondin, S., Dastidar, R., Larison, C., Miller, A.A., Andrews, J.E., Andrews, M., Anupama, G.C., Auchettl, K., Bánredi, D., Barna, B., Bostroem, K.A., Brink, T.G., Cartier, R., Chen, P., Christy, C.T., Coulter, D.A., Covarrubias, S., Davis, K.W., Dickinson, C.B., Dong, Y., Farah, J.R., Filippenko, A.V., Flörs, A., Foley, R.J., Franz, N., Fremling, C., Galbany, L., Gangopadhyay, A., Garg, A., Garnavich, P., Gates, E.L., Graur, O., Gordon, A.C., Hiramatsu, D., Hoang, E., Howell, D.A., Hsu, B., Johansson, J., Joshi, A., Kahinga, L.A., Kaur, R., Kumar, S., Kumnurdmanee, P., Kuncarayakti, H., LeBaron, N., Liu, C., Maeda, K., Maguire, K., McCully, C., Mehta, D., Menotti, L.M., Metevier, A.J., Misra, K., Murphey, C.T., Newsome, M., Padilla Gonzalez, E., Patra, K.C., Pearson, J., Piro, A.L., Polin, A., Ravi, A.P., Rest, A., Rehemtulla, N., Meza Retamal, N., Robinson, O.M., Rojas-Bravo, C., Sahu, D.K., Sand, D.J., Schmidt, B.P., Schulze, S., Schwab, M., Shrestha, M., Siebert, M.R., Simha, S., Smith, N., Sollerman, J., Subrayan, B.M., Szalai, T., Taggart, K., Teja, R.S., Temim, T., Terwel, J.H., Tinyanont, S., Valenti, S., Anais Vilchez, J., Vinkó, J., Westerling, A.L., Yang, Y., Zheng, W.: JWST and Ground-based Observations of the Type Iax Supernovae SN 2024pxl and SN 2024vjm: Evidence for Weak Deflagration Explosions. *ApJ* **989**(2), 33 (2025) <https://doi.org/10.3847/2041-8213/adf062> arXiv:2505.02944 [astro-ph.HE]

[44] Foley, R.J., Challis, P.J., Chornock, R., Ganeshalingam, M., Li, W., Marion, G.H., Morrell, N.I., Pignata, G., Stritzinger, M.D., Silverman, J.M., Wang, X., Anderson, J.P., Filippenko, A.V., Freedman, W.L., Hamuy, M., Jha, S.W., Kirshner, R.P., McCully, C., Persson, S.E., Phillips, M.M., Reichart, D.E., Soderberg, A.M.: Type Iax Supernovae: A New Class of Stellar Explosion. *ApJ* **767**(1), 57 (2013) <https://doi.org/10.1088/0004-637X/767/1/57> arXiv:1212.2209 [astro-ph.SR]

[45] Kawabata, M., Maeda, K., Yamanaka, M., Nakaoka, T., Kawabata, K.S., Aoki, K., Anupama, G.C., Burgaz, U., Dutta, A., Isogai, K., Kino, M., Kojiguchi, N., Kota, I., Kumar, B., Kuroda, D., Maehara, H., Matsubayashi, K., Morihana, K., Murata, K.L., Ohshima, T., Otsuka, M., Sahu, D.K., Singh, A., Sugitani, K., Takahashi, J., Takagi, K.: Intermediate luminosity type Iax supernova 2019muj with narrow absorption lines: Long-lasting radiation associated with a possible bound remnant predicted by the weak deflagration model. *PASJ* **73**(5), 1295–1314 (2021) <https://doi.org/10.1093/pasj/psab075>

arXiv:2107.02822 [astro-ph.HE]

- [46] Maeda, K., Kawabata, M.: Properties of Type Iax Supernova 2019muj in the Late Phase: Existence, Nature, and Origin of the Iron-rich Dense Core. *ApJ* **941**(1), 15 (2022) <https://doi.org/10.3847/1538-4357/ac9df2> arXiv:2210.14390 [astro-ph.HE]
- [47] Kilic, M., Allende Prieto, C., Brown, W.R., Koester, D.: The Lowest Mass White Dwarf. *ApJ* **660**(2), 1451–1461 (2007) <https://doi.org/10.1086/514327> arXiv:astro-ph/0611498 [astro-ph]
- [48] Kumar, A., Sarangi, A.: Type Iax supernovae as a source of iron-rich silicate dust. arXiv e-prints, 2511–15349 (2025) <https://doi.org/10.48550/arXiv.2511.15349> arXiv:2511.15349 [astro-ph.SR]
- [49] Ivezić, Ž., Kahn, S.M., Tyson, J.A., Abel, B., Acosta, E., Allsman, R., Alonso, D., AlSayyad, Y., Anderson, S.F., Andrew, J., Angel, J.R.P., Angeli, G.Z., Ansari, R., Antilogus, P., Araujo, C., Armstrong, R., Arndt, K.T., Astier, P., Aubourg, É., Auza, N., Axelrod, T.S., Bard, D.J., Barr, J.D., Barrau, A., Bartlett, J.G., Bauer, A.E., Bauman, B.J., Baumont, S., Bechtol, E., Bechtol, K., Becker, A.C., Becla, J., Beldica, C., Bellavia, S., Bianco, F.B., Biswas, R., Blanc, G., Blazek, J., Blandford, R.D., Bloom, J.S., Bogart, J., Bond, T.W., Booth, M.T., Borgland, A.W., Borne, K., Bosch, J.F., Boutigny, D., Brackett, C.A., Bradshaw, A., Brandt, W.N., Brown, M.E., Bullock, J.S., Burchat, P., Burke, D.L., Cagnoli, G., Calabrese, D., Callahan, S., Callen, A.L., Carlin, J.L., Carlson, E.L., Chandrasekharan, S., Charles-Emerson, G., Chesley, S., Cheu, E.C., Chiang, H.-F., Chiang, J., Chirino, C., Chow, D., Ciardi, D.R., Claver, C.F., Cohen-Tanugi, J., Cockrum, J.J., Coles, R., Connolly, A.J., Cook, K.H., Cooray, A., Covey, K.R., Cribbs, C., Cui, W., Cutri, R., Daly, P.N., Daniel, S.F., Daruich, F., Daubard, G., Daues, G., Dawson, W., Delgado, F., Dellapenna, A., de Peyster, R., de Val-Borro, M., Digel, S.W., Doherty, P., Dubois, R., Dubois-Felsmann, G.P., Durech, J., Economou, F., Eifler, T., Eracleous, M., Emmons, B.L., Fausti Neto, A., Ferguson, H., Figueroa, E., Fisher-Levine, M., Focke, W., Foss, M.D., Frank, J., Freemon, M.D., Gangler, E., Gawiser, E., Geary, J.C., Gee, P., Geha, M., Gessner, C.J.B., Gibson, R.R., Gilmore, D.K., Glanzman, T., Glick, W., Goldina, T., Goldstein, D.A., Goodenow, I., Graham, M.L., Gressler, W.J., Gris, P., Guy, L.P., Guyonnet, A., Haller, G., Harris, R., Haskell, P.A., Haupt, J., Hernandez, F., Herrmann, S., Hileman, E., Hoblitt, J., Hodgson, J.A., Hogan, C., Howard, J.D., Huang, D., Huffer, M.E., Ingraham, P., Innes, W.R., Jacoby, S.H., Jain, B., Jammes, F., Jee, M.J., Jenness, T., Jernigan, G., Jevremović, D., Johns, K., Johnson, A.S., Johnson, M.W.G., Jones, R.L., Juramy-Gilles, C., Jurić, M., Kalirai, J.S., Kallivayalil, N.J., Kalmbach, B., Kantor, J.P., Karst, P., Kasliwal, M.M., Kelly, H., Kessler, R., Kinnison, V., Kirkby, D., Knox, L., Kotov, I.V., Krabbendam, V.L., Krughoff, K.S., Kubánek, P., Kuczewski, J., Kulkarni, S., Ku, J., Kurita, N.R., Lage, C.S., Lambert, R., Lange, T., Langton, J.B., Le Guillou, L., Levine, D., Liang, M., Lim, K.-T.,

Lintott, C.J., Long, K.E., Lopez, M., Lotz, P.J., Lupton, R.H., Lust, N.B., MacArthur, L.A., Mahabal, A., Mandelbaum, R., Markiewicz, T.W., Marsh, D.S., Marshall, P.J., Marshall, S., May, M., McKercher, R., McQueen, M., Meyers, J., Migliore, M., Miller, M., Mills, D.J.: LSST: From Science Drivers to Reference Design and Anticipated Data Products. *ApJ* **873**(2), 111 (2019) <https://doi.org/10.3847/1538-4357/ab042c> arXiv:0805.2366 [astro-ph]

[50] Schlieder, J.E., Barclay, T., Barnes, A., Bray, E., Choi, A., Crome, B., Delker, T., Finch, T., Frater, E.H., Hill, R.J., Kruk, J., Lasco, J., Louie, D.R., Malhotra, S., McEnery, J.E., Mosby, G., Paine, J., Perkins, J.S., Rauscher, B.J., Rhoads, J.E., Rizzo, M., Sabatke, D., Schweickart, R., Shukis, D., Switzer, E.R., Wollack, E.J., Zellem, R.T., Zimmerman, N.T.: Survey science with the Nancy Grace Roman Space Telescope Wide Field Instrument. In: Coyle, L.E., Matsuura, S., Perrin, M.D. (eds.) *Space Telescopes and Instrumentation 2024: Optical, Infrared, and Millimeter Wave*. Society of Photo-Optical Instrumentation Engineers (SPIE) Conference Series, vol. 13092, p. 130920 (2024). <https://doi.org/10.1117/12.3020622>

[51] Krisciunas, K., Contreras, C., Burns, C.R., Phillips, M.M., Stritzinger, M.D., Morrell, N., Hamuy, M., Anais, J., Boldt, L., Busta, L., Campillay, A., Castellón, S., Folatelli, G., Freedman, W.L., González, C., Hsiao, E.Y., Krzeminski, W., Persson, S.E., Roth, M., Salgado, F., Serón, J., Suntzeff, N.B., Torres, S., Filippenko, A.V., Li, W., Madore, B.F., DePoy, D.L., Marshall, J.L., Rheault, J.-P., Villanueva, S.: The Carnegie Supernova Project. I. Third Photometry Data Release of Low-redshift Type Ia Supernovae and Other White Dwarf Explosions. *AJ* **154**(5), 211 (2017) <https://doi.org/10.3847/1538-3881/aa8df0> arXiv:1709.05146 [astro-ph.IM]

[52] Anand, G.S., Lee, J.C., Van Dyk, S.D., Leroy, A.K., Rosolowsky, E., Schinnerer, E., Larson, K., Kourkchi, E., Kreckel, K., Scheuermann, F., Rizzi, L., Thilker, D., Tully, R.B., Bigiel, F., Blanc, G.A., Boquien, M., Chandar, R., Dale, D., Emsellem, E., Deger, S., Glover, S.C.O., Grasha, K., Groves, B., S. Klessen, R., Kruijssen, J.M.D., Querejeta, M., Sánchez-Blázquez, P., Schruba, A., Turner, J., Ubeda, L., Williams, T.G., Whitmore, B.: Distances to PHANGS galaxies: New tip of the red giant branch measurements and adopted distances. *MNRAS* **501**(3), 3621–3639 (2021) <https://doi.org/10.1093/mnras/staa3668> arXiv:2012.00757 [astro-ph.GA]

[53] <https://ned.ipac.caltech.edu/>. NASA Extragalactic Database

[54] Schlegel, D.J., Finkbeiner, D.P., Davis, M.: Maps of Dust Infrared Emission for Use in Estimation of Reddening and Cosmic Microwave Background Radiation Foregrounds. *ApJ* **500**(2), 525–553 (1998) <https://doi.org/10.1086/305772> arXiv:astro-ph/9710327 [astro-ph]

[55] Schlafly, E.F., Finkbeiner, D.P.: Measuring Reddening with Sloan Digital Sky

Survey Stellar Spectra and Recalibrating SFD. *ApJ* **737**(2), 103 (2011) <https://doi.org/10.1088/0004-637X/737/2/103> arXiv:1012.4804 [astro-ph.GA]

- [56] Poznanski, D., Prochaska, J.X., Bloom, J.S.: An empirical relation between sodium absorption and dust extinction. *MNRAS* **426**(2), 1465–1474 (2012) <https://doi.org/10.1111/j.1365-2966.2012.21796.x> arXiv:1206.6107 [astro-ph.IM]
- [57] Arsenault, R., Madec, P.-Y., Hubin, N., Paufique, J., Stroebele, S., Soenke, C., Donaldson, R., Fedrigo, E., Oberti, S., Tordo, S., Downing, M., Kiekebusch, M., Conzelmann, R., Duchateau, M., Jost, A., Hackenberg, W., Bonaccini Calia, D., Delabre, B., Stuik, R., Biasi, R., Gallieni, D., Lazzarini, P., Lelouarn, M., Gindeman, A.: ESO adaptive optics facility. In: Hubin, N., Max, C.E., Wizinowich, P.L. (eds.) Adaptive Optics Systems. Society of Photo-Optical Instrumentation Engineers (SPIE) Conference Series, vol. 7015, p. 701524 (2008). <https://doi.org/10.1117/12.790359>
- [58] Ströbele, S., La Penna, P., Arsenault, R., Conzelmann, R.D., Delabre, B., Duchateau, M., Dorn, R., Fedrigo, E., Hubin, N., Quentin, J., Jolley, P., Kiekebusch, M., Kirchbauer, J.P., Klein, B., Kolb, J., Kuntschner, H., Le Louarn, M., Lizon, J.L., Madec, P.-Y., Pettazzi, L., Soenke, C., Tordo, S., Vernet, J., Muradore, R.: GALACSI system design and analysis. In: Ellerbroek, B.L., Marchetti, E., Véran, J.-P. (eds.) Adaptive Optics Systems III. Society of Photo-Optical Instrumentation Engineers (SPIE) Conference Series, vol. 8447, p. 844737 (2012). <https://doi.org/10.1117/12.926110>
- [59] Lyman, J.D., Taddia, F., Stritzinger, M.D., Galbany, L., Leloudas, G., Anderson, J.P., Eldridge, J.J., James, P.A., Krühler, T., Levan, A.J., Pignata, G., Stanway, E.R.: Investigating the diversity of supernovae type Iax: a MUSE and NOT spectroscopic study of their environments. *MNRAS* **473**(1), 1359–1387 (2018) <https://doi.org/10.1093/mnras/stx2414> arXiv:1707.04270 [astro-ph.HE]
- [60] Curti, M., Cresci, G., Mannucci, F., Marconi, A., Maiolino, R., Esposito, S.: New fully empirical calibrations of strong-line metallicity indicators in star-forming galaxies. *MNRAS* **465**(2), 1384–1400 (2017) <https://doi.org/10.1093/mnras/stw2766> arXiv:1610.06939 [astro-ph.GA]
- [61] Asplund, M., Grevesse, N., Sauval, A.J., Scott, P.: The Chemical Composition of the Sun. *ARA&A* **47**(1), 481–522 (2009) <https://doi.org/10.1146/annurev.astro.46.060407.145222> arXiv:0909.0948 [astro-ph.SR]
- [62] Yamanaka, M., Maeda, K., Kawabata, K.S., Tanaka, M., Tominaga, N., Akitaya, H., Nagayama, T., Kuroda, D., Takahashi, J., Saito, Y., Yanagisawa, K., Fukui, A., Miyanoshita, R., Watanabe, M., Arai, A., Isogai, M., Hattori, T., Hanayama, H., Itoh, R., Ui, T., Takaki, K., Ueno, I., Yoshida, M., Ali, G.B., Essam, A., Ozaki, A., Nakao, H., Hamamoto, K., Nogami, D., Morokuma, T., Oasa, Y., Izumiura, H., Sekiguchi, K.: OISTER Optical and Near-Infrared Observations

of Type Iax Supernova 2012Z. *ApJ* **806**(2), 191 (2015) <https://doi.org/10.1088/0004-637X/806/2/191> arXiv:1505.01593 [astro-ph.SR]

- [63] Magee, M.R., Kotak, R., Sim, S.A., Wright, D., Smartt, S.J., Berger, E., Chornock, R., Foley, R.J., Howell, D.A., Kaiser, N., Magnier, E.A., Wainscoat, R., Waters, C.: Growing evidence that SNe Iax are not a one-parameter family. The case of PS1-12bwh. *A&A* **601**, 62 (2017) <https://doi.org/10.1051/0004-6361/201629643> arXiv:1701.05459 [astro-ph.HE]
- [64] Jonas, J., MeerKAT Team: The MeerKAT Radio Telescope. In: MeerKAT Science: On the Pathway to the SKA, p. 1 (2016). <https://doi.org/10.22323/1.277.0001>
- [65] Ofek, E.O.: MATLAB package for astronomy and astrophysics (2014)
- [66] Ofek, E.O.: A Code for Robust Astrometric Solution of Astronomical Images. *PASP* **131**(999), 054504 (2019) <https://doi.org/10.1088/1538-3873/ab04df> arXiv:1903.02015 [astro-ph.IM]
- [67] Soumagnac, M.T., Ofek, E.O.: catsHTM: A Tool for Fast Accessing and Cross-matching Large Astronomical Catalogs. *PASP* **130**(989), 075002 (2018) <https://doi.org/10.1088/1538-3873/aac410> arXiv:1805.02666 [astro-ph.IM]
- [68] Ofek, E.O., Ben-Ami, S., Polishook, D., Segre, E., Blumenzweig, A., *et al.*: The Large Array Survey Telescope-System Overview and Performances. *PASP* **135**(1048), 065001 (2023) <https://doi.org/10.1088/1538-3873/acd8f0> arXiv:2304.04796 [astro-ph.IM]
- [69] Ben-Ami, S., Ofek, E.O., Polishook, D., Franckowiak, A., Hallakoun, N., *et al.*: The Large Array Survey Telescope – Science Goals. *arXiv e-prints*, 2304–02719 (2023) <https://doi.org/10.48550/arXiv.2304.02719> arXiv:2304.02719 [astro-ph.IM]
- [70] Shvartzvald, Y., Waxman, E., Gal-Yam, A., Ofek, E.O., Ben-Ami, S., Berge, D., Kowalski, M., Bühler, R., Worm, S., Rhoads, J.E., Arcavi, I., Maoz, D., Polishook, D., Stone, N., Trakhtenbrot, B., Ackermann, M., Aharanson, O., Birnholtz, O., Chelouche, D., Guetta, D., Hallakoun, N., Horesh, A., Kushnir, D., Mazeh, T., Nordin, J., Ofir, A., Ohm, S., Parsons, D., Pe'er, A., Perets, H.B., Perdelwitz, V., Poznanski, D., Sadeh, I., Sagiv, I., Shahaf, S., Soumagnac, M., Tal-Or, L., Van Santen, J., Zackay, B., Guttman, O., Rekhi, P., Townsend, A., Weinstein, A., Wold, I.: ULTRASAT: A wide-field time-domain UV space telescope. *arXiv e-prints*, 2304–14482 (2023) <https://doi.org/10.48550/arXiv.2304.14482> arXiv:2304.14482 [astro-ph.IM]
- [71] Gaia Collaboration, Prusti, T., de Bruijne, J.H.J., Brown, A.G.A., Vallenari, A., Babusiaux, C., Bailer-Jones, C.A.L., Bastian, U., Biermann, M., Evans, D.W., Eyer, L., Jansen, F., Jordi, C., Klioner, S.A., Lammers, U., Lindegren, L., Luri,

X., Mignard, F., Milligan, D.J., Panem, C.e.a.: The Gaia mission. *A&A* **595**, 1 (2016) <https://doi.org/10.1051/0004-6361/201629272> arXiv:1609.04153 [astro-ph.IM]

[72] Gaia Collaboration: VizieR Online Data Catalog: Gaia DR3 Part 1. Main source (Gaia Collaboration, 2022). *VizieR Online Data Catalog*, 355 (2022)

[73] Bertin, E., Arnouts, S.: SExtractor: Software for source extraction. *A&AS* **117**, 393–404 (1996) <https://doi.org/10.1051/aas:1996164>

[74] Bradley, L., Sipőcz, B., Robitaille, T., Tollerud, E., Vinícius, Z., Deil, C., Barbary, K., Wilson, T.J., Busko, I., Donath, A., Günther, H.M., Cara, M., Lim, P.L., Meßlinger, S., Burnett, Z., Conseil, S., Droettboom, M., Bostroem, A., Bray, E.M., Bratholm, L.A., Jamieson, W., Ginsburg, A., Barentsen, G., Craig, M., Pascual, S., Rathi, S., Perrin, M., Morris, B.M.: Astropy/photutils: 2.2.0. <https://doi.org/10.5281/zenodo.14889440> . <https://doi.org/10.5281/zenodo.14889440>

[75] Woudt, P.A., Steeghs, D., Karovska, M., Warner, B., Groot, P.J., Nelemans, G., Roelofs, G.H.A., Marsh, T.R., Nagayama, T., Smits, D.P., O'Brien, T.: The Expanding Bipolar Shell of the Helium Nova V445 Puppis. *ApJ* **706**(1), 738–746 (2009) <https://doi.org/10.1088/0004-637X/706/1/738> arXiv:0910.1069 [astro-ph.SR]

[76] Geier, S., Marsh, T.R., Wang, B., Dunlap, B., Barlow, B.N., Schaffenroth, V., Chen, X., Irrgang, A., Maxted, P.F.L., Ziegerer, E., Kupfer, T., Miszalski, B., Heber, U., Han, Z., Shporer, A., Telting, J.H., Gänsicke, B.T., Østensen, R.H., O'Toole, S.J., Napiwotzki, R.: A progenitor binary and an ejected mass donor remnant of faint type Ia supernovae. *A&A* **554**, 54 (2013) <https://doi.org/10.1051/0004-6361/201321395> arXiv:1304.4452 [astro-ph.SR]

[77] Kupfer, T., van Roestel, J., Brooks, J., Geier, S., Marsh, T.R., Groot, P.J., Bloemen, S., Prince, T.A., Bellm, E., Heber, U., Bildsten, L., Miller, A.A., Dyer, M.J., Dhillon, V.S., Green, M., Irawati, P., Laher, R., Littlefair, S.P., Shupe, D.L., Steidel, C.C., Rattansoon, S., Pettini, M.: PTF1 J082340.04+081936.5: A Hot Subdwarf B Star with a Low-mass White Dwarf Companion in an 87-minute Orbit. *ApJ* **835**(2), 131 (2017) <https://doi.org/10.3847/1538-4357/835/2/131> arXiv:1612.02019 [astro-ph.SR]

[78] Kupfer, T., Ramsay, G., van Roestel, J., Brooks, J., MacFarlane, S.A., Toma, R., Groot, P.J., Woudt, P.A., Bildsten, L., Marsh, T.R., Green, M.J., Breedt, E., Kilkenny, D., Freudenthal, J., Geier, S., Heber, U., Bagnulo, S., Blagorodnova, N., Buckley, D.A.H., Dhillon, V.S., Kulkarni, S.R., Lunnan, R., Prince, T.A.: The OmegaWhite Survey for Short-period Variable Stars. V. Discovery of an Ultracompact Hot Subdwarf Binary with a Compact Companion in a 44-minute Orbit. *ApJ* **851**(1), 28 (2017) <https://doi.org/10.3847/1538-4357/aa9522> arXiv:1710.07287 [astro-ph.SR]

- [79] Kupfer, T., Bauer, E.B., Marsh, T.R., van Roestel, J., Bellm, E.C., Burdge, K.B., Coughlin, M.W., Fuller, J., Hermes, J., Bildsten, L., Kulkarni, S.R., Prince, T.A., Szkody, P., Dhillon, V.S., Murawski, G., Burruss, R., Dekany, R., Delacroix, A., Drake, A.J., Duev, D.A., Feeney, M., Graham, M.J., Kaplan, D.L., Laher, R.R., Littlefair, S.P., Masci, F.J., Riddle, R., Rusholme, B., Serabyn, E., Smith, R.M., Shupe, D.L., Soumagnac, M.T.: The First Ultracompact Roche Lobe-Filling Hot Subdwarf Binary. *ApJ* **891**(1), 45 (2020) <https://doi.org/10.3847/1538-4357/ab72ff> arXiv:2002.01485 [astro-ph.SR]
- [80] Kupfer, T., Bauer, E.B., Burdge, K.B., Roestel, J.v., Bellm, E.C., Fuller, J., Hermes, J., Marsh, T.R., Bildsten, L., Kulkarni, S.R., Phinney, E.S., Prince, T.A., Szkody, P., Yao, Y., Irrgang, A., Heber, U., Schneider, D., Dhillon, V.S., Murawski, G., Drake, A.J., Duev, D.A., Feeney, M., Graham, M.J., Laher, R.R., Littlefair, S.P., Mahabal, A.A., Masci, F.J., Porter, M., Reiley, D., Rodriguez, H., Rusholme, B., Shupe, D.L., Soumagnac, M.T.: A New Class of Roche Lobe-filling Hot Subdwarf Binaries. *ApJ* **898**(1), 25 (2020) <https://doi.org/10.3847/2041-8213/aba3c2> arXiv:2007.05349 [astro-ph.SR]
- [81] Pelisoli, I., Neunteufel, P., Geier, S., Kupfer, T., Heber, U., Irrgang, A., Schneider, D., Bastian, A., van Roestel, J., Schaffenroth, V., Barlow, B.N.: A hot subdwarf-white dwarf super-Chandrasekhar candidate supernova Ia progenitor. *Nature Astronomy* **5**, 1052–1061 (2021) <https://doi.org/10.1038/s41550-021-01413-0> arXiv:2107.09074 [astro-ph.SR]
- [82] Kupfer, T., Bauer, E.B., van Roestel, J., Bellm, E.C., Bildsten, L., Fuller, J., Prince, T.A., Heber, U., Geier, S., Green, M.J., Kulkarni, S.R., Bloemen, S., Laher, R.R., Rusholme, B., Schneider, D.: Discovery of a Double-detonation Thermonuclear Supernova Progenitor. *ApJ* **925**(2), 12 (2022) <https://doi.org/10.3847/2041-8213/ac48f1> arXiv:2110.11974 [astro-ph.SR]
- [83] Yang, M., Yuan, H., Bai, Z., Li, Z., He, Y., Huang, X., Dong, Y., Wang, M., Chen, X., Wang, J., Cheng, Y., Zhang, H.: LAMOST J171013+532646: A detached short-period noneclipsing hot subdwarf + white dwarf binary. *A&A* **693**, 322 (2025) <https://doi.org/10.1051/0004-6361/202451415> arXiv:2412.02356 [astro-ph.SR]
- [84] Stringer, E.: (in prep.)
- [85] Pedregosa, F., Varoquaux, G., Gramfort, A., Michel, V., Thirion, B., Grisel, O., Blondel, M., Prettenhofer, P., Weiss, R., Dubourg, V., Vanderplas, J., Passos, A., Cournapeau, D., Brucher, M., Perrot, M., Duchesnay, E.: Scikit-learn: Machine learning in Python. *Journal of Machine Learning Research* **12**, 2825–2830 (2011)
- [86] Pastorello, A., Fraser, M.: Supernova impostors and other gap transients. *Nature Astronomy* **3**, 676–679 (2019) <https://doi.org/10.1038/s41550-019-0809-9> arXiv:1908.02323 [astro-ph.SR]

[87] Kulkarni, S.R., Ofek, E.O., Rau, A., Cenko, S.B., Soderberg, A.M., Fox, D.B., Gal-Yam, A., Capak, P.L., Moon, D.S., Li, W., Filippenko, A.V., Egami, E., Kartaltepe, J., Sanders, D.B.: An unusually brilliant transient in the galaxy M85. *Nature* **447**(7143), 458–460 (2007) <https://doi.org/10.1038/nature05822> [arXiv:0705.3668](https://arxiv.org/abs/0705.3668) [astro-ph]

[88] Pastorello, A., Della Valle, M., Smartt, S.J., Zampieri, L., Benetti, S., Cappellaro, E., Mazzali, P.A., Patat, F., Spiro, S., Turatto, M., Valenti, S.: A very faint core-collapse supernova in M85. *Nature* **449**(7164), 1–2 (2007) <https://doi.org/10.1038/nature06282> [arXiv:0710.3753](https://arxiv.org/abs/0710.3753) [astro-ph]

[89] Magee, M.R., Killestein, T.L., Pursiainen, M., Godson, B., Jarvis, D., Jiménez-Palau, C., Lyman, J.D., Steeghs, D., Warwick, B., Anderson, J.P., Butterley, T., Chen, T.-W., Dhillon, V.S., Galbany, L., González-Gaitán, S., Gromadzki, M., Inserra, C., Kelsey, L., Kumar, A., Leloudas, G., Mattila, S., Moran, S., Müller-Bravo, T.E., Noysena, K., Ramsay, G., Srivastav, S., Starling, R., Wilson, R.W., Young, D.R., Ackley, K., Breton, R.P., Casares Velázquez, J., Dyer, M.J., Galloway, D.K., Kankare, E., Kotak, R., Nuttall, L.K., O'Neill, D., Pessi, P., Pollacco, D., Ulaczyk, K., Yaron, O.: SN 2024bfu, SN 2025qe, and the early light curves of type Iax supernovae. *MNRAS* **543**(4), 3731–3753 (2025) <https://doi.org/10.1093/mnras/staf1675> [arXiv:2506.02118](https://arxiv.org/abs/2506.02118) [astro-ph.HE]

[90] Stritzinger, M.D., Valenti, S., Hoefflich, P., Baron, E., Phillips, M.M., Taddia, F., Foley, R.J., Hsiao, E.Y., Jha, S.W., McCully, C., Pandya, V., Simon, J.D., Benetti, S., Brown, P.J., Burns, C.R., Campillay, A., Contreras, C., Förster, F., Holmbo, S., Marion, G.H., Morrell, N., Pignata, G.: Comprehensive observations of the bright and energetic Type Iax SN 2012Z: Interpretation as a Chandrasekhar mass white dwarf explosion. *A&A* **573**, 2 (2015) <https://doi.org/10.1051/0004-6361/201424168> [arXiv:1408.1093](https://arxiv.org/abs/1408.1093) [astro-ph.HE]

[91] Tomasella, L., Cappellaro, E., Benetti, S., Pastorello, A., Hsiao, E.Y., Sand, D.J., Stritzinger, M., Valenti, S., McCully, C., Arcavi, I., Elias-Rosa, N., Harmanen, J., Harutyunyan, A., Hosseinzadeh, G., Howell, D.A., Kankare, E., Morales-Garoffolo, A., Taddia, F., Tartaglia, L., Terreran, G., Turatto, M.: Optical and near-infrared observations of SN 2014ck: an outlier among the Type Iax supernovae. *MNRAS* **459**(1), 1018–1038 (2016) <https://doi.org/10.1093/mnras/stw696> [arXiv:1603.07084](https://arxiv.org/abs/1603.07084) [astro-ph.HE]

[92] Barna, B., Szalai, T., Jha, S.W., Camacho-Neves, Y., Kwok, L., Foley, R.J., Kilpatrick, C.D., Coulter, D.A., Dimitriadis, G., Rest, A., Rojas-Bravo, C., Siebert, M.R., Brown, P.J., Burke, J., Padilla Gonzalez, E., Hiramatsu, D., Howell, D.A., McCully, C., Pellegrino, C., Dobson, M., Smartt, S.J., Swift, J.J., Stacey, H., Rahman, M., Sand, D.J., Andrews, J., Wyatt, S., Hsiao, E.Y., Anderson, J.P., Chen, T.-W., Della Valle, M., Galbany, L., Gromadzki, M., Inserra, C., Lyman, J., Magee, M., Maguire, K., Müller-Bravo, T.E., Nicholl, M., Srivastav, S., Williams, S.C.: SN 2019muj - a well-observed Type Iax supernova

that bridges the luminosity gap of the class. *MNRAS* **501**(1), 1078–1099 (2021) <https://doi.org/10.1093/mnras/staa3543> arXiv:2011.03068 [astro-ph.HE]

- [93] Singh, M., Kwok, L.A., Jha, S.W., Dastidar, R., Larison, C., Filippenko, A.V., Andrews, J.E., Andrews, M., Anupama, G.C., Arunachalam, P., Auchettl, K., BÁnhidi, D., Barna, B., Bostroem, K.A., Brink, T.G., Cartier, R., Chen, P., Christy, C.T., Coulter, D.A., Covarrubias, S., Davis, K.W., Dickinson, C.B., Dong, Y., Farah, J., FlÖrs, A., Foley, R.J., Franz, N., Fremling, C., Galbany, L., Gangopadhyay, A., Garg, A., Gates, E.L., Graur, O., Gordon, A.C., Hiramatsu, D., Hoang, E., Howell, D.A., Hsu, B., Johansson, J., Joshi, A., Kahinga, L.A., Kaur, R., Kumar, S., Kumnurdmanee, P., Kuncarayakti, H., Lebaron, N., Lidman, C., Liu, C., Maeda, K., Maguire, K., Martin, B., McCully, C., Mehta, D., Menotti, L.M., Metevier, A.J., Miller, A.A., Misra, K., Tanner Murphey, C., Newsome, M., Padilla Gonzalez, E., Patra, K.C., Pearson, J., Piro, A.L., Polin, A., Ravi, A.P., Rest, A., Rehemtulla, N., Meza Reta mal, N., Robinson, O.M., Rojas-Bravo, C., Sahu, D.K., Sand, D.J., Schmidt, B.P., Schulze, S., Schwab, M., Shrestha, M., Siebert, M.R., Simha, S., Smith, N., Sollerman, J., Srivastav, S., Subrayan, B.M., Szalai, T., Taggart, K., Singh Teja, R., Terwel, J.H., Tinyanont, S., Valenti, S., VinkÓ, J., Westerling, A.L., Yang, Y., Zheng, W.: Photometry and Spectroscopy of SN 2024pxl: A Luminosity Link Among Type Iax Supernovae. arXiv e-prints, 2505–02943 (2025) <https://doi.org/10.48550/arXiv.2505.02943> arXiv:2505.02943 [astro-ph.HE]
- [94] Magee, M.R., Kotak, R., Sim, S.A., Kromer, M., Rabinowitz, D., Smartt, S.J., Baltay, C., Campbell, H.C., Chen, T.-W., Fink, M., Gal-Yam, A., Galbany, L., Hillebrandt, W., Inserra, C., Kankare, E., Le Guillou, L., Lyman, J.D., Maguire, K., Pakmor, R., Röpke, F.K., Ruiter, A.J., Seitenzahl, I.R., Sullivan, M., Valenti, S., Young, D.R.: The type Iax supernova, SN 2015H. A white dwarf deflagration candidate. *A&A* **589**, 89 (2016) <https://doi.org/10.1051/0004-6361/201528036> arXiv:1603.04728 [astro-ph.HE]
- [95] Hoogendam, W.B., Ashall, C., Jones, D.O., Shappee, B.J., Tucker, M.A., Huber, M.E., Auchettl, K., Desai, D.D., Do, A., Hinkle, J.T., Kong, M.Y., Romagnoli, S., Shi, J., Syncatto, A., Kilpatrick, C.D.: Early and Extensive Ultraviolet through Near Infrared Observations of the Intermediate-luminosity Type Iax Supernovae 2024pxl. *ApJ* **988**(2), 209 (2025) <https://doi.org/10.3847/1538-4357/ade787> arXiv:2505.04610 [astro-ph.HE]
- [96] Kawabata, M., Kawabata, K.S., Maeda, K., Yamanaka, M., Nakaoka, T., Takaki, K., Fukushima, D., Kojiguchi, N., Masumoto, K., Matsumoto, K., Akitaya, H., Itoh, R., Kanda, Y., Moritani, Y., Takata, K., Uemura, M., Ui, T., Yoshida, M., Hattori, T., Lee, C.-H., Tominaga, N., Nomoto, K.: Extended optical/NIR observations of Type Iax supernova 2014dt: Possible signatures of a bound remnant. *PASJ* **70**(6), 111 (2018) <https://doi.org/10.1093/pasj/psy116> arXiv:1810.00922 [astro-ph.HE]

[97] Swartz, D.A., Sutherland, P.G., Harkness, R.P.: Gamma-Ray Transfer and Energy Deposition in Supernovae. *ApJ* **446**, 766 (1995) <https://doi.org/10.1086/175834> arXiv:astro-ph/9501005 [astro-ph]

[98] Junde, H., Su, H., Dong, Y.: Nuclear Data Sheets for $A = 56$. Nuclear Data Sheets **112**(6), 1513–1645 (2011) <https://doi.org/10.1016/j.nds.2011.04.004>

[99] Jeffery, D.J.: Radioactive Decay Energy Deposition in Supernovae and the Exponential/Quasi-Exponential Behavior of Late-Time Supernova Light Curves. arXiv e-prints, 9907015 (1999) <https://doi.org/10.48550/arXiv.astro-ph/9907015> arXiv:astro-ph/9907015 [astro-ph]

[100] Kushnir, D., Katz, B., Dong, S., Livne, E., Fernández, R.: Head-on Collisions of White Dwarfs in Triple Systems Could Explain Type Ia Supernovae. *ApJ* **778**(2), 37 (2013) <https://doi.org/10.1088/2041-8205/778/2/L37> arXiv:1303.1180 [astro-ph.HE]

[101] Pinto, P.A., Eastman, R.G.: The Physics of Type IA Supernova Light Curves. II. Opacity and Diffusion. *ApJ* **530**(2), 757–776 (2000) <https://doi.org/10.1086/308380>

[102] McCully, C., Jha, S.W., Scalzo, R.A., Howell, D.A., Foley, R.J., Zeng, Y., Liu, Z.-W., Hosseinzadeh, G., Bildsten, L., Riess, A.G., Kirshner, R.P., Marion, G.H., Camacho-Neves, Y.: Still Brighter than Pre-explosion, SN 2012Z Did Not Disappear: Comparing Hubble Space Telescope Observations a Decade Apart. *ApJ* **925**(2), 138 (2022) <https://doi.org/10.3847/1538-4357/ac3bbd> arXiv:2106.04602 [astro-ph.HE]

[103] Yaron, O., Gal-Yam, A.: WISeREP—An Interactive Supernova Data Repository. *Publications of the Astronomical Society of the Pacific* **124**, 668 (2012) <https://doi.org/10.1086/666656> arXiv:1204.1891 [astro-ph.IM]

[104] Vreeswijk: (in prep.)

[105] Zackay, B., Ofek, E.O., Gal-Yam, A.: Proper Image Subtraction—Optimal Transient Detection, Photometry, and Hypothesis Testing. *ApJ* **830**(1), 27 (2016) <https://doi.org/10.3847/0004-637X/830/1/27> arXiv:1601.02655 [astro-ph.IM]

[106] Brown, T.M., Baliber, N., Bianco, F.B., Bowman, M., Burleson, B., Conway, P., Crellin, M., Depagne, É., De Vera, J., Dilday, B., Dragomir, D., Dubberley, M., Eastman, J.D., Elphick, M., Falarski, M., Foale, S., Ford, M., Fulton, B.J., Garza, J., Gomez, E.L., Graham, M., Greene, R., Haldeman, B., Hawkins, E., Haworth, B., Haynes, R., Hidas, M., Hjelstrom, A.E., Howell, D.A., Hygelund, J., Lister, T.A., Lobdill, R., Martinez, J., Mullins, D.S., Norbury, M., Parrent, J., Paulson, R., Petry, D.L., Pickles, A., Posner, V., Rosing, W.E., Ross, R., Sand, D.J., Saunders, E.S., Shobbrook, J., Shporer, A., Street, R.A., Thomas, D., Tsapras, Y., Tufts, J.R., Valenti, S., Vander Horst, K., Walker,

Z., White, G., Willis, M.: Las Cumbres Observatory Global Telescope Network. *PASP* **125**(931), 1031 (2013) <https://doi.org/10.1086/673168> arXiv:1305.2437 [astro-ph.IM]

- [107] McCully, C., Turner, M., Volgenau, N., Harbeck, D., Valenti, S., Riba, A., Bachelet, E., Snyder, I.W., Kurczynski, B., Norbury, M., Street, R.: LCOGT/banzai: Initial Release. <https://doi.org/10.5281/zenodo.1257560>
- [108] Tonry, J.L., Denneau, L., Flewelling, H., Heinze, A.N., Onken, C.A., Smartt, S.J., Stalder, B., Weiland, H.J., Wolf, C.: The ATLAS All-Sky Stellar Reference Catalog. *ApJ* **867**(2), 105 (2018) <https://doi.org/10.3847/1538-4357/aae386> arXiv:1809.09157 [astro-ph.IM]
- [109] Tonry, J.L., Stubbs, C.W., Lykke, K.R., Doherty, P., Shivvers, I.S., Burgett, W.S., Chambers, K.C., Hodapp, K.W., Kaiser, N., Kudritzki, R.-P., Magnier, E.A., Morgan, J.S., Price, P.A., Wainscoat, R.J.: The Pan-STARRS1 Photometric System. *ApJ* **750**(2), 99 (2012) <https://doi.org/10.1088/0004-637X/750/2/99> arXiv:1203.0297 [astro-ph.IM]
- [110] Chen, P., Dong, S., Kochanek, C.S., Stanek, K.Z., Post, R.S., Stritzinger, M.D., Prieto, J.L., Filippenko, A.V., Kollmeier, J.A., Elias-Rosa, N., Katz, B., Tomasella, L., Bose, S., Ashall, C., Benetti, S., Bersier, D., Brimacombe, J., Brink, T.G., Brown, P., Buckley, D.A.H., Cappellaro, E., Christie, G.W., Fraser, M., Gromadzki, M., Holoiien, T.W.-S., Hu, S., Kankare, E., Koff, R., Lundqvist, P., Mattila, S., Milne, P.A., Morrell, N., Muñoz, J.A., Mutel, R., Natusch, T., Nicolas, J., Pastorello, A., Prentice, S., Roth, T., Shappee, B.J., Stone, G., Thompson, T.A., Villanueva, S., Zheng, W.: The First Data Release of CNIa0.02-A Complete Nearby (Redshift ≥ 0.02) Sample of Type Ia Supernova Light Curves. *ApJS* **259**(2), 53 (2022) <https://doi.org/10.3847/1538-4365/ac50b7> arXiv:2011.02461 [astro-ph.HE]
- [111] Chonis, T.S., Gaskell, C.M.: Setting UBVR Photometric Zero-Points Using Sloan Digital Sky Survey ugriz Magnitudes. *AJ* **135**(1), 264–267 (2008) <https://doi.org/10.1088/0004-6256/135/1/264> arXiv:0710.5801 [astro-ph]
- [112] Tartaglia, L., Sand, D.J., Valenti, S., Wyatt, S., Anderson, J.P., Arcavi, I., Ashall, C., Botticella, M.T., Cartier, R., Chen, T.-W., Cikota, A., Coulter, D., Della Valle, M., Foley, R.J., Gal-Yam, A., Galbany, L., Gall, C., Haislip, J.B., Harmanen, J., Hosseinzadeh, G., Howell, D.A., Hsiao, E.Y., Inserra, C., Jha, S.W., Kankare, E., Kilpatrick, C.D., Kouprianov, V.V., Kuncarayakti, H., Maccarone, T.J., Maguire, K., Mattila, S., Mazzali, P.A., McCully, C., Melandri, A., Morrell, N., Phillips, M.M., Pignata, G., Piro, A.L., Prentice, S., Reichart, D.E., Rojas-Bravo, C., Smartt, S.J., Smith, K.W., Sollerman, J., Stritzinger, M.D., Sullivan, M., Taddia, F., Young, D.R.: The Early Detection and Follow-up of the Highly Obscured Type II Supernova 2016ija/DLT16am. *ApJ* **853**(1), 62 (2018) <https://doi.org/10.3847/1538-4357/aaa014> arXiv:1711.03940 [astro-ph.HE]

[113] Steeghs, D., Galloway, D.K., Ackley, K., Dyer, M.J., Lyman, J., Ulaczyk, K., Cutter, R., Mong, Y.-L., Dhillon, V., O'Brien, P., Ramsay, G., Poshyachinda, S., Kotak, R., Nuttall, L.K., Pallé, E., Breton, R.P., Pollacco, D., Thrane, E., Aukkaravittayapun, S., Awiphan, S., Burhanudin, U., Chote, P., Chrimes, A., Daw, E., Duffy, C., Eyles-Ferris, R., Gompertz, B., Heikkilä, T., Irawati, P., Kennedy, M.R., Killestein, T., Kuncarayakti, H., Levan, A.J., Littlefair, S., Makrygianni, L., Marsh, T., Mata-Sanchez, D., Mattila, S., Maund, J., McCormac, J., Mkrtichian, D., Mullaney, J., Noysena, K., Patel, M., Rol, E., Sawangwit, U., Stanway, E.R., Starling, R., Strøm, P., Tooke, S., West, R., White, D.J., Wiersema, K.: The Gravitational-wave Optical Transient Observer (GOTO): prototype performance and prospects for transient science. *MNRAS* **511**(2), 2405–2422 (2022) <https://doi.org/10.1093/mnras/stac013> [arXiv:2110.05539](https://arxiv.org/abs/2110.05539) [astro-ph.IM]

[114] Lyman, J.: (in prep.)

[115] Tonry, J.L., Denneau, L., Flewelling, H., Heinze, A.N., Onken, C.A., Smartt, S.J., Stalder, B., Weiland, H.J., Wolf, C.: The ATLAS All-Sky Stellar Reference Catalog. *ApJ* **867**(2), 105 (2018) <https://doi.org/10.3847/1538-4357/aae386> [arXiv:1809.09157](https://arxiv.org/abs/1809.09157) [astro-ph.IM]

[116] Becker, A.: HOTPANTS: High Order Transform of PSF ANd Template Subtraction

[117] Drlica-Wagner, A., Ferguson, P.S., Adamów, M., Aguena, M., Allam, S., Andrade-Oliveira, F., Bacon, D., Bechtol, K., Bell, E.F., Bertin, E., Bilaji, P., Bocquet, S., Bom, C.R., Brooks, D., Burke, D.L., Carballo-Bello, J.A., Carlin, J.L., Carnero Rosell, A., Carrasco Kind, M., Carretero, J., Castander, F.J., Cerny, W., Chang, C., Choi, Y., Conselice, C., Costanzi, M., Crnojević, D., da Costa, L.N., de Vicente, J., Desai, S., Esteves, J., Everett, S., Ferrero, I., Fitzpatrick, M., Flaugher, B., Friedel, D., Frieman, J., García-Bellido, J., Gatti, M., Gaztanaga, E., Gerdes, D.W., Gruen, D., Gruendl, R.A., Gschwend, J., Hartley, W.G., Hernandez-Lang, D., Hinton, S.R., Hollowood, D.L., Honscheid, K., Hughes, A.K., Jacques, A., James, D.J., Johnson, M.D., Kuehn, K., Kuropatkin, N., Lahav, O., Li, T.S., Lidman, C., Lin, H., March, M., Marshall, J.L., Martínez-Delgado, D., Martínez-Vázquez, C.E., Massana, P., Mau, S., McNanna, M., Melchior, P., Menanteau, F., Miller, A.E., Miquel, R., Mohr, J.J., Morgan, R., Mutlu-Pakdil, B., Muñoz, R.R., Neilsen, E.H., Nidever, D.L., Nikutta, R., Nilo Castellon, J.L., Noël, N.E.D., Ogando, R.L.C., Olsen, K.A.G., Pace, A.B., Palmese, A., Paz-Chinchón, F., Pereira, M.E.S., Pieres, A., Plazas Malagón, A.A., Prat, J., Riley, A.H., Rodriguez-Monroy, M., Romer, A.K., Roodman, A., Sako, M., Sakowska, J.D., Sanchez, E., Sánchez, F.J., Sand, D.J., Santana-Silva, L., Santiago, B., Schubnell, M., Serrano, S., Sevilla-Noarbe, I., Simon, J.D., Smith, M., Soares-Santos, M., Stringfellow, G.S., Suchyta, E., Suson, D.J., Tan, C.Y., Tarle, G., Tavangar, K., Thomas, D., To, C., Tollerud, E.J., Troxel, M.A., Tucker, D.L., Varga, T.N., Vivas, A.K., Walker,

A.R., Weller, J., Wilkinson, R.D., Wu, J.F., Yanny, B., Zaborowski, E., Zenteno, A., Delve Collaboration, Des Collaboration, Astro Data Lab: The DECam Local Volume Exploration Survey Data Release 2. *ApJS* **261**(2), 38 (2022) <https://doi.org/10.3847/1538-4365/ac78eb> arXiv:2203.16565 [astro-ph.IM]

[118] Asquini, L., Landoni, M., Young, D., Marty, L., Smartt, S.J., Campana, S., Claudi, R., Schipani, P., Achren, J., Aliverti, M., Araiza-Durán, J.A., Arcavi, I., Battaini, F., Baruffolo, A., Ben-Ami, S., Bianco, A., Bichkovsky, A., Brucalassi, A., Bruch, R., Capasso, G., Cappellaro, E., Colapietro, M., Cosentino, R., D'Alessio, F., D'Avanzo, P., Della Valle, M., D'Orsi, S., Di Benedetto, R., Di Filippo, S., Gal-Yam, A., Genoni, M., Hernandez, M., Hershko, O., Kotilainen, J., Kuncarayakti, H., Li Causi, G., Mattila, S., Munari, M., Pariani, G., Pérez Ventura, H., Pignata, G., Radhakrishnan, K., Rappaport, M., Ricci, D., Riva, M., Rubin, A., Salasnich, B., Savarese, S., Stritzinger, M., Scuderi, S., Vitali, F., Zanmar Sanchez, R.: Automated scheduler for the SOXS instrument: design and performance. In: Ibsen, J., Chiozzi, G. (eds.) Software and Cyberinfrastructure for Astronomy VIII. Society of Photo-Optical Instrumentation Engineers (SPIE) Conference Series, vol. 13101, p. 131012 (2024). <https://doi.org/10.1117/12.3018271>

[119] <https://www.wis-tns.org/>. Transient Name Server

[120] Smartt, S.J., Valenti, S., Fraser, M., Inserra, C., Young, D.R., Sullivan, M., Pastorello, A., Benetti, S., Gal-Yam, A., Knapic, C., Molinaro, M., Smareglia, R., Smith, K.W., Taubenberger, S., Yaron, O., Anderson, J.P., Ashall, C., Balland, C., Baltay, C., Barbarino, C., Bauer, F.E., Baumont, S., Bersier, D., Blagorodnova, N., Bongard, S., Botticella, M.T., Bufano, F., Bulla, M., Cappellaro, E., Campbell, H., Cellier-Holzem, F., Chen, T.-W., Childress, M.J., Clocchiatti, A., Contreras, C., Dall'Ora, M., Danziger, J., de Jaeger, T., De Cia, A., Della Valle, M., Dennefeld, M., Elias-Rosa, N., Elman, N., Feindt, U., Fleury, M., Gall, E., Gonzalez-Gaitan, S., Galbany, L., Morales Garoffolo, A., Greggio, L., Guillou, L.L., Hachinger, S., Hadjiyska, E., Hage, P.E., Hillebrandt, W., Hodgkin, S., Hsiao, E.Y., James, P.A., Jerkstrand, A., Kangas, T., Kankare, E., Kotak, R., Kromer, M., Kuncarayakti, H., Leloudas, G., Lundqvist, P., Lyman, J.D., Hook, I.M., Maguire, K., Manulis, I., Margheim, S.J., Mattila, S., Maund, J.R., Mazzali, P.A., McCrum, M., McKinnon, R., Moreno-Raya, M.E., Nicholl, M., Nugent, P., Pain, R., Pignata, G., Phillips, M.M., Polshaw, J., Pumo, M.L., Rabinowitz, D., Reilly, E., Romero-Cañizales, C., Scalzo, R., Schmidt, B., Schulze, S., Sim, S., Sollerman, J., Taddia, F., Tartaglia, L., Terreran, G., Tomasella, L., Turatto, M., Walker, E., Walton, N.A., Wyrzykowski, L., Yuan, F., Zampieri, L.: PESSTO: survey description and products from the first data release by the Public ESO Spectroscopic Survey of Transient Objects. *A&A* **579**, 40 (2015) <https://doi.org/10.1051/0004-6361/201425237> arXiv:1411.0299 [astro-ph.SR]

[121] Hook, I.M., Jørgensen, I., Allington-Smith, J.R., Davies, R.L., Metcalfe, N.,

Murowinski, R.G., Crampton, D.: The Gemini-North Multi-Object Spectrograph: Performance in Imaging, Long-Slit, and Multi-Object Spectroscopic Modes. *PASP* **116**(819), 425–440 (2004) <https://doi.org/10.1086/383624>

[122] Gimeno, G., Roth, K., Chiboucas, K., Hibon, P., Boucher, L., White, J., Rippa, M., Labrie, K., Turner, J., Hanna, K., Lazo, M., Pérez, G., Rogers, R., Rojas, R., Placco, V., Murowinski, R.: On-sky commissioning of Hamamatsu CCDs in GMOS-S. In: Evans, C.J., Simard, L., Takami, H. (eds.) *Ground-based and Airborne Instrumentation for Astronomy VI*. Society of Photo-Optical Instrumentation Engineers (SPIE) Conference Series, vol. 9908, p. 99082 (2016). <https://doi.org/10.1117/12.2233883>

[123] Labrie, K., Simpson, C., Cardenes, R., Turner, J., Soraism, M., Quint, B., Oberdorf, O., Placco, V.M., Berke, D., Smirnova, O., Conseil, S., Vacca, W.D., Thomas-Osip, J.: DRAGONS-A Quick Overview. *Research Notes of the American Astronomical Society* **7**(10), 214 (2023) <https://doi.org/10.3847/2515-5172/ad0044> arXiv:2310.03048 [astro-ph.IM]

[124] Valenti, S.: Svalenti/floyds_pipeline: Floyds Pipeline (2016). https://github.com/svalenti/FLOYDS_{ }pipeline

[125] Vernet, J., Dekker, H., D’Odorico, S., Kaper, L., Kjaergaard, P., Hammer, F., Randich, S., Zerbi, F., Groot, P.J., Hjorth, J., Guinouard, I., Navarro, R., Adolfse, T., Albers, P.W., Amans, J.-P., Andersen, J.J., Andersen, M.I., Binetruy, P., Bristow, P., Castillo, R., Chemla, F., Christensen, L., Conconi, P., Conzelmann, R., Dam, J., de Caprio, V., de Ugarte Postigo, A., Delabre, B., di Marcantonio, P., Downing, M., Elswijk, E., Finger, G., Fischer, G., Flores, H., François, P., Goldoni, P., Guglielmi, L., Haigron, R., Hanenburg, H., Hendriks, I., Horrobin, M., Horville, D., Jessen, N.C., Kerber, F., Kern, L., Kiekebusch, M., Kleszcz, P., Klougart, J., Kragt, J., Larsen, H.H., Lizon, J.-L., Lucuix, C., Mainieri, V., Manuputy, R., Martayan, C., Mason, E., Mazzoleni, R., Michaelsen, N., Modigliani, A., Moehler, S., Møller, P., Norup Sørensen, A., Nørregaard, P., Péroux, C., Patat, F., Pena, E., Pragt, J., Reinero, C., Rigal, F., Riva, M., Roelfsema, R., Royer, F., Sacco, G., Santin, P., Schoenmaker, T., Spano, P., Sweers, E., Ter Horst, R., Tintori, M., Tromp, N., van Dael, P., van der Vliet, H., Venema, L., Vidali, M., Vinther, J., Vola, P., Winters, R., Wistisen, D., Wulterkens, G., Zacchei, A.: X-shooter, the new wide band intermediate resolution spectrograph at the ESO Very Large Telescope. *A&A* **536**, 105 (2011) <https://doi.org/10.1051/0004-6361/201117752> arXiv:1110.1944 [astro-ph.IM]

[126] Crawford, S.M., Still, M., Schellart, P., Balona, L., Buckley, D.A.H., Dugmore, G., Gulbis, A.A.S., Kniazev, A., Kotze, M., Loaring, N., Nordsieck, K.H., Pickering, T.E., Potter, S., Romero Colmenero, E., Vaisanen, P., Williams, T., Zietsman, E.: PySALT: the SALT science pipeline. In: Silva, D.R., Peck, A.B., Soifer, B.T. (eds.) *Observatory Operations: Strategies, Processes, and Systems III*. Society of Photo-Optical Instrumentation Engineers (SPIE) Conference

Series, vol. 7737, p. 773725 (2010). <https://doi.org/10.11117/12.857000>

- [127] Science Software Branch at STScI: PyRAF: Python Alternative for IRAF
- [128] Dressler, A., Bigelow, B., Hare, T., Sutin, B., Thompson, I., Burley, G., Epps, H., Oemler, J., Augustus, Bagish, A., Birk, C., Clardy, K., Gunnels, S., Kelson, D., Shectman, S., Osip, D.: IMACS: The Inamori-Magellan Areal Camera and Spectrograph on Magellan-Baade. *PASP* **123**(901), 288 (2011) <https://doi.org/10.1086/658908>
- [129] Kirkpatrick, J.D., Cushing, M.C., Gelino, C.R., Griffith, R.L., Skrutskie, M.F., Marsh, K.A., Wright, E.L., Mainzer, A., Eisenhardt, P.R., McLean, I.S., Thompson, M.A., Bauer, J.M., Benford, D.J., Bridge, C.R., Lake, S.E., Petty, S.M., Stanford, S.A., Tsai, C.-W., Bailey, V., Beichman, C.A., Bloom, J.S., Bochanski, J.J., Burgasser, A.J., Capak, P.L., Cruz, K.L., Hinz, P.M., Kartaltepe, J.S., Knox, R.P., Manohar, S., Masters, D., Morales-Calderón, M., Prato, L.A., Rodigas, T.J., Salvato, M., Schurr, S.D., Scoville, N.Z., Simcoe, R.A., Stapelfeldt, K.R., Stern, D., Stock, N.D., Vacca, W.D.: The First Hundred Brown Dwarfs Discovered by the Wide-field Infrared Survey Explorer (WISE). *ApJS* **197**(2), 19 (2011) <https://doi.org/10.1088/0067-0049/197/2/19> [arXiv:1108.4677](https://arxiv.org/abs/1108.4677) [astro-ph.SR]
- [130] <https://noirlab.edu/science/observing-noirlab/observing-ctio/observing-soar/data-reduction/triplespec-data>. TripleSpec
- [131] Cushing, M.C., Vacca, W.D., Rayner, J.T.: Spextool: A Spectral Extraction Package for SpeX, a 0.8-5.5 Micron Cross-Dispersed Spectrograph. *PASP* **116**(818), 362–376 (2004) <https://doi.org/10.1086/382907>
- [132] Vacca, W.D., Cushing, M.C., Rayner, J.T.: A Method of Correcting Near-Infrared Spectra for Telluric Absorption. *PASP* **115**(805), 389–409 (2003) <https://doi.org/10.1086/346193> [arXiv:astro-ph/0211255](https://arxiv.org/abs/astro-ph/0211255) [astro-ph]
- [133] Weilbacher, P.M., Palsa, R., Streicher, O., Bacon, R., Urrutia, T., Wisotzki, L., Conseil, S., Husemann, B., Jarno, A., Kelz, A., Pécontal-Rousset, A., Richard, J., Roth, M.M., Selman, F., Vernet, J.: The data processing pipeline for the MUSE instrument. *A&A* **641**, 28 (2020) <https://doi.org/10.1051/0004-6361/202037855> [arXiv:2006.08638](https://arxiv.org/abs/2006.08638) [astro-ph.IM]
- [134] Soto, K.T., Lilly, S.J., Bacon, R., Richard, J., Conseil, S.: ZAP - enhanced PCA sky subtraction for integral field spectroscopy. *MNRAS* **458**(3), 3210–3220 (2016) <https://doi.org/10.1093/mnras/stw474> [arXiv:1602.08037](https://arxiv.org/abs/1602.08037) [astro-ph.IM]